ISSN 2663-9084 (Print)
ISSN 2663-9092 (Online)

Ukrainian Neurosurgical Journal

Vol. 30, N4, 2024

Is a scholarly Open Access journal
Founded in April 1995. Quarterly.
State Registration Certificate KV No 23771-13611PR dated 14 February 2019
The journal is on the List of Scientific Professional Editions of Ukraine, where results of thesis research for earning academic degrees of doctor and candidate of sciences and PhD may be published (Order of the Ministry of Education and Science of Ukraine No. 1301 dated 15 October 2019)
The journal is included in the Scopus scientometric database.

Journal publishes peer-reviewed works.

Founders
Romodanov Neurosurgery Institute
Ukrainian Association of Neurosurgeons
National Academy of Medical Sciences of Ukraine

Publisher
Romodanov Neurosurgery Institute

Contact
32 Platona Mayborody st., Kyiv, 04050, Ukraine
tel. +380 44 483-91-98
fax +380 44 489-35-61
E-mail: unj.office@gmail.com
http://theunj.org

The journal went to press 05 December 2024
Format 60 × 841/8. Offset Paper No.1
Order No. 24-40

Circulation 300 copies

Polygraphic services
FOP Golosuy IE
Certificate AA No. 9221702
86 Kyrylivska st., Kyiv, 04080, Ukraine
Tel. +380 44 239-19-85

The master layout of the journal was approved and recommended for publication and distribution via the Internet at the joint meeting of the Editorial Board of the Ukrainian Neurosurgical Journal and the Academic Council of Romodanov Neurosurgery Institute (Meeting Minutes N. 17 dated 22 November 2024)

On the cover
Figures from the article by Ziia K. Melikov, Volodymyr V. Medvediev "The rat's sciatic nerve functional index dynamics after its transection and recovery by means of epineural neurorrhaphy", p. 33-42

Content

Review article

Ukr Neurosurg J. 2024;30(4):3-10
doi: 10.25305/unj.310374

Crossroads of Neurology and Virology: The Neurological Manifestations of COVID-19

Kirolos Eskandar

Diakonie Klinik Mosbach, Mosbach, Germany

Received: 22 August 2024
Accepted: 04 October 2024

Address for correspondence:
Kirolos Eskandar, Neckarburkener Str. 6, 74821 Mosbach, Germany, e-mail: kiroloss.eskandar@gmail.com

Introduction: The COVID-19 pandemic, caused by SARS-CoV-2, has led to an unprecedented global health crisis. While primarily recognized for its respiratory implications, the virus has shown a significant affinity for the nervous system, resulting in a wide spectrum of neurological manifestations. This literature review explores the intersection of neurology and virology, focusing on the acute and long-term neurological effects of COVID-19.

Methods: A comprehensive review of current literature was conducted using databases such as PubMed, Scopus, and Web of Science. Relevant studies were selected based on their focus on the pathophysiology, clinical presentations, and long-term neurological outcomes of COVID-19. Special attention was given to peer-reviewed articles, meta-analyses, and clinical case reports published between 2019 and 2024.

Results: The review identifies multiple mechanisms by which SARS-CoV-2 invades the nervous system, including direct viral entry and systemic inflammation. Acute neurological manifestations include encephalitis, stroke, and Guillain-Barré syndrome, while long-term sequelae encompass cognitive impairment, neurodegeneration, and psychiatric disorders. The findings underscore the complexity of COVID-19's impact on the nervous system, with both immediate and enduring effects.

Conclusion: Neuro-COVID represents a significant and evolving challenge in the context of the pandemic. Understanding the neurological implications of COVID-19 is crucial for improving patient outcomes and guiding future research. This review underscores the need for heightened clinical awareness and a multidisciplinary approach to effectively address the complex neuro-COVID spectrum.

Key words: *Neuro-COVID; SARS-CoV-2; Neurological manifestations; Long COVID; Neuroinvasion*

Introduction

The COVID-19 pandemic, caused by the novel coronavirus SARS-CoV-2, has profoundly affected global health, leading to millions of deaths and overwhelming healthcare systems worldwide. While the respiratory symptoms of COVID-19 were initially the primary concern, it soon became apparent that the virus could affect multiple organ systems, including the nervous system. This recognition has spurred an intense focus on understanding the neurological manifestations associated with COVID-19 [1].

The global impact of COVID-19 has been unprecedented. As of 2024, the virus has led to over 770 million confirmed cases and nearly 7 million deaths worldwide. The rapid spread of SARS-CoV-2, combined with its potential for severe complications, especially in vulnerable populations, has created a significant public health challenge [2]. This global crisis has prompted extensive research into various aspects of the disease, including its neurological implications.

Viral infections have long been known to affect the nervous system. Neurotropic viruses, such as herpes simplex virus and West Nile virus, can directly invade the central nervous system (CNS), leading to conditions like encephalitis and meningitis. Other viruses can cause neurological damage indirectly through immune-mediated mechanisms or by causing systemic conditions that affect the brain, such as hypoxia or coagulopathies. SARS-CoV-2 appears to have a multifaceted impact on the nervous system, potentially through direct viral invasion, immune responses, and vascular involvement, leading to a range of neurological symptoms [3].

The rationale behind studying the neurological manifestations of COVID-19 lies in the broad spectrum of neurological symptoms reported in patients, ranging from mild headaches and anosmia to severe conditions like stroke, encephalitis, and Guillain-Barré syndrome [3]. Understanding these manifestations is crucial for improving clinical management and outcomes for patients with COVID-19. Early recognition of neurological symptoms can lead to timely interventions that may reduce morbidity and mortality associated with the disease. Furthermore, studying the mechanisms by which SARS-CoV-2 affects the nervous system could

provide insights into the broader field of neurovirology, potentially leading to advances in the treatment of other viral infections that impact the nervous system [2].

Methodology:

This literature review was conducted using a systematic approach in accordance with the PRISMA (Preferred Reporting Items for Systematic reviews and Meta-Analyses) guidelines to ensure a comprehensive and unbiased selection of relevant studies related to the neurological manifestations of COVID-19.

Search Strategy:

A thorough literature search was performed across several reputable databases, including PubMed, Scopus, Web of Science, and Google Scholar. The search was conducted over a period from [start date] to [end date], covering all relevant studies published during this timeframe. The search strategy incorporated a combination of specific keywords and Medical Subject Headings (MeSH) terms, including "Neuro-COVID", "SARS-CoV-2", "Neurological manifestations", "Long COVID" and "Neuroinvasion." Boolean operators (AND, OR) were used to refine the search results and ensure that a wide range of pertinent literature was captured.

Inclusion and Exclusion Criteria:

To be included in this review, studies had to meet the following criteria:

- Language: Only studies published in English were considered to avoid language bias.
- Population: Studies focusing specifically on patients diagnosed with COVID-19.
- Focus: Articles that reported on neurological manifestations related to COVID-19.
- Study Design: All types of peer-reviewed studies were included, such as case reports, cohort studies, cross-sectional studies, and reviews. Non-peer-reviewed articles, editorials, and commentaries were excluded.

Study Selection and Screening Process:

Initially, 168 articles were retrieved from the databases. After the removal of duplicate records, 120 unique articles remained. These articles were subjected to a multi-stage screening process:

1. Title and Abstract Screening: The titles and abstracts of the remaining articles were screened independently by two reviewers to assess their relevance to the topic. Articles that did not meet the inclusion criteria were excluded at this stage.

2. Full-text Screening: The full texts of the remaining 70 articles were then reviewed in detail to confirm their eligibility based on the predefined inclusion criteria. This process resulted in the exclusion of 30 additional studies that did not adequately focus on the neurological aspects of COVID-19.

Ultimately, 40 studies were included in this review after the rigorous screening process. Any discrepancies between the reviewers during the screening process were resolved through discussion or consultation with a third reviewer.

Data Extraction and Synthesis:

Data were extracted from the included studies using a standardized data extraction form. The extracted data included study characteristics (author, year, study design, sample size), patient demographics, types of neurological manifestations, and key findings related to the mechanisms and outcomes of these neurological conditions. The extracted data were then synthesized to provide a comprehensive overview of the neurological manifestations associated with COVID-19.

Quality Assessment:

The quality of the included studies was assessed using the Newcastle-Ottawa Scale for observational studies and the Cochrane Risk of Bias tool for randomized controlled trials. This assessment ensured that the findings presented in this review were based on high-quality evidence.

To provide a clear overview of the study selection process, a PRISMA flow diagram ***(Fig. 1)*** is included, illustrating the number of records identified, screened, and included in the review, along with reasons for exclusion at each stage.

Results:

The systematic review of the literature identified 40 studies that met the inclusion criteria and were analyzed for the neurological manifestations of COVID-19. The findings reveal a broad spectrum of both acute and long-term neurological complications associated with SARS-CoV-2 infection.

Acute Neurological Manifestations:

- Central Nervous System (CNS): Encephalitis, meningitis, acute disseminated encephalomyelitis (ADEM), and ischemic stroke were frequently reported. Patients presented with symptoms ranging from mild confusion and headaches to severe cases involving coma and large-vessel strokes. Stroke, particularly in younger patients, emerged as a critical concern, with hypercoagulable states induced by the virus as a contributing factor.
- Peripheral Nervous System (PNS): Guillain-Barré Syndrome (GBS) and its variants were commonly observed, presenting as ascending paralysis. Additionally, anosmia (loss of smell) and ageusia (loss of taste) were among the most prevalent early symptoms, often linked to the virus's impact on the olfactory nerve.

Long-term Neurological Sequelae:

- Cognitive and Psychiatric Disorders: Cognitive impairments, often termed "brain fog," along with headaches, fatigue, and dizziness, were recurrent in patients experiencing "Long COVID." These symptoms were compounded by mental health issues such as anxiety, depression, and PTSD.
- Neurodegenerative Concerns: There is growing evidence suggesting that SARS-CoV-2 may accelerate or contribute to the onset of neurodegenerative diseases like Parkinson's and Alzheimer's. Persistent neuroinflammation and immune dysregulation are hypothesized as underlying mechanisms.

This article contains some figures that are displayed in color online but in black and white in the print edition

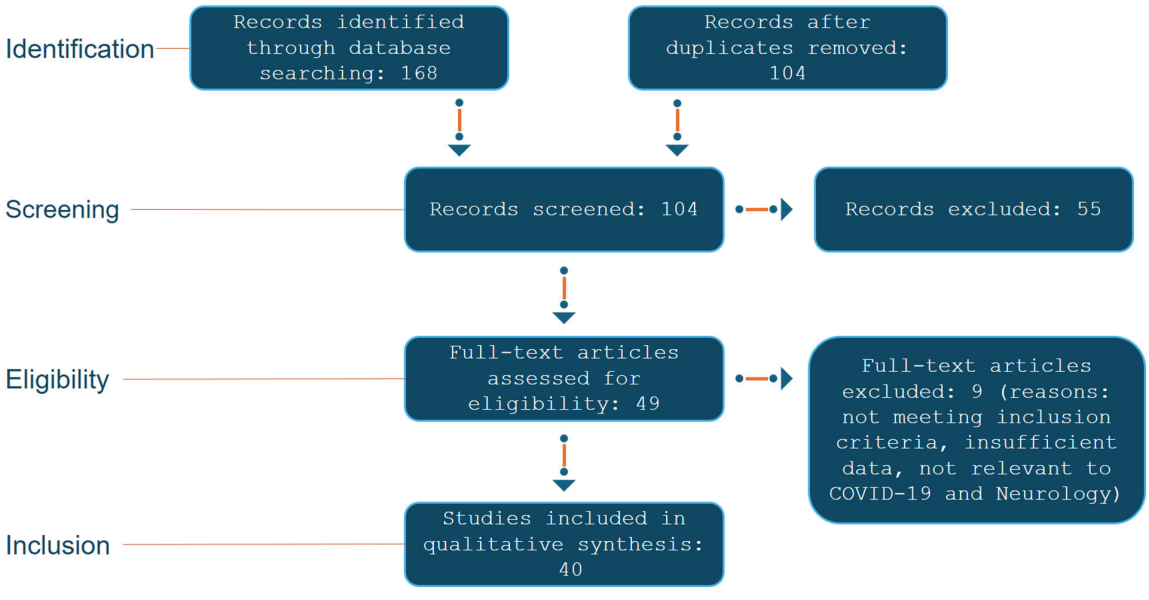

Fig. 1. Illustrates the PRIMSA flow diagram

Pediatric Considerations: Conditions like Multisystem Inflammatory Syndrome in Children (MIS-C) have shown severe neurological complications, including encephalopathy and cerebrovascular events. Long-term cognitive and developmental outcomes in children who suffered from severe COVID-19 or MIS-C are still under investigation but are a significant concern.

Immunological and Molecular Insights:

The review highlighted the critical role of the immune system in the neurological impact of COVID-19, particularly the cytokine storm and its effects on the blood-brain barrier (BBB). Autoimmune responses, potentially triggered by molecular mimicry, were linked to conditions like GBS and other neuropathies, raising concerns about long-term neurodegenerative risks.

Diagnostic Challenges:

The review underscored the complexity of diagnosing COVID-19-related neurological symptoms, with neuroimaging and biomarkers like neurofilament light chain (NfL) and S100B playing crucial roles. However, the specificity of these diagnostic tools remains an area for further research.

Therapeutic Approaches:

Management strategies for these neurological manifestations have evolved, with corticosteroids like dexamethasone proving effective in reducing severe outcomes. Long-term management, particularly for "Long COVID," includes cognitive rehabilitation and neuropsychiatric support, with ongoing research into neuroprotective therapies.

Discussion:

Pathophysiology of SARS-CoV-2

The pathophysiology of SARS-CoV-2's interaction with the central nervous system (CNS) is a multifaceted process, involving both direct and indirect mechanisms of neuroinvasion. One key aspect is the virus's ability to enter the CNS, a process known as neuroinvasion. This can occur through several potential routes: direct viral entry, systemic inflammatory responses, or a combination of both.

SARS-CoV-2, like other coronaviruses, has a known neurotropic potential, which means it can infect nerve tissues. The mechanisms of neuroinvasion primarily involve two pathways: direct viral entry into the brain and the systemic inflammatory response triggered by the virus. Direct viral entry can occur through the hematogenous route, where the virus in the bloodstream crosses the blood-brain barrier (BBB) and enters the CNS. Alternatively, the virus can spread through retrograde neuronal transport, utilizing nerves like the olfactory nerve as a conduit to the brain [4].

The hematogenous spread is a critical route for neuroinvasion. After the initial infection in the respiratory system, the virus can enter the bloodstream, potentially disrupting the BBB, a protective barrier that normally restricts the entry of pathogens into the brain. SARS-CoV-2 can bind to ACE2 receptors on the endothelial cells of the BBB, leading to increased permeability and allowing the virus to penetrate the CNS. This disruption of the BBB can also result in inflammation and edema, further facilitating viral entry [5].

Another significant pathway is the olfactory route. The olfactory nerve, which extends from the nasal cavity to the brain, provides a direct route for viral entry. SARS-CoV-2 can infect the olfactory epithelial cells, which express the ACE2 receptors, and travel along the olfactory nerve into the CNS. This route of entry is particularly associated with the neurological symptom of anosmia, or loss of smell, which has been widely reported in COVID-19 patients [5, 6].

The role of the BBB in SARS-CoV-2 neuroinvasion is complex. The BBB is composed of tightly joined endothelial cells that prevent most pathogens from entering the brain. However, SARS-CoV-2 can increase the permeability of the BBB through various mechanisms, including the release of pro-inflammatory cytokines

during the systemic inflammatory response known as the cytokine storm. This increased permeability allows not only the virus but also immune cells and inflammatory mediators to enter the CNS, potentially leading to neuroinflammation and neurological damage [7].

Acute Neurological Manifestations

The neurological manifestations of COVID-19 encompass a range of acute conditions involving both the central nervous system (CNS) and peripheral nervous system (PNS). Among CNS manifestations, encephalitis and meningitis are prominent, often presenting with symptoms like confusion, altered mental status, and in severe cases, coma. Acute disseminated encephalomyelitis (ADEM) has also been reported, characterized by an inflammatory attack on the brain and spinal cord, likely driven by the immune response to SARS-CoV-2 [8]. Stroke, particularly ischemic stroke, is another significant concern, with COVID-19 patients at increased risk due to hypercoagulable states induced by the virus. Reports from China and the United States have documented large-vessel strokes in younger patients, raising concerns about the broader impact of COVID-19 on cerebrovascular health [8, 9]. Seizures and status epilepticus, though less common, have been noted, particularly in severe COVID-19 cases, suggesting that SARS-CoV-2 can provoke severe neurological sequelae [10].

In the peripheral nervous system, Guillain-Barré Syndrome (GBS) and its variants, such as Miller Fisher syndrome, have been increasingly associated with COVID-19. GBS typically presents as an ascending paralysis and is thought to result from a post-infectious dysregulation of the immune system, potentially triggered by molecular mimicry between the virus and peripheral nerve components. The clinical spectrum includes acute inflammatory demyelinating polyneuropathy (AIDP) and acute motor-sensory axonal neuropathy (AMSAN), with some COVID-19 patients requiring intensive care due to respiratory failure [11, 12]. Additionally, COVID-19 has been linked to various forms of neuropathy and myopathy, with patients often experiencing muscle pain and weakness, likely due to direct viral invasion of muscle tissue or secondary to systemic inflammation [11]. Anosmia and ageusia, or the loss of smell and taste, are among the most common early symptoms, thought to result from viral invasion of the olfactory nerve or the supportive cells in the nasal epithelium, underscoring the virus's ability to affect the nervous system even in mild cases [13].

Long-term Neurological Sequelae

The long-term neurological sequelae of COVID-19, often referred to as "Long COVID," have emerged as a significant concern in the aftermath of the pandemic. These sequelae, collectively termed Post-Acute Sequelae of SARS-CoV-2 Infection (PASC), encompass a range of persistent neurological symptoms that extend beyond the acute phase of the infection. Among the most commonly reported symptoms are cognitive impairments, often referred to as "brain fog," headaches, fatigue, and dizziness [14]. Cognitive impairments can manifest as difficulties in concentration, memory, and executive function, significantly impacting daily activities and quality of life. These symptoms are believed to arise from persistent neuroinflammation and dysregulation of the immune system, as well as potential direct viral damage to the central nervous system [15].

In addition to these cognitive and sensory disturbances, Long COVID has been associated with a significant burden of mental health issues. Anxiety, depression, and post-traumatic stress disorder (PTSD) have been widely reported among survivors, exacerbating the already complex neurological landscape of Long COVID [16]. The interplay between ongoing neurological symptoms and psychological distress creates a challenging environment for both patients and healthcare providers, necessitating a multidisciplinary approach to management.

Emerging evidence also suggests that COVID-19 may accelerate or precipitate neurodegenerative processes. There is growing concern about the potential links between COVID-19 and the development of neurodegenerative diseases such as Parkinson's disease and Alzheimer's disease. The mechanisms underlying these associations are thought to involve chronic neuroinflammation and persistent immune activation, which could potentially contribute to the pathophysiology of these conditions [17]. Moreover, the virus's impact on the blood-brain barrier and its potential to trigger neuroinflammatory cascades may further contribute to the risk of neurodegeneration [18].

The chronic neuroinflammatory responses triggered by COVID-19 may not only be confined to acute illness but could have lasting effects on brain health, underscoring the importance of ongoing research in this area [19]. These findings highlight the need for long-term monitoring of individuals who have recovered from COVID-19, particularly those who experience persistent neurological symptoms, to better understand the potential for long-term neurodegenerative consequences.

Immunological and Molecular Insights

The immunological and molecular mechanisms underlying the neurological complications of COVID-19 are multifaceted and complex. One of the most significant contributors to these complications is the "cytokine storm," a hyperinflammatory response triggered by the immune system's overreaction to SARS-CoV-2. This storm involves the excessive release of pro-inflammatory cytokines such as IL-6, IL-1β, and TNF-α, which can have detrimental effects on the central nervous system (CNS). The blood-brain barrier (BBB) can become compromised during this process, allowing these cytokines and other immune cells to infiltrate the CNS, leading to inflammation, neuronal damage, and a variety of neurological symptoms [20, 21].

Autoimmunity also plays a crucial role in the neurological manifestations of COVID-19. SARS-CoV-2 has been shown to induce autoimmune responses, wherein the immune system mistakenly attacks the body's own tissues, including neural tissues. This can result from molecular mimicry, where viral antigens resemble human proteins, leading to cross-reactivity. For instance, certain SARS-CoV-2 proteins have been found to share similarities with neural antigens, potentially triggering autoimmune conditions such as Guillain-Barré Syndrome (GBS) and other neuropathies [12, 22].

Molecular mimicry and cross-reactivity are particularly concerning because they suggest a mechanism by which COVID-19 could precipitate or

exacerbate chronic neurological conditions. The immune response to SARS-CoV-2 might not only cause acute neurological symptoms but could also set the stage for long-term neurodegenerative diseases. The persistent immune activation and chronic inflammation observed in some COVID-19 patients could potentially contribute to the development or progression of conditions like Parkinson's disease and Alzheimer's disease [23, 24].

Pediatric Neurological Manifestations

The pediatric population has demonstrated a unique spectrum of neurological manifestations related to COVID-19, notably through conditions such as Multisystem Inflammatory Syndrome in Children (MIS-C) and Pediatric Acute-onset Neuropsychiatric Syndrome (PANS). MIS-C, a hyperinflammatory condition often triggered by SARS-CoV-2 infection, presents with a range of neurological complications including severe encephalopathy, cerebrovascular events, and acute demyelinating syndromes. These manifestations are frequently associated with systemic inflammation and may involve direct viral invasion or autoimmune mechanisms [25, 26].

PANS, which can occur after COVID-19, has been linked to neuropsychiatric symptoms like sudden onset of obsessive-compulsive disorder, tics, and other severe behavioral changes. The pathophysiology is thought to involve immune dysregulation and molecular mimicry, where the immune response against the virus cross-reacts with neural tissues, leading to neuroinflammation [26].

Moreover, there is growing concern about the long-term cognitive and developmental outcomes in children who have experienced severe COVID-19 or MIS-C. Emerging evidence suggests that these children may face persistent challenges, including cognitive deficits, memory issues, and difficulties in executive functioning, potentially due to ongoing neuroinflammation or direct neuronal injury. These long-term effects are still being studied, but they highlight the need for continued monitoring and early intervention strategies [27, 28].

Diagnostic Challenges and Biomarkers

The neurological manifestations of COVID-19 present complex diagnostic challenges, necessitating a multifaceted approach involving advanced neuroimaging techniques and biomarkers to differentiate these symptoms from other neurological disorders. Neuroimaging, including MRI, CT, and PET scans, plays a critical role in identifying the structural and functional alterations in the brain associated with COVID-19. MRI has been particularly useful in detecting white matter hyperintensities, microhemorrhages, and cortical abnormalities, which are indicative of the neuroinflammatory processes triggered by SARS-CoV-2 infection. PET scans, although less frequently utilized, have shown changes in glucose metabolism, especially in the frontal and temporal lobes, correlating with cognitive deficits like "brain fog" commonly reported in long COVID cases [28].

Cerebrospinal fluid (CSF) analysis offers another diagnostic avenue, providing insights into the immune response and neuronal injury associated with COVID-19. Elevated levels of neurofilament light chain (NfL) in the CSF have been correlated with neuronal damage, and this marker has been proposed as a potential biomarker for assessing the severity of neurological involvement in COVID-19. Additionally, the presence of oligoclonal bands (OCBs) in the CSF has been linked to intrathecal antibody synthesis, suggesting an ongoing immune response within the central nervous system [29].

Differential diagnosis remains a critical challenge, as many of the neurological symptoms of COVID-19 overlap with other conditions, such as autoimmune encephalitis, stroke, and neurodegenerative diseases. Biomarkers like NfL and S100B, combined with neuroimaging findings, are essential for distinguishing COVID-19-related neurological damage from other etiologies [30]. However, the specificity and sensitivity of these biomarkers are still under investigation, and further research is needed to refine their diagnostic utility [31].

Therapeutic Approaches and Management

The therapeutic management of neurological complications associated with COVID-19 encompasses a broad range of strategies tailored to address both acute and long-term effects. The complexity of these neurological manifestations requires a multidisciplinary approach that combines pharmacological interventions, rehabilitation programs, and ongoing research into neuroprotective and anti-inflammatory therapies.

In the acute phase of COVID-19, early recognition and treatment of neurological complications are critical. Corticosteroids, particularly dexamethasone, have demonstrated significant efficacy in reducing inflammation and preventing severe neurological outcomes such as stroke, encephalitis, and seizures. Dexamethasone works by dampening the hyperinflammatory response associated with severe COVID-19, which is a key contributor to the development of neurological complications. Additionally, antiviral agents like remdesivir, when used in conjunction with corticosteroids, have been shown to synergistically reduce the frequency and severity of neurological manifestations, thereby improving overall patient outcomes [32].

As the pandemic has progressed, the focus has increasingly shifted towards managing the long-term neurological sequelae of COVID-19, commonly referred to as "long COVID" or post-acute sequelae of SARS-CoV-2 infection (PASC). These long-term symptoms include cognitive impairments such as "brain fog," chronic headaches, fatigue, and neuropsychiatric disorders like anxiety, depression, and post-traumatic stress disorder (PTSD). Cognitive rehabilitation, which includes strategies to enhance memory, attention, and executive function, has become a cornerstone of management for these patients. Furthermore, neuropsychiatric rehabilitation, including psychotherapy and pharmacotherapy, is crucial for addressing the mental health challenges associated with long COVID [33].

Research into neuroprotective agents is ongoing, with a focus on their potential to prevent or mitigate long-term neurodegenerative processes that may be initiated by COVID-19. Agents such as N-acetylcysteine (NAC) and melatonin are being investigated for their antioxidant properties and their ability to reduce oxidative stress and inflammation in the brain. These agents could play a role in protecting neuronal integrity and preventing the progression of neurodegenerative diseases in patients with a history of COVID-19 [34].

Given the central role of inflammation in COVID-19-related neurological damage, anti-inflammatory therapies are a key area of interest. Beyond corticosteroids, other anti-inflammatory agents, including interleukin-6 (IL-6) inhibitors (e.g., tocilizumab) and Janus kinase (JAK) inhibitors, are being explored for their potential to modulate the immune response and reduce neuroinflammation. These therapies aim to target the chronic inflammatory state that persists in some patients post-COVID-19, which is thought to contribute to the development of long-term neurological complications [35].

Rehabilitation plays an essential role in the recovery of patients with neurological complications from COVID-19. Multidisciplinary rehabilitation programs that incorporate physical therapy, occupational therapy, speech therapy, and neuropsychological support are vital for helping patients regain function and improve their quality of life. Telemedicine has also emerged as a valuable tool in delivering rehabilitation services to patients with long COVID, providing access to care while minimizing the risk of infection [36].

Future Directions and Research Gaps

The neurological impact of COVID-19 has revealed several critical gaps in our understanding, necessitating focused future research. A primary area of concern is the lack of comprehensive longitudinal studies that can track the neurological effects of COVID-19 over time. These studies are essential to discern the long-term consequences, particularly the risk of developing chronic neurodegenerative conditions like Alzheimer's or Parkinson's disease. Current evidence suggests that SARS-CoV-2 may accelerate neurodegenerative processes, but definitive conclusions can only be drawn through extensive follow-up research over many years [37, 38].

In parallel, there is a growing interest in developing targeted therapies for neuro-COVID. These include anti-inflammatory treatments to mitigate neuroinflammation, which has been implicated in both acute and long-term neurological symptoms of COVID-19. Researchers are also exploring the potential of neuroprotective agents that could safeguard against the neuronal damage observed in severe cases. Importantly, there is an emerging need to personalize these therapies based on individual patient profiles, taking into account factors such as genetic predispositions and the severity of initial COVID-19 infection [39].

Ethical considerations are paramount in this ongoing research. The urgency to develop treatments must be balanced with the need for thorough testing to avoid unintended consequences. Furthermore, addressing neuro-COVID requires a multidisciplinary approach, involving neurologists, immunologists, psychologists, and other healthcare professionals. This collaboration is crucial to ensure that all aspects of the condition are understood and effectively managed [40].

Conclusion

In conclusion, this review highlights the profound and multifaceted neurological impact of COVID-19, ranging from acute manifestations such as encephalitis and stroke to long-term sequelae like cognitive impairment and neurodegeneration. The pathophysiology of SARS-CoV-2's neuroinvasion involves complex mechanisms including direct viral entry, systemic inflammation, and disruption of the blood-brain barrier. Emerging therapeutic strategies are being developed to address these neurological complications, though the field still faces significant challenges. Future research must focus on longitudinal studies to fully understand the chronic effects of COVID-19 on the nervous system, and interdisciplinary collaboration will be crucial in developing effective treatments and addressing the ethical considerations inherent in this rapidly evolving area of study.

Disclosure

Ethics approval and consent to participate:

Not applicable

Consent for publication:

Not applicable

Availability of data and material:

Data sharing not applicable to this article as no datasets were generated or analyzed during the current study

Competing interests:

The authors declare that they have no competing interests.

Funding:

Not applicable

Acknowledgements:

Not applicable

References

1. Yu H, Sun T, Feng J. Complications and Pathophysiology of COVID-19 in the Nervous System. Front Neurol. 2020 Dec 4;11:573421. doi: 10.3389/fneur.2020.5734216
2. Oxley TJ, Mocco J, Majidi S, Kellner CP, Shoirah H, Singh IP, De Leacy RA, Shigematsu T, Ladner TR, Yaeger KA, Skliut M, Weinberger J, Dangayach NS, Bederson JB, Tuhrim S, Fifi JT. Large-Vessel Stroke as a Presenting Feature of Covid-19 in the Young. N Engl J Med. 2020 May 14;382(20):e60. doi: 10.1056/NEJMc20097874
3. Varatharaj A, Thomas N, Ellul MA, Davies NWS, Pollak TA, Tenorio EL, Sultan M, Easton A, Breen G, Zandi M, Coles JP, Manji H, Al-Shahi Salman R, Menon DK, Nicholson TR, Benjamin LA, Carson A, Smith C, Turner MR, Solomon T, Kneen R, Pett SL, Galea I, Thomas RH, Michael BD; CoroNerve Study Group. Neurological and neuropsychiatric complications of COVID-19 in 153 patients: a UK-wide surveillance study. Lancet Psychiatry. 2020 Oct;7(10):875-882. doi: 10.1016/S2215-0366(20)30287-X
4. Meinhardt J, Radke J, Dittmayer C, Franz J, Thomas C, Mothes R, Laue M, Schneider J, Brünink S, Greuel S, Lehmann M, Hassan O, Aschman T, Schumann E, Chua RL, Conrad C, Eils R, Stenzel W, Windgassen M, Rößler L, Goebel HH, Gelderblom HR, Martin H, Nitsche A, Schulz-Schaeffer WJ, Hakroush S, Winkler MS, Tampe B, Scheibe F, Körtvélyessy P, Reinhold D, Siegmund B, Kühl AA, Elezkurtaj S, Horst D, Oesterhelweg L, Tsokos M, Ingold-Heppner B, Stadelmann C, Drosten C, Corman VM, Radbruch H, Heppner FL. Olfactory transmucosal SARS-CoV-2 invasion as a port of central nervous system entry in individuals with COVID-19. Nat Neurosci. 2021 Feb;24(2):168-175. doi: 10.1038/s41593-020-00758-5
5. Paniz-Mondolfi A, Bryce C, Grimes Z, Gordon RE, Reidy J, Lednicky J, Sordillo EM, Fowkes M. Central nervous system involvement by severe acute respiratory syndrome coronavirus-2 (SARS-CoV-2). J Med Virol. 2020 Jul;92(7):699-702. doi: 10.1002/jmv.259150
6. Kabbani N, Olds JL. Does COVID19 Infect the Brain? If So, Smokers Might Be at a Higher Risk. Mol Pharmacol. 2020 May;97(5):351-353. doi: 10.1124/molpharm.120.0000148
7. Nath A. Neurologic complications of coronavirus infections. Neurology. 2020 May 12;94(19):809-810. doi: 10.1212/WNL.0000000000009455

8. Baig AM. Chronic COVID syndrome: Need for an appropriate medical terminology for long-COVID and COVID long-haulers. J Med Virol. 2021 May;93(5):2555-2556. doi: 10.1002/jmv.26624
9. Li Y, Li M, Wang M, Zhou Y, Chang J, Xian Y, Wang D, Mao L, Jin H, Hu B. Acute cerebrovascular disease following COVID-19: a single center, retrospective, observational study. Stroke Vasc Neurol. 2020 Sep;5(3):279-284. doi: 10.1136/svn-2020-0004314
10. Mao L, Jin H, Wang M, Hu Y, Chen S, He Q, Chang J, Hong C, Zhou Y, Wang D, Miao X, Li Y, Hu B. Neurologic Manifestations of Hospitalized Patients With Coronavirus Disease 2019 in Wuhan, China. JAMA Neurol. 2020 Jun 1;77(6):683-690. doi: 10.1001/jamaneurol.2020.11278
11. Paterson RW, Brown RL, Benjamin L, Nortley R, Wiethoff S, Bharucha T, Jayaseelan DL, Kumar G, Raftopoulos RE, Zambreanu L, Vivekanandam V, Khoo A, Geraldes R, Chinthapalli K, Boyd E, Tuzlali H, Price G, Christofi G, Morrow J, McNamara P, McLoughlin B, Lim ST, Mehta PR, Levee V, Keddie S, Yong W, Trip SA, Foulkes AJM, Hotton G, Miller TD, Everitt AD, Carswell C, Davies NWS, Yoong M, Attwell D, Sreedharan J, Silber E, Schott JM, Chandratheva A, Perry RJ, Simister R, Checkley A, Longley N, Farmer SF, Carletti F, Houlihan C, Thom M, Lunn MP, Spillane J, Howard R, Vincent A, Werring DJ, Hoskote C, Jäger HR, Manji H, Zandi MS. The emerging spectrum of COVID-19 neurology: clinical, radiological and laboratory findings. Brain. 2020 Oct 1;143(10):3104-3120. doi: 10.1093/brain/awaa2407
12. Caress JB, Castoro RJ, Simmons Z, Scelsa SN, Lewis RA, Ahlawat A, Narayanaswami P. COVID-19-associated Guillain-Barré syndrome: The early pandemic experience. Muscle Nerve. 2020 Oct;62(4):485-491. doi: 10.1002/mus.270240
13. Keddie S, Pakpoor J, Mousele C, Pipis M, Machado PM, Foster M, Record CJ, Keh RYS, Fehmi J, Paterson RW, Bharambe V, Clayton LM, Allen C, Price O, Wall J, Kiss-Csenki A, Rathnasabapathi DP, Geraldes R, Yermakova T, King-Robson J, Zosmer M, Rajakulendran S, Sumaria S, Farmer SF, Nortley R, Marshall CR, Newman EJ, Nirmalananthan N, Kumar G, Pinto AA, Holt J, Lavin TM, Brennan KM, Zandi MS, Jayaseelan DL, Pritchard J, Hadden RDM, Manji H, Willison HJ, Rinaldi S, Carr AS, Lunn MP. Epidemiological and cohort study finds no association between COVID-19 and Guillain-Barré syndrome. Brain. 2021 Mar 3;144(2):682-693. doi: 10.1093/brain/awaa4339
14. Giacomelli A, Pezzati L, Conti F, Bernacchia D, Siano M, Oreni L, Rusconi S, Gervasoni C, Ridolfo AL, Rizzardini G, Antinori S, Galli M. Self-reported Olfactory and Taste Disorders in Patients With Severe Acute Respiratory Coronavirus 2 Infection: A Cross-sectional Study. Clin Infect Dis. 2020 Jul 28;71(15):889-890. doi: 10.1093/cid/ciaa3308
15. NIH study identifies features of Long COVID neurological symptoms. National Institutes of Health (NIH). 2023, May 5. https://www.nih.gov/news-events/news-releases/nih-study-identifies-features-long-covid-neurological-symptoms#:~:text=People%20with%20post%2Dacute%20sequelae,SARS%2DCoV%2D2%20infection
16. Zubair AS, McAlpine LS, Gardin T, Farhadian S, Kuruvilla DE, Spudich S. Neuropathogenesis and Neurologic Manifestations of the Coronaviruses in the Age of Coronavirus Disease 2019: A Review. JAMA Neurol. 2020 Aug 1;77(8):1018-1027. doi: 10.1001/jamaneurol.2020.20657
17. Sudre CH, Murray B, Varsavsky T, Graham MS, Penfold RS, Bowyer RC, Pujol JC, Klaser K, Antonelli M, Canas LS, Molteni E, Modat M, Jorge Cardoso M, May A, Ganesh S, Davies R, Nguyen LH, Drew DA, Astley CM, Joshi AD, Merino J, Tsereteli N, Fall T, Gomez MF, Duncan EL, Menni C, Williams FMK, Franks PW, Chan AT, Wolf J, Ourselin S, Spector T, Steves CJ. Attributes and predictors of long COVID. Nat Med. 2021 Apr;27(4):626-631. doi: 10.1038/s41591-021-01292-y
18. Heneka MT, Golenbock D, Latz E, Morgan D, Brown R. Immediate and long-term consequences of COVID-19 infections for the development of neurological disease. Alzheimers Res Ther. 2020 Jun 4;12(1):69. doi: 10.1186/s13195-020-00640-31
19. Taquet M, Geddes JR, Husain M, Luciano S, Harrison PJ. 6-month neurological and psychiatric outcomes in 236 379 survivors of COVID-19: a retrospective cohort study using electronic health records. Lancet Psychiatry. 2021 May;8(5):416-427. doi: 10.1016/S2215-0366(21)00084-58
20. Holder K, Reddy PH. The COVID-19 Effect on the Immune System and Mitochondrial Dynamics in Diabetes, Obesity, and Dementia. Neuroscientist. 2021 Aug;27(4):331-339. doi: 10.1177/1073858420960443
21. Schreiner P, Harrer T, Scheibenbogen C, Lamer S, Schlosser A, Naviaux RK, Prusty BK. Human Herpesvirus-6 Reactivation, Mitochondrial Fragmentation, and the Coordination of Antiviral and Metabolic Phenotypes in Myalgic Encephalomyelitis/Chronic Fatigue Syndrome. Immunohorizons. 2020 Apr 23;4(4):201-215. doi: 10.4049/immunohorizons.2000006
22. Roep BO. Molecular mimicry in autoimmune neurological disease after viral infection. Curr Med Chem. 2003 Oct;10(19):1939-43.
23. Baig AM, Khaleeq A, Ali U, Syeda H. Evidence of the COVID-19 Virus Targeting the CNS: Tissue Distribution, Host-Virus Interaction, and Proposed Neurotropic Mechanisms. ACS Chem Neurosci. 2020 Apr 1;11(7):995-998. doi: 10.1021/acschemneuro.0c00122
24. Wang Y, Liu S, Liu H, Li W, Lin F, Jiang L, Li X, Xu P, Zhang L, Zhao L, Cao Y, Kang J, Yang J, Li L, Liu X, Li Y, Nie R, Mu J, Lu F, Zhao S, Lu J, Zhao J. SARS-CoV-2 infection of the liver directly contributes to hepatic impairment in patients with COVID-19. J Hepatol. 2020 Oct;73(4):807-816. doi: 10.1016/j.jhep.2020.05.0020
25. Santos MO, Gonçalves LC, Silva PAN, Moreira ALE, Ito CRM, Peixoto FAO, Wastowski IJ, Carneiro LC, Avelino MAG. Multisystem inflammatory syndrome (MIS-C): a systematic review and meta-analysis of clinical characteristics, treatment, and outcomes. J Pediatr (Rio J). 2022 Jul-Aug;98(4):338-349. doi: 10.1016/j.jped.2021.08.0061
26. LaRovere KL, Riggs BJ, Poussaint TY, Young CC, Newhams MM, Maamari M, Walker TC, Singh AR, Dapul H, Hobbs CV, McLaughlin GE, Son MBF, Maddux AB, Clouser KN, Rowan CM, McGuire JK, Fitzgerald JC, Gertz SJ, Shein SL, Munoz AC, Thomas NJ, Irby K, Levy ER, Staat MA, Tenforde MW, Feldstein LR, Halasa NB, Giuliano JS Jr, Hall MW, Kong M, Carroll CL, Schuster JE, Doymaz S, Loftis LL, Tarquinio KM, Babbitt CJ, Nofziger RA, Kleinman LC, Keenaghan MA, Cvijanovich NZ, Spinella PC, Hume JR, Wellnitz K, Mack EH, Michelson KN, Flori HR, Patel MM, Randolph AG; Overcoming COVID-19 Investigators. Neurologic Involvement in Children and Adolescents Hospitalized in the United States for COVID-19 or Multisystem Inflammatory Syndrome. JAMA Neurol. 2021 May 1;78(5):536-547. doi: 10.1001/jamaneurol.2021.05049
27. Morand, A.; Urbina, D.; Fabre, A. COVID-19 and Kawasaki Like Disease: The Known-Known, the Unknown-Known and the Unknown-Unknown. Preprints 2020, 2020050160. doi: 10.20944/preprints202005.0160.v1
28. Nalbandian A, Sehgal K, Gupta A, Madhavan MV, McGroder C, Stevens JS, Cook JR, Nordvig AS, Shalev D, Sehrawat TS, Ahluwalia N, Bikdeli B, Dietz D, Der-Nigoghossian C, Liyanage-Don N, Rosner GF, Bernstein EJ, Mohan S, Beckley AA, Seres DS, Choueiri TK, Uriel N, Ausiello JC, Accili D, Freedberg DE, Baldwin M, Schwartz A, Brodie D, Garcia CK, Elkind MSV, Connors JM, Bilezikian JP, Landry DW, Wan EY. Post-acute COVID-19 syndrome. Nat Med. 2021 Apr;27(4):601-615. doi: 10.1038/s41591-021-01283-z7
29. Avittan H, Kustovs D. Cognition and Mental Health in Pediatric Patients Following COVID-19. Int J Environ Res Public Health. 2023 Mar 13;20(6):5061. doi: 10.3390/ijerph200650618
30. Sharma VK, Singh TG, Mehta V, Mannan A. Biomarkers: Role and Scope in Neurological Disorders. Neurochem Res. 2023 Jul;48(7):2029-2058. doi: 10.1007/s11064-023-03873-4
31. Kanberg N, Simrén J, Edén A, Andersson LM, Nilsson S, Ashton NJ, Sundvall PD, Nellgård B, Blennow K, Zetterberg H, Gisslén M. Neurochemical signs of astrocytic and neuronal injury in acute COVID-19 normalizes during long-term follow-up. EBioMedicine. 2021 Aug;70:103512. doi: 10.1016/j.ebiom.2021.1035128
32. Paterson RW, Benjamin LA, Mehta PR, Brown RL, Athauda

D, Ashton NJ, Leckey CA, Ziff OJ, Heaney J, Heslegrave AJ, Benedet AL, Blennow K, Checkley AM, Houlihan CF, Mummery CJ, Lunn MP, Manji H, Zandi MS, Keddie S, Chou M, Vinayan Changaradil D, Solomon T, Keshavan A, Barker S, Jäger HR, Carletti F, Simister R, Werring DJ, Spyer MJ, Nastouli E, Gauthier S, Rosa-Neto P; UCLH Queen Square COVID-19 Biomarker Study Group; Zetterberg H, Schott JM. Serum and cerebrospinal fluid biomarker profiles in acute SARS-CoV-2-associated neurological syndromes. Brain Commun. 2021 May 12;3(3):fcab099. doi: 10.1093/braincomms/fcab0999

33. Barbosa-Silva MC, Lima MN, Battaglini D, Robba C, Pelosi P, Rocco PRM, Maron-Gutierrez T. Infectious disease-associated encephalopathies. Crit Care. 2021 Jul 6;25(1):236. doi: 10.1186/s13054-021-03659-65
34. Kiani L. Preventing COVID-19 neurological complications. Nat Rev Neurol. 2022 Dec;18(12):699. doi: 10.1038/s41582-022-00744-42
35. Rolin S, Chakales A, Verduzco-Gutierrez M. Rehabilitation Strategies for Cognitive and Neuropsychiatric Manifestations of COVID-19. Curr Phys Med Rehabil Rep. 2022;10(3):182-187. doi: 10.1007/s40141-022-00352-97
36. Fotuhi M, Mian A, Meysami S, Raji CA. Neurobiology of COVID-19. J Alzheimers Dis. 2020;76(1):3-19. doi: 10.3233/JAD-2005817
37. Thankachen SS, Devasenapathy N, Bassi A, Ghosh A, Arfin S, Gummidi B, Basheer A, Bangi A, Sahu D, Bhalla A, Blesson M, Jain M, Jha V. Colchicine to reduce coronavirus disease-19-related inflammation and cardiovascular complications in high-risk patients post-acute infection with SARS-COV-2-a study protocol for a randomized controlled trial. Trials. 2024 Jun 12;25(1):378. doi: 10.1186/s13063-024-08205-76
38. Daniels K, Mourad J, Bonnechère B. Exploring the Use of Mobile Health for the Rehabilitation of Long COVID Patients: A Scoping Review. Healthcare (Basel). 2024 Feb 10;12(4):451. doi: 10.3390/healthcare120404516
39. D'Arcy RCN, Sandhu JK, Marshall S, Besemann M. Mitigating Long-Term COVID-19 Consequences on Brain Health. Front Neurol. 2021 Sep 27;12:630986. doi: 10.3389/fneur.2021.6309864
40. Frank MG, Ball JB, Hopkins S, Kelley T, Kuzma AJ, Thompson RS, Fleshner M, Maier SF. SARS-CoV-2 S1 subunit produces a protracted priming of the neuroinflammatory, physiological, and behavioral responses to a remote immune challenge: A role for corticosteroids. Brain Behav Immun. 2024 Oct;121:87-103. doi: 10.1016/j.bbi.2024.07.034

Review article

Ukr Neurosurg J. 2024;30(4):11-22
doi: 10.25305/unj.310442

Age-related aspects of glioma: current understanding. Literature review

Serhii P. Luhovskyi, Tetiana Y. Kvitnytska-Ryzhova

Laboratory of Morphology and Cytology, D.F. Chebotarev Institute of Gerontology of the National Academy of Medical Sciences of Ukraine, Kyiv, Ukraine

Received: 24 Augustl 2024
Accepted: 07 October 2024

Address for correspondence:
Serhii Pavlovych Luhovskyi, Laboratory of Morphology and Cytology, D.F. Chebotarev Institute of Gerontology, Vyshhorodska St., 67, Kyiv, 04114, Ukraine, e-mail: lugsp61@gmail.com

The updated 2021 WHO Classification of Central Nervous System (CNS) Tumors introduces, for the first time, an age-based approach to glioma classification, leveraging advances in molecular biology and epigenetics of CNS tumors. This classification groups gliomas within the category "Gliomas, glioneuronal tumors, and neuronal tumors," distinguishing between adult-type and pediatric-type diffuse gliomas, corresponding to low-grade and high-grade malignancies (LGG and HGG), highlighting the fundamental role of age in gliomagenesis. A review of current literature deepens the understanding of age-related characteristics, differences, and patterns in gliomagenesis across age groups, which is essential for effective diagnosis and treatment.

Pediatric-type and adult-type low-grade gliomas (pLGG and aLGG) differ in location, biological behavior, and molecular-genetic profiles. Inherited syndromes (e.g., NF-1, TSC) associated with glioma development are linked to specific LGG subtypes occurring in childhood, adolescence, and adulthood. Moreover, pLGG differs from aLGG in its potential for malignant transformation and spontaneous regression, as well as in mutations affecting the MAPK (mitogen-activated protein kinase) pathway.

While pediatric-type and adult-type high-grade gliomas (pHGG and aHGG) share histological features, they differ in location, biological behavior, molecular-genetic profiles, and prognosis. A major distinction between aHGG and pHGG lies in mutations such as *IDH 1/2*, *EGFR* gene expression, *TERT* mutations, chromosome alterations (+7/-10), and *TP53* mutations, all contributing to a poorer prognosis in HGG gliomas. Additionally, changes in histone proteins H3.3 or 3.1 (H3.3 K27 and H3 G34) in pHGG, as opposed to aHGG, carry diagnostic and prognostic significance.

An analysis of data on glioma epidemiology, risk factors, and characteristic molecular-genetic features considering age is provided. The next publication will cover certain clinical aspects of this issue.

Keywords: *glioma; age-related differences in gliomas; adult-type and pediatric-type gliomas; low-grade and high-grade gliomas*

Introduction

The diagnosis and treatment of gliomas—the most common tumors of the central nervous system (CNS)—represent a significant healthcare burden worldwide. In the United States alone, approximately 18,500 cases of malignant gliomas are diagnosed annually. Medical care for one patient, including surgical intervention and radiation therapy, costs between $50,600 and $92,700 USD per year [1]. Adding chemotherapy (temozolomide and bevacizumab) for glioblastoma (GBM) treatment further increases expenses, costing €20,587.53 and €5,581.49 per year per patient, respectively, for caregivers providing support [2]. Identifying causes and risk factors for glioma development enables the timely implementation of preventive measures to reduce incidence across different population groups—an approach that is more cost-effective than the expenses associated with treatment, rehabilitation, and patient care.

The literature increasingly emphasizes the relevance of age in gliomagenesis [3]. Glioma incidence rises significantly with age, particularly after 65 years [3-5]. *Low-grade gliomas* (LGG) are more common in children, while *high-grade gliomas* (HGG) are typically observed in adults.

In 2021, the WHO Classification of tumors of the central nervous system was updated. The primary distinction in this edition was the introduction of an age-based approach to glioma characterization [6-8]. This marks the sixth version of the international standard for CNS tumor classification, with previous editions published by WHO in 1979, 1993, 2000, 2007, and 2016.

Building on the 2016 WHO CNS Tumor Classification [8] and recommendations from the *Consortium to Inform Molecular and Practical Approaches to CNS Tumor Taxonomy* (cIMPACT-NOW) [9], a number of significant changes and additions have been made to the WHO Classification of brain and spinal cord tumors (2021) [6, 10]. Gliomas are now classified within the family "Gliomas, glioneuronal tumors, and neuronal tumors," with the following types: *circumscribed astrocytic gliomas*, *adult-type diffuse gliomas*, *pediatric-type diffuse low-grade gliomas* (pLGG), and *pediatric-type diffuse high-grade gliomas* (pHGG). The division of diffuse gliomas into adult- and pediatric-type categories underscores the important role of age, which may substantially influence gliomagenesis, biological behavior, molecular-genetic profiles, and prognosis, and should be considered in the diagnosis and treatment of gliomas across all age groups [6, 10-13].

Epidemiology of gliomas considering age and other factors

Recent large-scale clinico-epidemiological studies conducted in recent years indicate that the incidence, prevalence, and mortality rates of gliomas depend on factors such as age, gender, race, geographic region, and other variables [14].

Gliomas account for approximately 24.5% of all primary brain tumors and about 81% of all malignant central nervous system (CNS) tumors in adults [15]. About 62% of gliomas are located in the supratentorial region: 27.0% in the frontal lobe, 20.2% in the temporal lobe, 11.6% in the parietal lobe, and 2.8% in the occipital lobe. Tumor location influences the surgical approach. Gliomas may also be found in the brainstem (4.3%), cerebellum (2.8%), and other CNS areas (around 20.0%) [16]. The most common glioma is glioblastoma (GBM), accounting for 14.2% of all CNS tumors, 50.1% of all malignant CNS tumors, and approximately 45% of all gliomas, with a higher incidence among men (incidence rate ratio of 1.57) [17–19]. GBM is the most aggressive CNS tumor with a poor prognosis; the five-year relative *overall survival* (OS) rate is less than 5% [18].

Current reports, such as those from the *Central Brain Tumor Registry of the United States* (CBTRUS), provide data on glioma incidence, prevalence, and mortality derived from registries that classify glioma cases according to the 2007 and 2016 WHO CNS classifications. Thus, the tumor nomenclature, particularly for gliomas, differs from that in the 2021 WHO Classification of tumors of the brain and spinal cord [8,13,20]. The types of gliomas according to the WHO Classification of Brain and Spinal Cord Tumours (2021) are presented in a table ***(Table 1)***, facilitating a better understanding and assessment of studies conducted before the updated classification was adopted.

According to extensive epidemiological research by Q.T. Ostrom et al. [14, 16–19], astrocytic tumors, specifically GBM, represent 77.5% of all gliomas. Among malignant gliomas, other notable types include diffuse astrocytoma (7.3% of all gliomas), anaplastic astrocytoma – 6.8%, oligodendroglioma – 3.5%, anaplastic oligodendroglioma – 1,7%, pilocytic astrocytoma – 5.0%, and unspecified gliomas (NOS) - 7.9%.

The highest incidence of GBM among adults is 3.23 per 100,000 population, while rates for diffuse and anaplastic astrocytoma are 0.46 and 0.42 per 100,000, respectively. For oligodendroglioma and anaplastic oligodendroglioma, the rates are 0.23 and 0.11 per 100,000 [16,17,19]. The peak ages for diffuse astrocytoma and oligodendroglioma are at mean age of 46 and 43 years, respectively, while anaplastic astrocytoma and oligodendroglioma peak at ages 53 and 49. GBM is a prevalent tumor among adults, particularly the elderly (average age of 65), whereas GBM is rare in children [15].

In children, gliomas account for 45% of all malignant CNS tumors [21, 22]. Among pediatric gliomas, midline glioma ranks first, representing 31.1% of all childhood gliomas, while pilocytic astrocytoma accounts for 18.3%, diffuse and anaplastic astrocytoma for 5.3%, and glioblastoma multiforme (GBM) for 2%.

In the age group 0–19 years, the incidence of diffuse midline glioma is 0.31 per 100,000 population, while diffuse astrocytoma and GBM have incidences of 0.23 and 0.17 per 100,000 population, respectively [15]. Anaplastic astrocytoma, oligodendroglioma, and anaplastic oligodendroglioma are rare in this age group, with incidences of 0.09, 0.04, and 0.01 per 100,000 population, respectively.

The highest incidence rate of gliomas is registered in males (5.51 and 3.65 per 100,000 population, respectively), although females have a higher incidence of diffuse midline glioma—0.324 and 0.288 per 100,000 population, respectively [14, 15].

In the United States, malignant CNS tumors in children (aged 0–14 years) rank second in pediatric mortality rates, and in 2016 they were the leading cause of death among children [23,24]. The incidence rate of malignant CNS tumors in the pediatric population from 1998 to 2013 remained relatively stable, with an *annual percent change* (APC) of 0.16% per year (95% confidence interval (CI) 0.21–0.53). An increase in incidence was recorded for certain tumor types, including gliomas (APC 0.77% per year (95% CI 0.29–1.26)) and pilocytic astrocytoma (APC 0.89% per year (95% CI 0.21–0.53)), while a decrease in LGG gliomas (12.9% of all gliomas; APC -2.85 (95% CI 1.46–4.23)) and an increase in HGG gliomas (21.3% of all gliomas; APC -1.25 (95% CI 0.68–1.83)) and other gliomas (65.8% of all gliomas; APC -1.55 (95% CI 0.18–2.95)) were observed [15, 23]. These results are consistent with those reported by R. McKean-Cowdin et al. [25], obtained from 1973–2009, indicating that factors such as availability of specialized neurosurgical care, the quality of glioma diagnostics, and the accuracy and completeness of registry data on glioma cases influence these findings.

Epidemiological studies suggest regional variability in glioma incidence. It is hypothesized that the aging populations observed in recent decades in Europe and North America may partially explain the high glioma incidence, especially GBM, which increased on average by 2.9% per year from 1978 to 1992 [26–29]. The incidence of malignant gliomas increased from 1998 to

2008 among the elderly, while the CBTRUS registry data indicate relative stability among those aged ≥40 years from 2000 to 2016 [16, 20, 30].

Brainstem gliomas (BSG) represent a type of malignant CNS tumor that is rare in adults (1–2% of all gliomas) but common in children (20% of all gliomas) and has a poorer prognosis in children than in adults [31, 32]. The 5-year OS rates are 94.7% for pilocytic astrocytoma and 6.8% for GBM [14, 15, 26].

Table 1. Classification of gliomas according to the 2021 WHO Classification of tumors of the Brain and Spinal Cord

Type of glioma	WHO CNS Grade	Characteristic molecular and genetic alterations *
Circumscribed astrocytic gliomas		
Pilocytic astrocytoma	1	*KIAA1549-BRAF, BRAF, NF1*
High-grade astrocytoma with pi14locytic features	NS‡	*BRAF, NF1, ATRX, CDKN2A/B (methylome)*
Pleomorphic xanthoastrocytoma	2, 3	*BRAF, CDKN2A/B*
Subependymal giant cell astrocytoma	1	*TSC1, TSC2*
Chordoid glioma	2	*PRKCA*
Astroblastoma, MN1-altered	NS	*MN1*
Adult-type diffuse gliomas (aDG)		
Astrocytoma, IDH-mutant	2, 3, 4	*IDH1, IDH2, ATRX, TP53, CDKN2A/B*
Oligodendroglioma, IDH-mutant and 1p/19q codeleted	2, 3	*IDH1, IDH2, 1p/19q, TERT promoter, CIC, FUBP1, NOTCH1*
Glioblastoma, IDH wild-type	4	*IDH-wildtype, TERT promoter chromosomes 7/10, EGFR*
Pediatric low-grade diffuse gliomas (pLGG)		
Diffuse astrocytoma, MYB - or MYBL1 altered	1	*MYB, MYBL1*
Angiocentric glioma	1	*MYB*
Polymorphous low-grade neuroepithelial tumor of young	NS*	*BRAF, FGFR family*
Diffuse low-grade glioma, MAPK pathway-altered		*FGFR1, BRAF*
Pediatric high-grade diffuse gliomas (pHGG)		
Diffuse midline glioma, H3 K27-altered	4	*H3 K27, TP53 , ACVR1 , PDGFRA, EGFR, EZHIP*
Diffuse hemispheric glioma, H3 G34-mutant	4	*H3 G34, TP53 , ATRX*
Diffuse pediatric-type high-grade glioma, H3-wildtype and IDH-wild-type	4	*IDH- wild-type, H3- wild-type, PDGFRA, MYCN, EGFR (methylome)*
Infant-type hemispheric glioma	NS‡	*NTRK family, ALK, ROS, MET*

Notes: * - molecular and genetic changes, which are often common, are listed first. "methylome" is specified only for gliomas where it is recommended for diagnostic purposes. NS – not specified; NS * – not specified for LGG; not specified NS ‡ – not specified for HGG. Genes: BRAF – proto-oncogene B-Raf, serine/threonine kinase; KIAA1549-BRAF – gene fusion;NF1 – neurofibromin 1; ATRX – alpha-thalassemia/mental retardation syndrome, linked to the X chromosome; CDKN2A/B – cyclin-dependent kinase inhibitor; TSC1, TSC2 – tuberous sclerosis proteins 1 and 2; PRKCA – protein kinase C alpha; MN1 – proto-oncogene, transcription regulator; IDH – isocitrate dehydrogenase; TERT – telomerase reverse transcriptase; CIC – transcriptional repressor HMG-box; FUBP1 – oncogene; NOTCH1 – single-pass transmembrane receptor; NTRK – neurotrophic tyrosine receptor kinase gene family; EGFR – epidermal growth factor receptor; MYB – proto-oncogene, transcription factor; MYBL1 – MYB-like proto-oncogene 1; FGFR – fibroblast growth factor receptor; H3 – histones H3 K27 and H3 G34; ACVR1 – activin type I receptor; PDGFRA – platelet-derived growth factor receptor alpha; EZHIP – EZH inhibitory protein; TP53 – transcription factor p53; MYCN – proto-oncogene, transcription factor bHLH; ALK – anaplastic lymphoma receptor tyrosine kinase; ROS – proto-oncogene receptor tyrosine kinase; MET – proto-oncogene, receptor tyrosine kinase.

Risk factors (determinants) of gliomas

The risk factors, or determinants, for the development of gliomas are not yet fully defined, and data from the literature are contradictory. However, understanding these factors is useful for the prevention and early diagnosis of gliomas. Despite numerous publications on identifying glioma risk factors, only a few are considered proven, including genetic factors (hereditary disorders and syndromes) and ionizing radiation [14, 33-36].

Genetic (hereditary) disorders and syndromes. It is known that most gliomas occur without a burdensome family history, with only 5% of cases having such a history, and in 1% of cases, established hereditary disorders/syndromes are present in patients with glioma [14, 33]. Studies on the associations between genetic disorders and the risk of CNS tumors indicate that certain hereditary disorders are closely linked to glioma risk [14]. The most significant hereditary disorders and syndromes, their modes of inheritance, and chromosomal and genetic changes associated with glioma risk are presented in ***Table 2***. Among hereditary disorders, particular attention is given to Li-Fraumeni syndrome, caused by alterations in the *TP53* gene, which encodes the tumor suppressor protein P53; Turcot's syndrome type 1, which combines primary brain tumors with colorectal cancer; neurofibromatosis type 1; and tuberous sclerosis. These conditions are associated with the highest risk [14, 33-35].

Aging is associated with telomere shortening, while the risk of gliomas is linked to telomere lengthening [33, 36]. Shortened telomeres suppress cell proliferative activity, potentially inhibiting tumor development. In contrast, telomere lengthening is associated with high proliferative activity, which may increase the likelihood of somatic mutations, and thus, the risk of brain tumors, including gliomas (odds ratio (OR) = 1.16, 95% CI 1.02–1.31) [36]. The mean telomere length in glioma patients is 31 bp (5.7%) longer than in controls, and with each increase in telomere length septile, the glioma risk rises (OR = 1.12, 95% CI 0.90–1.62). It is known that *single nucleotide polymorphisms* (SNPs) in *TERC* and *TERT* alleles, which are associated with telomere length, may play a central role in gliomagenesis [33, 34, 36].

Ionizing Radiation is one of the most thoroughly studied and proven risk factors for gliomas in children, adolescents, and adults [34]. The International agency for research on cancer (IARC) classifies ionizing radiation as a Group 1 carcinogen [37]. In IARC's publication, studies involving large cohorts of children and adolescents (up to age 19) who received therapeutic radiation for medical reasons showed a twofold increase in glioma risk within nine years post-treatment. Glioma risk was found to have a linear dose-response relationship, with the highest risk per unit of absorbed dose (1 Gy) observed in children under five.

Non-Ionizing Radiation (NIR), which includes microwave radiation in the radiofrequency range and extremely low-frequency magnetic fields, has also been studied. The IARC has classified radiation within the 30–300 GHz range as a Group 2B possible human carcinogen [38]. Concerns about NIR's role in glioma development have risen in recent decades due to the widespread use of mobile (cellular) communication devices [14, 39-42]. Mobile phones are a common source of NIR, with 97-99% of absorbed energy impacting the brain hemispheres, and 50-60% affecting the temporal lobe and cerebellum. Despite numerous large clinical and epidemiological studies (INTERPHONE, CERENAT, COSMOS) conducted in recent decades, their results on glioma risk from NIR exposure remain inconclusive [39-44]. This issue is the subject of ongoing debate in the scientific community and is discussed in government and international institutions, especially with the active adoption of new 5G technologies [45, 46].

Table 2. Hereditary disorders and syndromes associated with glioma (adapted from [14]

Syndrome/disorder	Inheritance type	Gene alterations (chromosomes)
Li-Fraumeni syndrome (LFS)	Dominant	*TP53 (17p13.1)*
Turcot's syndrome Type 1 (ST1)	Autosomal recessive	*MLH1, PMS2*
Familial adenomatous polyposis, Turcot's syndrome Type 2 (ST2)	Dominant	*APC, MMR (5q21)*
Neurofibromatosis 1 (NF1)	Dominant	*NF1 (17q11.2)*
Tuberous sclerosis (TSC)	Dominant	*TSC1,TSC2 (9q34.14,16p13.3)*
Rubinstein-Taybi syndrome	Dominant	*CREBBP, EP30 (16p13.3; 22q13.2)*
Ollier disease	Acquired postzygotic mosaicism, dominant with reduced penetrance	*IDH1/IDH2 (2q33,3/15q26,1)*
Lynch syndrome	Dominant	*MSH2, MLH1, MSH6, PMS2*
Mismatch repair deficiency syndrome	Recessive	*MSH2, MLH1, MSH6, PMS2*
Retinoblastoma syndrome	Dominant	*RB1 (13q14)*
Melanoma-neural system tumor syndrome	Dominant	*CDKN2A (9p21.3)*
Ataxia-telangiectasia	Autosomal recessive	*ATM (11q22.3)*

Biological factors, including infectious disease agents such as Herpes Simplex Virus types 1 and 2 (HSV), Human Papillomavirus (HPV), Varicella-Zoster Virus (VZV), Cytomegalovirus (CMV), Epstein-Barr Virus (EBV), and others, are of interest to researchers not only for assessing glioma risk but also for exploring immunotherapy options through antiviral vaccines [47-50].

For many years, CMV infection was thought to be associated with gliomagenesis [47]. A meta-analysis [49] found that previous CMV infection increased the incidence of glioma (OR 3.95, 95% CI 1.7–5.3). However, the results of other studies have shown that individuals with a previous VZV-associated infection had a significantly reduced risk of LGG gliomas (HR 0.85, 95% CI 0.76-0.96) [51], and the risk of GBM was 30% lower compared with control group. This may be because VZV can trigger immune response reactions aimed at viral infections, which cross-react with GBM cell membrane proteins, thus generating an immune response against tumor cells [18]. The decrease in anti-VZV IgG levels in GBM compared with control group supports its protective role in gliomagenesis. A prospective study of the association between infections caused by HS, VZV, CMV, and EBV viruses and glioma risk indicate that EBV infection is associated with a lower risk of glioma development (OR = 0.57, 95% CI 0.38–0.85) [52]. There is no evidence of an increased risk of glioma in the presence of HPV infection [52, 53]. Consequently, there are no definitive conclusions about the causal relationship between viral infections and the risk of glioma development. The study of this issue is relevant because of the likelihood of distant consequences of infection due to the *SARS-COV-2* virus that caused the outbreak of the 2019 coronavirus disease pandemic (COVID-19) [54]. Upon entry into the body by respiratory route, *SARS-CoV-2* virus interacts with target cells and initiates a complex cascade of immune response reactions. At the same time, the tropism of SARS-CoV-2 virus to receptors on the surface of certain cell types can cause a high risk of severe course of the disease and its long-term consequences [55, 56].

It is known that the *SARS-CoV-2* S-glycoprotein can interact with receptor proteins on the surface of target cells, specifically with angiotensin-converting enzyme 2 (ACE2), which facilitates viral entry into cells [57]. This interaction plays a key role in the pathogenesis of COVID-19. The expression of ACE2 on the surface of glial cells and neurons characterizes them as potential targets for *SARS-CoV-2* [56]. Glioma cells express epidermal growth factor (EGFR), vascular endothelial growth factor (VEGFR), and hepatocyte growth factor (HGFR/c-MET) receptors, which are associated with tumor development and invasion [58]. ACE2 expression on cell surfaces enables the initiation of signaling pathways that play a central role in tumorigenesis. Recent studies have shown that the S glycoprotein of *SARS-CoV-2* has high affinity for the receptor proteins EGFR, VEGFR, and c-MET, which may indicate a potential role of COVID-19 in the development of gliomas [59, 60].

Age-related differences in low-grade gliomas

Gliomas represent about one-third of CNS tumors. In children and adolescents, two-thirds of gliomas are categorized as pediatric low-grade gliomas (pLGG). In adults and the elderly, aLGG gliomas are rare (15–20% of all gliomas) [63–65].

The research results by L. Greuter et al. [65] indicate that pLGG and aLGG gliomas have several age-related differences in terms of localization, malignancy grade, molecular-genetic status, potential for malignant transformation, association with hereditary pathology, prognosis, and so on, which are relevant for diagnosis, treatment, and prognosis ***(Table 3)***.

In children and adolescents, most gliomas are classified as diffuse Grade 1 gliomas according to the WHO Classification of Tumors of the Central Nervous System (2021), while in adults, most LGG gliomas are Grade 2 [66]. Most pLGG gliomas are located in the cerebellum, whereas in adults, they are typically found in the supratentorial region of the brain. pLGG gliomas are characterized by a more favorable prognosis compared to aLGG gliomas [65]. The majority of aLGG gliomas can undergo malignant transformation into HGG gliomas, whereas malignant transformation in pLGG gliomas is rare [67–69]. Approximately 6% of pLGG gliomas have the ability to spread to other areas of the CNS, while in adults, this capability is observed only in HGG gliomas [70, 71].

Hereditary syndromes, as noted above ***(see Table 2)***, are associated with the risk of LGG glioma development in both children and adults [14,15,35,65,72]. Specifically, NF-1 syndrome is associated with a risk of optic pathway glioma in 6% of patients aged 3–4 years and is characterized by a relatively benign course and favorable prognosis [73–75]. In 1% of NF-1 patients, brainstem glioma has been reported, often accompanied by hydrocephalus [76]. TSC is a multisystem autosomal dominant hamartoma syndrome caused by mutations in the TSC1 or TSC2 genes, which enhance the regulation of cell cycle signaling pathways and lead to the development of certain types of gliomas, primarily of astrocytic origin, with only a few cases reported in the literature [77]. These tumors mostly occur in children and young adults and are not found in adults.

Surgical intervention assessment indicates that *gross total resection* (GTR) of glioma correlates with increased overall survival (OS) and *progression-free survival* (PFS) in both children and adults. It is reported that *subtotal resection* (STR) with minimal residual tumor shows similar outcomes to GTR, although data on this are conflicting [65, 78].

Glioma localization is a factor that determines an unfavorable prognosis for pLGG located in the brainstem and for *optic pathway gliomas* (OPG), though not for OPG in patients with NF-1. Prognostic factors include STR, young age, and tumor location, particularly within the brainstem or optic pathway [14, 65, 79].

In adults with LGG glioma, the likelihood of a favorable GTR outcome increases if the tumor is detected without specific symptoms and at an early stage, as opposed to cases with pronounced glioma symptoms. According to AJ Gogos et al. [78], the average growth rate of such "incidental gliomas" is 3.9 cm^3/year. Gross total resection (GTR) is achieved in 57% of cases compared to 24% in patients with characteristic glioma symptoms. In cases with STR, the residual tumor volume averaged 2.9 cm^3, impacting glioma prognosis (OS for patients with

"incidental gliomas" is around 14.6 years) [78]. For aLGG, early GTR after tumor detection increases the likelihood of a favorable prognosis compared to delayed tumor resection, indicating the importance of GTR as a primary treatment method for both aLGG and pLGG gliomas. However, GTR is found to be more effective for pLGG gliomas than aLGG gliomas, likely due to differences in their morphology and biological behavior.

Molecular-genetic, diagnostic, and prognostic factors. Recent research on the molecular-genetic profile of pLGG gliomas has revealed changes in the MAPK/ERK pathway (*mitogen-activated protein kinase/ extracellular signal-regulated kinase*) caused by BRAF gene mutations or fusions, which are not characteristic of aLGG gliomas [80–83]. Alterations in the MAPK pathway are also typical for NF-1 syndrome, which predisposes to pLGG [83]. It is reported that 84% of pLGG gliomas are characterized by a mutation in the *BRAF* gene encoding the B-Raf protein (*B-Raf proto-oncogene, serine/threonine kinase*). The *KIAA1549-BRAF* fusion is common in pilocytic astrocytoma (35%), while *BRAFV600E* mutations and NF-1 are observed in only 17% of pLGG cases [81]. Molecular-genetic profiling of gliomas at the diagnostic stage is crucial for treatment and prognosis [11,13,82,83]. The *KIAA1549-BRAF* alteration is characteristic of cerebellar pLGG gliomas and is associated with significantly higher 5-year progression-free survival (PFS) compared to pLGG with a *BRAFV600E* mutation (69% vs. 52%) and 10-year overall survival (OS) (97% vs. 89%) [81]. Most pLGG gliomas typically exhibit at least one mutation impacting the MAPK pathway.

Age-specific features of malignant transformation (MT) in LGG are observed in only 2.9–6.7% of pLGG cases [65,85]. In children, MT is often associated with previous chemotherapy and/or radiotherapy. In contrast, MT occurs more frequently in adults (13–86% of all aLGG gliomas), especially in pregnant women, which may be associated with hemodynamic and metabolic changes due to elevated levels of progesterone and insulin-like growth factor-1 (IGF-1), which particularly correlates with astrocytoma development [85,86].

Spontaneous regression of pLGG has been documented as a phenomenon in certain types of pLGG gliomas, particularly in rare cases of cerebellar gliomas. Regression has been recorded in 30% of cerebellar pLGG gliomas on average 11.9 months after STR. Other studies report spontaneous regression in 32.5–48% of cerebellar pLGG glioma cases [65].

Thus, pLGG and aLGG gliomas differ in anatomical localization, biological behavior, and molecular-genetic profiles, which is essential for the diagnosis, treatment, and prognosis of LGG gliomas in children and adults. Hereditary syndromes, such as NF-1 or TSC, are associated with specific types of pLGG gliomas that arise in childhood.

Table 3. Differences between pediatric and adult low-grade gliomas (adapted from [65]

Indicator	pLGG	aLGG
Localization	Supratentorial (30%) Infratentorial (30%)	Supratentorial (80%)
Histological grading	Grade 1* (74%) Grade 2* (26%) Pilocytic astrocytoma (65%)	Grade 1* (10–15%) Grade 2* (85–90%) Diffuse glioma LGG (60%)
Associated hereditary disorders	NF-1 (TSC)	-
Molecular alterations	*BRAF600 (17%)*	*IDH-mutant (70%)*
Treatment	GTR increases OS	GTR increases OS
Malignant transformation	Rare (2.9–6.7%), may increase post-CT or RT	Frequent (86%)
10-Year OS, %	>90	~60
Prognosis	OPG and brainstem glioma – unfavorable; OPG with NF-1 – favorable; GTR – favorable; young age – unfavorable	Gliomas (typical sites) – unfavorable; GTR – favorable; Diffuse Grade 1 gliomas* – unfavorable; age <40 – favorable

*Note.** – according to the WHO Classification of Tumors of the brain and spinal cord tumors (2021); NF-1 – neurofibromatosis type 1; TSC – tuberous sclerosis; BRAF600 – B-Raf proto-oncogene serine/ threonine kinase; IDH – isocitrate dehydrogenase gene; OPG – optic pathway glioma; GTR – gross total resection; CT – chemotherapy; RT – radiotherapy.

Age-related differences in high-grade gliomas

According to the WHO Classification of Tumors of the Central Nervous System (2021), HGG gliomas include circumscribed WHO CNS grade 3 gliomas, as well as diffuse adult-type WHO CNS Grade 3 and 4 gliomas (*IDH*-mutant astrocytoma, *IDH*-mutant oligodendroglioma with 1p/19q codeletion, *IDH*-wild-type glioblastoma) and all pediatric-type diffuse HGG gliomas ***(Table 1)***.

Age-related differences in glioma localization. In adults, *IDH*-mutant astrocytoma can occur in any part of the brain, most commonly in the subtentorial region and frontal lobe. The average age of patients with this type of glioma is 30–40 years, rarely over 55 years [87,88]. The average age for patients with WHO CNS Grade 4 *IDH*-mutant astrocytoma is 42 years, while for Grade 2-3 it is 38 years. *IDH*-mutant oligodendroglioma with 1p/19q codeletion is most often observed in patients aged 40–50 years and is very rarely seen in children. Most tumors are located in the frontal lobe, less frequently in the temporal or parietal lobes, and very rarely in the brainstem [88]. *IDH*-wild-type GBM, which is also characterized by EGFR amplification and/or *telomerase reverse transcriptase* (TERT) promoter mutation and/or chromosomal alterations (+7/–10), accounts for half of all malignant brain tumors in adults and elderly individuals, with 10,000 new cases reported annually [89]. GBM develops between 18 and 89 years, most frequently (58%) between 50 and 69 years [88, 90, 91]. Comorbidities in older individuals result in a poorer prognosis for glioma compared to younger patients, due to limitations in standard glioma treatments caused by concurrent diseases.

In children and adolescents, diffuse HGG gliomas account for 3 to 15% of primary CNS tumors, with pHGG patient OS averaging 10–73 months [89,92]. Diffuse midline glioma, H3K27-altered, develops in individuals aged 2 to 65 years, with a median age of 11–14 years. Its pathognomonic feature is localization in the brainstem, thalamus, hypothalamus, as well as the cerebellum and spinal cord. The median age for brainstem glioma is 7 years, for thalamic glioma 24 years, and for spinal cord glioma 25 years. The prognosis for this glioma is poor, with an OS of 1 year [92].

Diffuse hemispheric glioma, H3G34-mutant, is most common between ages 15 and 19, and according to some studies, between 18 and 26 years. The prognosis for this glioma is generally poor (OS from 12 to 36 months) [92, 93].

H3-wild-type and *IDH-wild-type pHGG* gliomas are usually located in the brain hemispheres and rarely in other brain regions. These gliomas are often detected in early childhood but can also occur in adolescence and early adulthood. The prognosis for such gliomas is unfavorable (OS of 22 months) [90, 92, 93].

Molecular-genetic, diagnostic, and prognostic factors in aHGG and pHGG gliomas. Among HGG gliomas, diffuse gliomas are the most common. Although there are practically no histological differences between diffuse aHGG and pHGG gliomas, they differ in biological behavior, molecular-genetic characteristics, treatment response, and prognosis [92, 94, 95]. The defining differences between diffuse aHGG and pHGG gliomas, as reflected in the WHO Classification of CNS Tumors (2021), are molecular-genetic characteristics ***(Table 4)***.

Table 4. Age-related differences in the molecular-genetic profile of diffuse high-grade gliomas [92]

Molecular and genetic alterations	pHGG	aHGG	Implications
IDH1 Mutation	In 16.3–35.0% of cases in children over 14 years old	~50% of primary HGG gliomas	Astrocytoma, IDH-mutant
EGFR Expression	In approximately 80% of cases	Amplification and overexpression in 27–60% of cases	Grade 4 glioma*
TERT Promoter mutations	Rarely	In 40–70% of cases	Grade 4 glioma*
Chromosomal alterations +7/–10	NS	У 50–70% випадків	Grade 4 glioma*
TP53 Mutation	In 33–58% of pediatric cases	In 30–60% of GBM cases	p53 – tumor suppressor
Loss or Mutation of PTEN	In 0–20% of cases	In 27–60% of cases	Alterations in the PI3K/AKT/mTOR signaling pathway
H3 K27- mutant	In 60–80% of cases	NS	Pediatric diffuse midline glioma, Grade 4*
H3 G34- mutant	In approximately 20% of cases	NS	Pediatric diffuse hemispheric glioma, Grade 4*

Note. * Based on the WHO Classification of Tumors of the Central Nervous System (2021); EGFR – epidermal growth factor receptor gene; TERT – telomerase reverse transcriptase promoter gene; TP53 – p53 tumor suppressor gene; PTEN – phosphatase and tensin homolog gene; IDH – isocitrate dehydrogenase gene; H3 K27 and H3 G34 – histone H3 proteins; Not specified – NS.

The key difference between aHGG and pHGG is the *IDH 1/2* gene mutations, which have diagnostic and prognostic significance, since *IDH* mutation in HGG gliomas determines a significantly better prognosis for adult and paediatric gliomas compared with *IDH*-wild-type gliomas [7,13,93,96]. Astrocytoma, *IDH*-mutant with homozygous deletion of *CDK2A/B*, is classified as a WHO CNS Grade 4 glioma with a poor prognosis ***(see Table 1)***. For gliomas, *IDH*-wild type, the presence of mutations such as *EGFR* amplification, *TERT* promoter mutations and chromosome +7/-10 alterations are a factor of unfavourable prognosis for patients ***(see Table 4)***.

EGFR amplification affects the tyrosine kinase receptor involved in cell proliferation and differentiation, as well as malignant growth processes. It is observed in 60% of GBM cases in adults, while it is rare in pHGG diffuse gliomas [92, 97, 98, 99].

Among other genes that cause age-related differences in gliomas, the *phosphatase and tensin homologue* (*PTEN*) suppressor gene, which is able to inhibit tumour invasion and blood vessel formation, occupies an important place. Its mutations are frequently reported in aHGG and rarely in pHGG. The *TP53* gene is also a tumour suppressor gene with alterations in the majority of adult GBM cases [96, 99].

In the case of pHGG gliomas, in contrast to aHGG gliomas, alterations in histone proteins, particularly H3, are important for diagnosis and prognosis. Thus, diffuse medial glioma of pHGG is characterised by K27M mutation in histones H3.3 or H3.1. Diffuse hemispheric gliomas of pHGG are characterised by the presence of H3 G34R or H3 G34V mutation. pHGG gliomas with histone mutations usually have a poor prognosis and significantly lower OS compared to diffuse H3-wild-type and *IDH*-wild-type gliomas [98, 100-101]. In diffuse pHGG gliomas, TP53 mutations are often found together with H3 mutations. Therefore, histone mutation status may play a key role in gliomagenesis, especially in children, adolescents, and young adults, which is important for diagnosis, selection of adequate treatment methods, and prognosis of diffuse gliomas of pHGG.

Amplification of the platelet-derived growth factor receptor A (*PDGFRA*) gene in diffuse H3G34-mutant hemispheric gliomas is associated with an unfavorable prognosis, while O6-methylguanine DNA methyltransferase MGMT-methylation is associated with a more favorable prognosis, including increased survival. Specific molecular-genetic alterations in H3 wild-type and *IDH* wild-type diffuse pHGG gliomas also significantly impact prognosis. For example, the OS of patients with gliomas showing *MYCN* amplification averages 14 months, with *PDGFRA* amplification – 21 months, and with *TERT* or *EGFR* mutation 44 months [92, 96].

Conclusions

1. In light of recent research findings, the 2016 WHO Classification of Tumors of the Central Nervous System has been revised, and in 2021, an updated version was approved. According to this new classification, gliomas are grouped within the "Gliomas, glioneuronal, and neuronal tumors" family, divided into the following types: circumscribed astrocytic gliomas, adult-type diffuse gliomas, pediatric-type low-grade diffuse gliomas, and pediatric-type high-grade diffuse gliomas. The distinction of gliomas into adult and pediatric types, which share similar histological characteristics but differ substantially in biological behavior, molecular-genetic profile, and prognosis, emphasizes the significant role of age in influencing gliomagenesis. This must be considered in both diagnosis and treatment of gliomas.

2. Analysis of the current literature on the theoretical and applied aspects of gliomas—the most common CNS tumor types—provides an opportunity to deepen understanding of the age-related features, differences, and patterns of gliomagenesis across all age groups affected by gliomas. Additionally, this analysis highlights distinct and shared characteristics of gliomas in adults and children, which can enhance prevention measures, improve diagnostics, treatment, and prognostication for patients of various ages.

3. Pediatric- and adult-type low-grade gliomas differ in anatomical location, biological behavior, and molecular-genetic profile, which has crucial implications for diagnosis, treatment, and prognosis. Hereditary syndromes associated with glioma development (NF-1, TSC) are linked to specific low-grade glioma types that can arise in childhood, adolescence, and adulthood. In contrast to aLGG, pLGG is characterized by the presence of at least one mutation affecting the MAPK pathway. Furthermore, pLGGs differ from aLGGs in their potential for malignant transformation and spontaneous regression.

4. Pediatric- and adult-type high-grade gliomas share similar histological characteristics but differ in location, biological behavior, molecular-genetic changes, and prognosis, which should be considered in diagnosis and treatment. The primary difference between aHGG and pHGG lies in *IDH 1/2* gene mutations, as well as *EGFR* gene expression, *TERT* promoter mutations, chromosomal changes (+7/−10), and *TP53* gene mutations, all of which are often associated with a poor prognosis in glioma patients. In contrast to aHGG, pHGG diagnostics and prognostics rely on changes in histone proteins H3.3 or H3.1 (H3.3 K27 and H3 G34).

Disclosure

Conflict of Interest

The authors declare no conflict of interest.

Funding

The study received no sponsorship.

References

1. Raizer JJ, Fitzner KA, Jacobs DI, Bennett CL, Liebling DB, Luu TH, Trifilio SM, Grimm SA, Fisher MJ, Haleem MS, Ray PS, McKoy JM, DeBoer R, Tulas KM, Deeb M, McKoy JM. Economics of Malignant Gliomas: A Critical Review. J Oncol Pract. 2015 Jan;11(1):e59-65. doi: 10.1200/JOP.2012.000560
2. Boele FW, Meads D, Jansen F, Verdonck-de Leeuw IM, Heimans JJ, Reijneveld JC, Short SC, Klein M. Healthcare utilization and productivity loss in glioma patients and family caregivers: the impact of treatable psychological symptoms. J Neurooncol. 2020 Apr;147(2):485-494. doi: 10.1007/s11060-020-03454-3
3. Zozulya YuA, red. Gliomy golovnogo mozga (sovremennoe sostoyanie problemyi i puti dalneyshih poiskov). K.: UIPK «EksOb»; 2007. Russian.
4. Li K, Lu D, Guo Y, Wang C, Liu X, Liu Y, Liu D. Trends and patterns of incidence of diffuse glioma in adults in the United States, 1973-2014. Cancer Med. 2018 Oct;7(10):5281-5290.

doi: 10.1002/cam4.1757
5. Grochans S, Cybulska AM, Simińska D, Korbecki J, Kojder K, Chlubek D, Baranowska-Bosiacka I. Epidemiology of Glioblastoma Multiforme-Literature Review. Cancers (Basel). 2022 May 13;14(10):2412. doi: 10.3390/cancers14102412
6. Louis DN, Perry A, Wesseling P, Brat DJ, Cree IA, Figarella-Branger D, Hawkins C, Ng HK, Pfister SM, Reifenberger G, Soffietti R, von Deimling A, Ellison DW. The 2021 WHO Classification of Tumors of the Central Nervous System: a summary. Neuro Oncol. 2021 Aug 2;23(8):1231-1251. doi: 10.1093/neuonc/noab106
7. Gianno F, Giovannoni I, Cafferata B, Diomedi-Camassei F, Minasi S, Barresi S, Buttarelli FR, Alesi V, Cardoni A, Antonelli M, Puggioni C, Colafati GS, Carai A, Vinci M, Mastronuzzi A, Miele E, Alaggio R, Giangaspero F, Rossi S. Paediatric-type diffuse high-grade gliomas in the 5th CNS WHO Classification. Pathologica. 2022 Dec;114(6):422-435. doi: 10.32074/1591-951X-830
8. Louis DN, Perry A, Reifenberger G, von Deimling A, Figarella-Branger D, Cavenee WK, Ohgaki H, Wiestler OD, Kleihues P, Ellison DW. The 2016 World Health Organization Classification of Tumors of the Central Nervous System: a summary. Acta Neuropathol. 2016 Jun;131(6):803-20. doi: 10.1007/s00401-016-1545-1
9. Louis DN, Aldape K, Brat DJ, Capper D, Ellison DW, Hawkins C, Paulus W, Perry A, Reifenberger G, Figarella-Branger D, Wesseling P, Batchelor TT, Cairncross JG, Pfister SM, Rutkowski S, Weller M, Wick W, von Deimling A. Announcing cIMPACT-NOW: the Consortium to Inform Molecular and Practical Approaches to CNS Tumor Taxonomy. Acta Neuropathol. 2017 Jan;133(1):1-3. doi: 10.1007/s00401-016-1646-x
10. Thomas DL. 2021 updates to the World Health Organization classification of adult-type and pediatric-type diffuse gliomas: a clinical practice review. Chin Clin Oncol. 2023 Feb;12(1):7. doi: 10.21037/cco-22-120
11. Pfister SM, Reyes-Múgica M, Chan JKC, Hasle H, Lazar AJ, Rossi S, Ferrari A, Jarzembowski JA, Pritchard-Jones K, Hill DA, Jacques TS, Wesseling P, López Terrada DH, von Deimling A, Kratz CP, Cree IA, Alaggio R. A Summary of the Inaugural WHO Classification of Pediatric Tumors: Transitioning from the Optical into the Molecular Era. Cancer Discov. 2022 Feb;12(2):331-355. doi: 10.1158/2159-8290.CD-21-1094
12. Wen PY, Packer RJ. The 2021 WHO Classification of Tumors of the Central Nervous System: clinical implications. Neuro Oncol. 2021 Aug 2;23(8):1215-1217. doi: 10.1093/neuonc/noab120
13. Torp SH, Solheim O, Skjulsvik AJ. The WHO 2021 Classification of Central Nervous System tumours: a practical update on what neurosurgeons need to know-a minireview. Acta Neurochir (Wien). 2022 Sep;164(9):2453-2464. doi: 10.1007/s00701-022-05301-y
14. Ostrom QT, Adel Fahmideh M, Cote DJ, Muskens IS, Schraw JM, Scheurer ME, Bondy ML. Risk factors for childhood and adult primary brain tumors. Neuro Oncol. 2019 Nov 4;21(11):1357-1375. doi: 10.1093/neuonc/noz123
15. Pellerino A, Caccese M, Padovan M, Cerretti G, Lombardi G. Epidemiology, risk factors, and prognostic factors of gliomas. Clin Transl Imaging. 2022; 10: 467–475. doi: 10.1007/s40336-022-00489-6
16. Ostrom QT, Patil N, Cioffi G, Waite K, Kruchko C, Barnholtz-Sloan JS. CBTRUS Statistical Report: Primary Brain and Other Central Nervous System Tumors Diagnosed in the United States in 2013-2017. Neuro Oncol. 2020 Oct 30;22(12 Suppl 2):iv1-iv96. doi: 10.1093/neuonc/noaa200
17. Ostrom QT, Gittleman H, Farah P, Ondracek A, Chen Y, Wolinsky Y, Stroup NE, Kruchko C, Barnholtz-Sloan JS. CBTRUS statistical report: Primary brain and central nervous system tumors diagnosed in the United States in 2006-2010. Neuro Oncol. 2013 Nov;15 Suppl 2(Suppl 2):ii1-56. doi: 10.1093/neuonc/not151
18. Ostrom QT, Bauchet L, Davis FG, Deltour I, Fisher JL, Langer CE, Pekmezci M, Schwartzbaum JA, Turner MC, Walsh KM, Wrensch MR, Barnholtz-Sloan JS. The epidemiology of glioma in adults: a "state of the science" review. Neuro Oncol. 2014 Jul;16(7):896-913. doi: 10.1093/neuonc/nou087
19. Ostrom QT, Price M, Neff C, Cioffi G, Waite KA, Kruchko C, Barnholtz-Sloan JS. CBTRUS Statistical Report: Primary Brain and Other Central Nervous System Tumors Diagnosed in the United States in 2015-2019. Neuro Oncol. 2022 Oct 5;24(Suppl 5):v1-v95. doi: 10.1093/neuonc/noac202
20. Louis DN, Ohgaki H, Wiestler OD, Cavenee WK, Burger PC, Jouvet A, Scheithauer BW, Kleihues P. The 2007 WHO classification of tumours of the central nervous system. Acta Neuropathol. 2007 Aug;114(2):97-109. doi: 10.1007/s00401-007-0243-4
21. Hoffman LM, Veldhuijzen van Zanten SEM, Colditz N, Baugh J, Chaney B, Hoffmann M, Lane A, Fuller C, Miles L, Hawkins C, Bartels U, Bouffet E, Goldman S, Leary S, Foreman NK, Packer R, Warren KE, Broniscer A, Kieran MW, Minturn J, Comito M, Broxson E, Shih CS, Khatua S, Chintagumpala M, Carret AS, Escorza NY, Hassall T, Ziegler DS, Gottardo N, Dholaria H, Doughman R, Benesch M, Drissi R, Nazarian J, Jabado N, Boddaert N, Varlet P, Giraud G, Castel D, Puget S, Jones C, Hulleman E, Modena P, Giagnacovo M, Antonelli M, Pietsch T, Gielen GH, Jones DTW, Sturm D, Pfister SM, Gerber NU, Grotzer MA, Pfaff E, von Bueren AO, Hargrave D, Solanki GA, Jadrijevic Cvrlje F, Kaspers GJL, Vandertop WP, Grill J, Bailey S, Biassoni V, Massimino M, Calmon R, Sanchez E, Bison B, Warmuth-Metz M, Leach J, Jones B, van Vuurden DG, Kramm CM, Fouladi M. Clinical, Radiologic, Pathologic, and Molecular Characteristics of Long-Term Survivors of Diffuse Intrinsic Pontine Glioma (DIPG): A Collaborative Report From the International and European Society for Pediatric Oncology DIPG Registries. J Clin Oncol. 2018 Jul 1;36(19):1963-1972. doi: 10.1200/JCO.2017.75.9308
22. Patil N, Kelly ME, Yeboa DN, Buerki RA, Cioffi G, Balaji S, Ostrom QT, Kruchko C, Barnholtz-Sloan JS. Epidemiology of brainstem high-grade gliomas in children and adolescents in the United States, 2000-2017. Neuro Oncol. 2021 Jun 1;23(6):990-998. doi: 10.1093/neuonc/noaa295
23. Siegel RL, Miller KD, Jemal A. Cancer statistics, 2016. CA Cancer J Clin. 2016 Jan-Feb;66(1):7-30. doi: 10.3322/caac.21332
24. Siegel RL, Miller KD, Jemal A. Cancer Statistics, 2017. CA Cancer J Clin. 2017 Jan;67(1):7-30. doi: 10.3322/caac.21387
25. McKean-Cowdin R, Razavi P, Barrington-Trimis J, Baldwin RT, Asgharzadeh S, Cockburn M, Tihan T, Preston-Martin S. Trends in childhood brain tumor incidence, 1973-2009. J Neurooncol. 2013 Nov;115(2):153-60. doi: 10.1007/s11060-013-1212-5
26. Leece R, Xu J, Ostrom QT, Chen Y, Kruchko C, Barnholtz-Sloan JS. Global incidence of malignant brain and other central nervous system tumors by histology, 2003-2007. Neuro Oncol. 2017 Oct 19;19(11):1553-1564. doi: 10.1093/neuonc/nox091
27. Girardi F, Matz M, Stiller C, You H, Marcos Gragera R, Valkov MY, Bulliard JL, De P, Morrison D, Wanner M, O'Brian DK, Saint-Jacques N, Coleman MP, Allemani C; CONCORD Working Group. Global survival trends for brain tumors, by histology: analysis of individual records for 556,237 adults diagnosed in 59 countries during 2000-2014 (CONCORD-3). Neuro Oncol. 2023 Mar 14;25(3):580-592. doi: 10.1093/neuonc/noac217
28. Ratnapradipa KL, Yellala A, Shonka N. Exploratory analysis of the spatial distribution of adult glioma age-adjusted county incidence rates, Nebraska Medicine, 2009-2019. Neurooncol Pract. 2023 Aug 25;11(1):64-68. doi: 10.1093/nop/npad050
29. Lin D, Wang M, Chen Y, Gong J, Chen L, Shi X, Lan F, Chen Z, Xiong T, Sun H, Wan S. Trends in Intracranial Glioma Incidence and Mortality in the United States, 1975-2018. Front Oncol. 2021 Nov 1;11:748061. doi: 10.3389/fonc.2021.748061
30. Ostrom QT, Egan KM, Nabors LB, Gerke T, Thompson RC, Olson JJ, LaRocca R, Chowdhary S, Eckel-Passow JE, Armstrong G, Wiencke JK, Bernstein JL, Claus EB, Il'yasova D, Johansen C, Lachance DH, Lai RK, Merrell RT, Olson SH, Sadetzki S, Schildkraut JM, Shete S, Houlston RS, Jenkins RB, Wrensch MR, Melin B, Amos CI, Huse JT, Barnholtz-Sloan JS, Bondy ML. Glioma risk associated with extent of

estimated European genetic ancestry in African Americans and Hispanics. Int J Cancer. 2020 Feb 1;146(3):739-748. doi: 10.1002/ijc.32318
31. Li S, Zhao Y, Huang H. Clinical characteristics and prognostic factors of adult brainstem gliomas: A retrospective analysis of histologically-proven 40 cases. Medicine (Baltimore). 2024 May 3;103(18):e37910. doi: 10.1097/MD.0000000000037910
32. Khalid SI, Kelly R, Adogwa O, Carlton A, Tam E, Naqvi S, Kushkuley J, Ahmad S, Woodward J, Khanna R, Davison M, Munoz L, Byrne R. Pediatric Brainstem Gliomas: A Retrospective Study of 180 Patients from the SEER Database. Pediatr Neurosurg. 2019;54(3):151-164. doi: 10.1159/000497440
33. Howell AE, Zheng J, Haycock PC, McAleenan A, Relton C, Martin RM, Kurian KM. Use of Mendelian Randomization for Identifying Risk Factors for Brain Tumors. Front Genet. 2018 Nov 12;9:525. doi: 10.3389/fgene.2018.00525
34. Sioutas G, Nikova A, Birbilis T. Risk factors for pediatric glioma. Folia Med (Plovdiv). 2022 Aug 31;64(4):566-571. doi: 10.3897/folmed..e64431
35. Malbari F, Lindsay H. Genetics of Common Pediatric Brain Tumors. Pediatr Neurol. 2020 Mar;104:3-12. doi: 10.1016/j.pediatrneurol.2019.08.004
36. Andersson U, Degerman S, Dahlin AM, Wibom C, Johansson G, Bondy ML, Melin BS. The association between longer relative leukocyte telomere length and risk of glioma is independent of the potentially confounding factors allergy, BMI, and smoking. Cancer Causes Control. 2019 Feb;30(2):177-185. doi: 10.1007/s10552-018-1120-2
37. IARC. Working Group on the Evaluation of Carcinogenic Risks to Humans. Radiation. Lyon (FR): International Agency for Research on Cancer; 2012. (IARC Monographs on the Evaluation of Carcinogenic Risks to Humans, No. 100D.) https://www.ncbi.nlm.nih.gov/books/NBK304362/
38. IARC Working Group on the Evaluation of Carcinogenic Risks to Humans. Non-Ionizing Radiation, Part 2: Radiofrequency Electromagnetic Fields. Lyon (FR): International Agency for Research on Cancer; 2013. (IARC Monographs on the Evaluation of Carcinogenic Risks to Humans, No. 102.) https://www.ncbi.nlm.nih.gov/books/NBK304630/
39. Hardell L, Carlberg M. Mobile phones, cordless phones and rates of brain tumors in different age groups in the Swedish National Inpatient Register and the Swedish Cancer Register during 1998-2015. PLoS One. 2017 Oct 4;12(10):e0185461. doi: 10.1371/journal.pone.0185461
40. Elwood JM, Win SS, Aye PS, Sanagou M. Trends in brain cancers (glioma) in New Zealand from 1995 to 2020, with reference to mobile phone use. Cancer Epidemiol. 2022 Oct;80:102234. doi: 10.1016/j.canep.2022.102234
41. Uddin M, Dhanta R, Pitti T, Barsasella D, Scholl J, Jian WS, Li YJ, Hsu MH, Syed-Abdul S. Incidence and Mortality of Malignant Brain Tumors after 20 Years of Mobile Use. Cancers (Basel). 2023 Jul 4;15(13):3492. doi: 10.3390/cancers15133492
42. Feychting M, Schüz J, Toledano MB, Vermeulen R, Auvinen A, Harbo Poulsen A, Deltour I, Smith RB, Heller J, Kromhout H, Huss A, Johansen C, Tettamanti G, Elliott P. Mobile phone use and brain tumour risk - COSMOS, a prospective cohort study. Environ Int. 2024 Mar;185:108552. doi: 10.1016/j.envint.2024.108552
43. Brzozek C, Abramson MJ, Benke G, Karipidis K. Comment on Choi et al. Cellular Phone Use and Risk of Tumors: Systematic Review and Meta-Analysis. Int. J. Environ. Res. Public Health 2020, 17, 8079. Int J Environ Res Public Health. 2021 May 20;18(10):5459. doi: 10.3390/ijerph18105459
44. Moskowitz JM, Frank JW, Melnick RL, Hardell L, Belyaev I, Héroux P, Kelley E, Lai H, Maisch D, Mallery-Blythe E, Philips A; International Commission on the Biological Effects of Electromagnetic Fields. COSMOS: A methodologically-flawed cohort study of the health effects from exposure to radiofrequency radiation from mobile phone use. Environ Int. 2024 Aug;190:108807. doi: 10.1016/j.envint.2024.108807
45. Feychting M, Schüz J, Toledano MB, Vermeulen R, Auvinen A, Harbo Poulsen A, Deltour I, Smith RB, Heller J, Kromhout H, Huss A, Johansen C, Tettamanti G, Elliott P. Response to the letter to the editor regarding "Mobile phone use and brain tumour risk - COSMOS, a prospective cohort study". Environ Int. 2024 Jul;189:108808. doi: 10.1016/j.envint.2024.108808
46. Nyberg R, McCredden J, Hardell L. The European Union assessments of radiofrequency radiation health risks - another hard nut to crack (Review). Rev Environ Health. 2023 Aug 23. doi: 10.1515/reveh-2023-0046
47. Dziurzynski K, Chang SM, Heimberger AB, Kalejta RF, McGregor Dallas SR, Smit M, Soroceanu L, Cobbs CS; HCMV and Gliomas Symposium. Consensus on the role of human cytomegalovirus in glioblastoma. Neuro Oncol. 2012 Mar;14(3):246-55. doi: 10.1093/neuonc/nor227
48. Duinkerken S, van Kooyk Y, Garcia-Vallejo JJ. Human cytomegalovirus-based immunotherapy to treat glioblastoma: Into the future. Oncoimmunology. 2016 Jul 25;5(9):e1214791. doi: 10.1080/2162402X.2016.1214791
49. Cai Z, Yang S, Li X, Chen F, Li W. Viral infection and glioma: a meta-analysis of prognosis. BMC Cancer. 2020 Jun 12;20(1):549. doi: 10.1186/s12885-020-06796-3
50. Cuoco JA, Benko MJ, Busch CM, Rogers CM, Prickett JT, Marvin EA. Vaccine-Based Immunotherapeutics for the Treatment of Glioblastoma: Advances, Challenges, and Future Perspectives. World Neurosurg. 2018 Dec;120:302-315. doi: 10.1016/j.wneu.2018.08.202
51. Zhong S, Yang W, Zhang Z, Xie Y, Pan L, Ren J, Ren F, Li Y, Xie H, Chen H, Deng D, Lu J, Li H, Wu B, Chen Y, Peng F, Puduvalli VK, Sai K, Li Y, Cheng Y, Mou Y. Association between viral infections and glioma risk: a two-sample bidirectional Mendelian randomization analysis. BMC Med. 2023 Dec 5;21(1):487. doi: 10.1186/s12916-023-03142-9
52. Coghill AE, Kim Y, Hodge JM, Bender N, Smith-Warner SA, Teras LR, Grimsrud TK, Waterboer T, Egan KM. Prospective investigation of herpesvirus infection and risk of glioma. Int J Cancer. 2022 Jul 15;151(2):222-228. doi: 10.1002/ijc.33987
53. Vidone M, Alessandrini F, Marucci G, Farnedi A, de Biase D, Ricceri F, Calabrese C, Kurelac I, Porcelli AM, Cricca M, Gasparre G. Evidence of association of human papillomavirus with prognosis worsening in glioblastoma multiforme. Neuro Oncol. 2014 Jan;16(2):298-302. doi: 10.1093/neuonc/not140
54. Desai AD, Lavelle M, Boursiquot BC, Wan EY. Long-term complications of COVID-19. Am J Physiol Cell Physiol. 2022 Jan 1;322(1):C1-C11. doi: 10.1152/ajpcell.00375.2021
55. Zhang L, Wei C, Li D, He J, Liu S, Deng H, Cheng J, Du J, Liu X, Chen H, Sun S, Yu H, Fu J. COVID-19 receptor and malignant cancers: Association of CTSL expression with susceptibility to SARS-CoV-2. Int J Biol Sci. 2022 Mar 6;18(6):2362-2371. doi: 10.7150/ijbs.70172
56. Baig AM, Khaleeq A, Ali U, Syeda H. Evidence of the COVID-19 Virus Targeting the CNS: Tissue Distribution, Host-Virus Interaction, and Proposed Neurotropic Mechanisms. ACS Chem Neurosci. 2020 Apr 1;11(7):995-998. doi: 10.1021/acschemneuro.0c00122
57. Paules CI, Marston HD, Fauci AS. Coronavirus Infections-More Than Just the Common Cold. JAMA. 2020 Feb 25;323(8):707-708. doi: 10.1001/jama.2020.0757
58. Pearson JRD, Regad T. Targeting cellular pathways in glioblastoma multiforme. Signal Transduct Target Ther. 2017 Sep 29;2:17040. doi: 10.1038/sigtrans.2017.40
59. Khan I, Hatiboglu MA. Can COVID-19 induce glioma tumorogenesis through binding cell receptors? Med Hypotheses. 2020 Nov;144:110009. doi: 10.1016/j.mehy.2020.110009
60. Wan Y, Shang J, Graham R, Baric RS, Li F. Receptor Recognition by the Novel Coronavirus from Wuhan: an Analysis Based on Decade-Long Structural Studies of SARS Coronavirus. J Virol. 2020 Mar 17;94(7):e00127-20. doi: 10.1128/JVI.00127-20
61. Banerjee S, Wang X, Du S, Zhu C, Jia Y, Wang Y, Cai Q. Comprehensive role of SARS-CoV-2 spike glycoprotein in regulating host signaling pathway. J Med Virol. 2022 Sep;94(9):4071-4087. doi: 10.1002/jmv.27820
62. Behboudi E, Nooreddin Faraji S, Daryabor G, Mohammad Ali Hashemi S, Asadi M, Edalat F, Javad Raee M, Hatam G. SARS-CoV-2 mechanisms of cell tropism in various organs considering host factors. Heliyon. 2024 Feb

20;10(4):e26577. doi: 10.1016/j.heliyon.2024.e26577
63. Diwanji TP, Engelman A, Snider JW, Mohindra P. Epidemiology, diagnosis, and optimal management of glioma in adolescents and young adults. Adolesc Health Med Ther. 2017 Sep 22;8:99-113. doi: 10.2147/AHMT.S53391
64. Rasmussen BK, Hansen S, Laursen RJ, Kosteljanetz M, Schultz H, Nørgård BM, Guldberg R, Gradel KO. Epidemiology of glioma: clinical characteristics, symptoms, and predictors of glioma patients grade I-IV in the the Danish Neuro-Oncology Registry. J Neurooncol. 2017 Dec;135(3):571-579. doi: 10.1007/s11060-017-2607-5
65. Greuter L, Guzman R, Soleman J. Pediatric and Adult Low-Grade Gliomas: Where Do the Differences Lie? Children (Basel). 2021 Nov 22;8(11):1075. doi: 10.3390/children8111075
66. Bandopadhayay P, Bergthold G, London WB, Goumnerova LC, Morales La Madrid A, Marcus KJ, Guo D, Ullrich NJ, Robison NJ, Chi SN, Beroukhim R, Kieran MW, Manley PE. Long-term outcome of 4,040 children diagnosed with pediatric low-grade gliomas: an analysis of the Surveillance Epidemiology and End Results (SEER) database. Pediatr Blood Cancer. 2014 Jul;61(7):1173-9. doi: 10.1002/pbc.24958
67. Soleman J, Roth J, Ram Z, Yalon M, Constantini S. Malignant transformation of a conservatively managed incidental childhood cerebral mass lesion: controversy regarding management paradigm. Childs Nerv Syst. 2017 Dec;33(12):2169-2175. doi: 10.1007/s00381-017-3566-z
68. Soleman J, Kozyrev DA, Ben-Sira L, Constantini S, Roth J. Management of incidental brain tumors in children: a systematic review. Childs Nerv Syst. 2020 Aug;36(8):1607-1619. doi: 10.1007/s00381-020-04658-8
69. Jakola AS, Bouget D, Reinertsen I, Skjulsvik AJ, Sagberg LM, Bø HK, Gulati S, Sjåvik K, Solheim O. Spatial distribution of malignant transformation in patients with low-grade glioma. J Neurooncol. 2020 Jan;146(2):373-380. doi: 10.1007/s11060-020-03391-1
70. Chamdine O, Broniscer A, Wu S, Gajjar A, Qaddoumi I. Metastatic Low-Grade Gliomas in Children: 20 Years' Experience at St. Jude Children's Research Hospital. Pediatr Blood Cancer. 2016 Jan;63(1):62-70. doi: 10.1002/pbc.25731
71. Munshey A, Moore J, Maclean C, Longano A, Goldschlager T. Cranial Pilocytic Astrocytoma With Spinal Drop Metastasis in an Adult: Case Report and Literature Review. World Neurosurg. 2017 Feb;98:883.e7-883.e12. doi: 10.1016/j.wneu.2016.08.013
72. Shofty B, Ben Sira L, Constantini S. Neurofibromatosis 1-associated optic pathway gliomas. Childs Nerv Syst. 2020 Oct;36(10):2351-2361. doi: 10.1007/s00381-020-04697-1
73. Evans DGR, Salvador H, Chang VY, Erez A, Voss SD, Schneider KW, Scott HS, Plon SE, Tabori U. Cancer and Central Nervous System Tumor Surveillance in Pediatric Neurofibromatosis 1. Clin Cancer Res. 2017 Jun 15;23(12):e46-e53. doi: 10.1158/1078-0432.CCR-17-0589
74. Campen CJ, Gutmann DH. Optic Pathway Gliomas in Neurofibromatosis Type 1. J Child Neurol. 2018 Jan;33(1):73-81. doi: 10.1177/0883073817739509
75. Tang Y, Gutmann DH. Neurofibromatosis Type 1-Associated Optic Pathway Gliomas: Current Challenges and Future Prospects. Cancer Manag Res. 2023 Jul 13;15:667-681. doi: 10.2147/CMAR.S36267
76. Roth J, Ber R, Constantini S. Neurofibromatosis Type 1-Related Hydrocephalus: Treatment Options and Considerations. World Neurosurg. 2019 Aug;128:e664-e668. doi: 10.1016/j.wneu.2019.04.231
77. Corlette L, Reid A, Roberts-Thomson S, Christie M, Gaillard F. Solitary subependymal giant cell astrocytoma: Case report and review of the literature. J Clin Neurosci. 2020 Dec;82(Pt A):26-28. doi: 10.1016/j.jocn.2020.10.017
78. Gogos AJ, Young JS, Pereira MP, Morshed RA, Potts MB, Hervey-Jumper SL, Berger MS. Surgical management of incidentally discovered low-grade gliomas. J Neurosurg. 2020 Oct 2;135(2):480-487. doi: 10.3171/2020.6.JNS201296
79. Khatua S, Gutmann DH, Packer RJ. Neurofibromatosis type 1 and optic pathway glioma: Molecular interplay and therapeutic insights. Pediatr Blood Cancer. 2018 Mar;65(3). doi: 10.1002/pbc.26838
80. Ryall S, Zapotocky M, Fukuoka K, Nobre L, Guerreiro Stucklin A, Bennett J, Siddaway R, Li C, Pajovic S, Arnoldo A, Kowalski PE, Johnson M, Sheth J, Lassaletta A, Tatevossian RG, Orisme W, Qaddoumi I, Surrey LF, Li MM, Waanders AJ, Gilheeney S, Rosenblum M, Bale T, Tsang DS, Laperriere N, Kulkarni A, Ibrahim GM, Drake J, Dirks P, Taylor MD, Rutka JT, Laughlin S, Shroff M, Shago M, Hazrati LN, D'Arcy C, Ramaswamy V, Bartels U, Huang A, Bouffet E, Karajannis MA, Santi M, Ellison DW, Tabori U, Hawkins C. Integrated Molecular and Clinical Analysis of 1,000 Pediatric Low-Grade Gliomas. Cancer Cell. 2020 Apr 13;37(4):569-583.e5. doi: 10.1016/j.ccell.2020.03.011
81. Peeters SM, Muftuoglu Y, Na B, Daniels DJ, Wang AC. Pediatric Gliomas: Molecular Landscape and Emerging Targets. Neurosurg Clin N Am. 2021 Apr;32(2):181-190. doi: 10.1016/j.nec.2020.12.001
82. Bennett J, Yeo KK, Tabori U, Hawkins C, Lim-Fat MJ. Pediatric-type low-grade gliomas in adolescents and young adults-challenges and emerging paradigms. Childs Nerv Syst. 2024 May 18. doi: 10.1007/s00381-024-06449-x
83. Fangusaro J, Onar-Thomas A, Young Poussaint T, Wu S, Ligon AH, Lindeman N, Banerjee A, Packer RJ, Kilburn LB, Goldman S, Pollack IF, Qaddoumi I, Jakacki RI, Fisher PG, Dhall G, Baxter P, Kreissman SG, Stewart CF, Jones DTW, Pfister SM, Vezina G, Stern JS, Panigrahy A, Patay Z, Tamrazi B, Jones JY, Haque SS, Enterline DS, Cha S, Fisher MJ, Doyle LA, Smith M, Dunkel IJ, Fouladi M. Selumetinib in paediatric patients with BRAF-aberrant or neurofibromatosis type 1-associated recurrent, refractory, or progressive low-grade glioma: a multicentre, phase 2 trial. Lancet Oncol. 2019 Jul;20(7):1011-1022. doi: 10.1016/S1470-2045(19)30277-3
84. Lassaletta A, Zapotocky M, Mistry M, Ramaswamy V, Honnorat M, Krishnatry R, Guerreiro Stucklin A, Zhukova N, Arnoldo A, Ryall S, Ling C, McKeown T, Loukides J, Cruz O, de Torres C, Ho CY, Packer RJ, Tatevossian R, Qaddoumi I, Harreld JH, Dalton JD, Mulcahy-Levy J, Foreman N, Karajannis MA, Wang S, Snuderl M, Nageswara Rao A, Giannini C, Kieran M, Ligon KL, Garre ML, Nozza P, Mascelli S, Raso A, Mueller S, Nicolaides T, Silva K, Perbet R, Vasiljevic A, Faure Conter C, Frappaz D, Leary S, Crane C, Chan A, Ng HK, Shi ZF, Mao Y, Finch E, Eisenstat D, Wilson B, Carret AS, Hauser P, Sumerauer D, Krskova L, Larouche V, Fleming A, Zelcer S, Jabado N, Rutka JT, Dirks P, Taylor MD, Chen S, Bartels U, Huang A, Ellison DW, Bouffet E, Hawkins C, Tabori U. Therapeutic and Prognostic Implications of BRAF V600E in Pediatric Low-Grade Gliomas. J Clin Oncol. 2017 Sep 1;35(25):2934-2941. doi: 10.1200/JCO.2016.71.8726
85. Hanada T, Rahayu TU, Yamahata H, Hirano H, Yoshioka T, Arita K. Rapid malignant transformation of low-grade astrocytoma in a pregnant woman. J Obstet Gynaecol Res. 2016 Oct;42(10):1385-1389. doi: 10.1111/jog.13072
86. Schmidt BT, Hanna A. Deadly Proliferation and Transformation of Pilocytic Astrocytoma in Pregnancy. World Neurosurg. 2020 Jan;133:99-103. doi: 10.1016/j.wneu.2019.09.125
87. Barresi V, Eccher A, Simbolo M, Cappellini R, Ricciardi GK, Calabria F, Cancedda M, Mazzarotto R, Bonetti B, Pinna G, Sala F, Ghimenton C, Scarpa A. Diffuse gliomas in patients aged 55 years or over: A suggestion for IDH mutation testing. Neuropathology. 2020 Feb;40(1):68-74. doi: 10.1111/neup.12608
88. Nafe R, Porto L, Samp PF, You SJ, Hattingen E. Adult-type and Pediatric-type Diffuse Gliomas : What the Neuroradiologist Should Know. Clin Neuroradiol. 2023 Sep;33(3):611-624. doi: 10.1007/s00062-023-01277-z
89. Davis ME. Glioblastoma: Overview of Disease and Treatment. Clin J Oncol Nurs. 2016 Oct 1;20(5 Suppl):S2-8. doi: 10.1188/16.CJON.S1.2-8
90. Ostrom QT, Cioffi G, Waite K, Kruchko C, Barnholtz-Sloan JS. CBTRUS Statistical Report: Primary Brain and Other Central Nervous System Tumors Diagnosed in the United States in 2014-2018. Neuro Oncol. 2021 Oct 5;23(12 Suppl 2):iii1-iii105. doi: 10.1093/neuonc/noab200
91. Bakas S, Sako C, Akbari H, Bilello M, Sotiras A, Shukla G, Rudie JD, Santamaría NF, Kazerooni AF, Pati S, Rathore S, Mamourian E, Ha SM, Parker W, Doshi J, Baid U, Bergman

M, Binder ZA, Verma R, Lustig RA, Desai AS, Bagley SJ, Mourelatos Z, Morrissette J, Watt CD, Brem S, Wolf RL, Melhem ER, Nasrallah MP, Mohan S, O'Rourke DM, Davatzikos C. The University of Pennsylvania glioblastoma (UPenn-GBM) cohort: advanced MRI, clinical, genomics, & radiomics. Sci Data. 2022 Jul 29;9(1):453. doi: 10.1038/s41597-022-01560-7

92. Aggarwal P, Luo W, Pehlivan KC, Hoang H, Rajappa P, Cripe TP, Cassady KA, Lee DA, Cairo MS. Pediatric versus adult high grade glioma: Immunotherapeutic and genomic considerations. Front Immunol. 2022 Nov 22;13:1038096. doi: 10.3389/fimmu.2022.1038096
93. Korshunov A, Schrimpf D, Ryzhova M, Sturm D, Chavez L, Hovestadt V, Sharma T, Habel A, Burford A, Jones C, Zheludkova O, Kumirova E, Kramm CM, Golanov A, Capper D, von Deimling A, Pfister SM, Jones DTW. H3-/IDH-wild type pediatric glioblastoma is comprised of molecularly and prognostically distinct subtypes with associated oncogenic drivers. Acta Neuropathol. 2017 Sep;134(3):507-516. doi: 10.1007/s00401-017-1710-1
94. Solomon DA, Wood MD, Tihan T, Bollen AW, Gupta N, Phillips JJ, Perry A. Diffuse Midline Gliomas with Histone H3-K27M Mutation: A Series of 47 Cases Assessing the Spectrum of Morphologic Variation and Associated Genetic Alterations. Brain Pathol. 2016 Sep;26(5):569-80. doi: 10.1111/bpa.12336
95. Roux A, Pallud J, Saffroy R, Edjlali-Goujon M, Debily MA, Boddaert N, Sanson M, Puget S, Knafo S, Adam C, Faillot T, Cazals-Hatem D, Mandonnet E, Polivka M, Dorfmüller G, Dauta A, Desplanques M, Gareton A, Pages M, Tauziede-Espariat A, Grill J, Bourdeaut F, Doz F, Dhermain F, Mokhtari K, Chretien F, Figarella-Branger D, Varlet P. High-grade gliomas in adolescents and young adults highlight histomolecular differences from their adult and pediatric counterparts. Neuro Oncol. 2020 Aug 17;22(8):1190-1202. doi: 10.1093/neuonc/noaa024
96. Joyner DA, Garrett J, Batchala PP, Rama B, Ravicz JR, Patrie JT, Lopes MB, Fadul CE, Schiff D, Jain R, Patel SH. MRI features predict tumor grade in isocitrate dehydrogenase (IDH)-mutant astrocytoma and oligodendroglioma. Neuroradiology. 2023 Jan;65(1):121-129. doi: 10.1007/s00234-022-03038-0
97. Sabbah DA, Hajjo R, Sweidan K. Review on Epidermal Growth Factor Receptor (EGFR) Structure, Signaling Pathways, Interactions, and Recent Updates of EGFR Inhibitors. Curr Top Med Chem. 2020;20(10):815-834. doi: 10.2174/1568026620666200303123102
98. Rallis KS, George AM, Wozniak AM, Bigogno CM, Chow B, Hanrahan JG, Sideris M. Molecular Genetics and Targeted Therapies for Paediatric High-grade Glioma. Cancer Genomics Proteomics. 2022 Jul-Aug;19(4):390-414. doi: 10.21873/cgp.20328
99. Yang Z, Ling F, Ruan S, Hu J, Tang M, Sun X, Long W. Clinical and Prognostic Implications of 1p/19q, IDH, BRAF, MGMT Promoter, and TERT Promoter Alterations, and Expression of Ki-67 and p53 in Human Gliomas. Cancer Manag Res. 2021 Nov 23;13:8755-8765. doi: 10.2147/CMAR.S336213
100. Picart T, Barritault M, Poncet D, Berner LP, Izquierdo C, Tabouret E, Figarella-Branger D, Idbaïh A, Bielle F, Bourg V, Vandenbos FB, Moyal EC, Uro-Coste E, Guyotat J, Honnorat J, Gabut M, Meyronet D, Ducray F. Characteristics of diffuse hemispheric gliomas, H3 G34-mutant in adults. Neurooncol Adv. 2021 Apr 19;3(1):vdab061. doi: 10.1093/noajnl/vdab061
101. Lim KY, Won JK, Park CK, Kim SK, Choi SH, Kim T, Yun H, Park SH. H3 G34-mutant high-grade glioma. Brain Tumor Pathol. 2021 Jan;38(1):4-13. doi: 10.1007/s10014-020-00378-8

Original article

Ukr Neurosurg J. 2024;30(4):23-29
doi: 10.25305/unj.309045

The impact of the number of aneurysms on the course of the acute period of subarachnoid hemorrhage in patients with multiple intracranial aneurysms

Yuliia O. Solodovnikova, Anatoliy S. Son

Department of Neurology and Neurosurgery, Odesa National Medical University, Odesa, Ukraine

Received: 25 July 2024
Accepted: 02 September 2024

Address for correspondence:
Yuliia O. Solodovnikova, Department of Neurology and Neurosurgery, Odesa National Medical University, 8 Tinysta Street., Odesa , 65125, Ukraine, e-mail: julie-sinel@ukr.net

Objective to determine the effect of the number of multiple intracranial aneurysms (MIA) on the course of the acute period of subarachnoid hemorrhage (SAH).

Materials and methods: A cross-sectional retrospective study was conducted involving 92 patients in the acute phase of SAH due to the rupture of MIA. Patients were divided into two groups depending on the number of aneurysms. Demographic indicators (age, gender) and clinical-instrumental factors (comorbidities, extent of hemorrhage, severity at admission, clinical manifestations), treatment characteristics, and outcomes were analyzed using descriptive statistics and logistic regression.

Results: Comorbidities were 3.4 times more common among patients with three or more aneurysms (p=0.143). Patients in group 2 were 1.9 times more likely to be admitted with a World Federation of Neurosurgical Societies (WFNS) grade 2 (p=0.335). WFNS grade 3 at admission was observed twice as often in group 1 (p=0.447). Patients from group 1 and group 2 were equally likely to present with WFNS grade 4 (p=0.978). The probability of being admitted with a WFNS grade 5 was 1.8 times higher in group 2 (p=0.830). The presence of meningeal syndrome increased the risk of having 3 or more aneurysms by more than four times (OR 4.41, CI 0.41-47.13, p=0.21). The presence of motor impairments significantly reduced the risk of having 3 or more aneurysms (OR 0.63, CI 0.09-4.18, p=0.63). Patients in group 2 were slightly more likely to develop vasospasm than those in group 1 (OR 1.22, CI 0.34-4.31, p=0.752). The presence of comorbidities increased with the number of aneurysms (OR 3.42, CI 0.65-17.62, p=0.143).

Conclusions: The presence of comorbidities more than triples the chances of having 3 or more aneurysms. Patients with fewer aneurysms are twice as likely to be admitted in a milder condition (WFNS grade 2). The probability of severe condition (WFNS grade 5) at hospital admission for patients in group 2 is 1.8 times higher than in group 1. The likelihood of motor disorders decreases by 4.4 times with an increasing number of aneurysms. The probability of vasospasm development slightly increased with the number of aneurysms. These data emphasize the importance of a comprehensive approach to the assessment of SAH patients and the need for careful monitoring of patients at high risk of vasospasm.

Key words: *subarachnoid hemorrhage; multiple intracranial aneurysms; clinical course*

Introduction

Multiple intracranial aneurysms (MIA) account for 20–34% of all intracranial aneurysms and carry a higher risk of rupture compared to solitary aneurysms. Key risk factors for rupture include age, sex, and aneurysm location. The annual rupture risk for multiple aneurysms is 1–2%, depending on additional factors such as hypertension and a personal or family history of hemorrhages [1, 2].

Recent studies have identified complex genetic and molecular mechanisms influencing MIA rupture [3]. Inherited genetic mutations are often associated with an increased risk of aneurysm development and rupture. Conditions such as Ehlers-Danlos and Marfan syndromes, as well as Factor VII deficiency, are known to compromise vascular wall integrity, increasing the likelihood of MIA formation [4].

Molecular mechanisms involving mitochondrial protein dysfunction also play a significant role in the pathogenesis of MIA rupture. Proteins such as AIF1, CCDC90B, and tRNA PusA are linked to an elevated rupture risk due to their influence on cellular energy metabolism and structural processes in vascular walls [5]. Inflammatory processes caused by immune cell dysfunction can promote the development of MIA, particularly in the presence of hypertension [4].

Multiple cerebral aneurysms are associated with a higher risk of complications, especially rupture, compared to solitary aneurysms. The rupture risk varies depending on the aneurysm's location, size, and morphology. In our study, the size of ruptured aneurysms in most cases ranged from 5 to 10 mm, but this factor needs further investigation because of differences between studies. Aneurysms located in the anterior communicating artery ruptured more frequently, while fewer ruptures were observed in the internal carotid and middle cerebral arteries. Ruptures were observed only in patients with two or three aneurysms, with the highest rupture frequency in the MIA group [6].

Aneurysms in the posterior cerebral circulation or with a diameter exceeding 5 mm were more prone to rupture. Additionally, patients with a history of aneurysmal subarachnoid hemorrhage (SAH) faced an increased risk of rebleeding from another aneurysm [1, 2].

The course of MIA presents several challenges for diagnosis and treatment. Often asymptomatic, these aneurysms may only become clinically evident upon rupture, resulting in life-threatening conditions such as SAH. While symptoms like severe headache, nausea, loss of consciousness, or stroke-like presentations may occur after rupture, early signs are often minimal or absent. MIAs can vary in size and location, with some remaining stable while others grow or rupture due to factors like hypertension or additional risk conditions. Monitoring is complicated as each aneurysm carries a unique rupture risk [4].

When MIAs are located in different vascular regions, complications such as recurrent hemorrhages can occur even after surgical intervention on one aneurysm. For example, following treatment of one aneurysm, another may remain undetected or form anew at another site [5]. Studies show that MIA patients are at risk of developing new (*de novo*) aneurysms, underscoring the need for continuous monitoring, particularly after surgical treatment. Contributing factors include hypertension, atherosclerosis, smoking, and genetic predispositions affecting vascular wall stability [4].

Hypertension is a major risk factor for aneurysm rupture, as increased arterial pressure can weaken vessel walls already compromised by aneurysms. Patients with hypertension must closely monitor their blood pressure to mitigate this risk [2, 7].

A multivariate analysis of the risk of MIA rupture revealed a particularly negative impact of age under 40, smoking more than 20 cigarettes per day, uncontrolled hypertension, and aneurysm location on the C_7 segment of the internal carotid artery or anterior communicating artery. Ruptured aneurysms tend to be larger and had a wider neck [8].

Atherosclerotic changes reduce vascular elasticity, increasing rupture susceptibility under hemodynamic stress [1].

While evidence on the direct impact of diabetes on aneurysm rupture is conflicting, it is believed that diabetes may worsen the overall health of the vessels and reduce their ability to recover from damage, indirectly increasing the risk of rupture. Smoking-related toxins damage vessel walls, promoting aneurysm formation and rupture. Smoking is also associated with the development of new aneurysms and its rupture [2].

Objective: To analyze the impact of the number of arterial aneurysms on the acute phase of subarachnoid hemorrhage.

Materials and Methods

Study Participants

The study analyzed 480 medical records of patients who underwent inpatient treatment at Odesa City Clinical Hospital No. 11 between 2000 and 2023, of whom 92 were diagnosed with multiple intracranial aneurysms (MIA).

The study was approved by the ethics and bioethics committee of Odesa National Medical University (minutes No. 7, dated September 30, 2019). All patients provided informed and voluntary written consent to participate in the study and for the publication of their data.

Inclusion Criteria

Patients in the acute phase of subarachnoid hemorrhage (SAH) caused by the rupture of MIA.

Group Characteristics

Patients with ruptured MIA were divided into two groups based on the number of aneurysms: Group 1 (n = 71): Patients with two arterial aneurysms (AA), Group 2 (n = 21): Patients with three or more arterial aneurysms (≥3 AA).

The groups were comparable in terms of age ***(Fig. 1)***. However, women were significantly more prevalent in Group 2 ***(Fig. 2)***.

In Group 2, the number of patients with 3 AAs was 16 patients (76.2%), 4 AAs - 4 (19%), 5 AAs - 1 (2.4%) and 6 AAs - 1 (2.4%)

Most patients with MIA were admitted in a mild condition, with preserved or only slightly impaired consciousness. Only 2.2% of patients were admitted in a critical condition. Differences in severity between the groups were observed: the proportion of patients with ≥3 AAs admitted in critical condition was significantly higher ***(Fig. 3)***.

Study Design

A cross-sectional, retrospective study was conducted. The analysis included demographic factors (age, gender), clinical and instrumental features of SAH progression (comorbidities, hemorrhage extent, severity at admission, clinical manifestations), treatment specifics, and outcomes.

Statistical Analysis

Descriptive statistics and logistic regression were used in the study. A significance threshold (p-value) of 0.05 was applied for hypothesis testing. All calculations were performed using Microsoft Excel.

This article contains some figures that are displayed in color online but in black and white in the print edition.

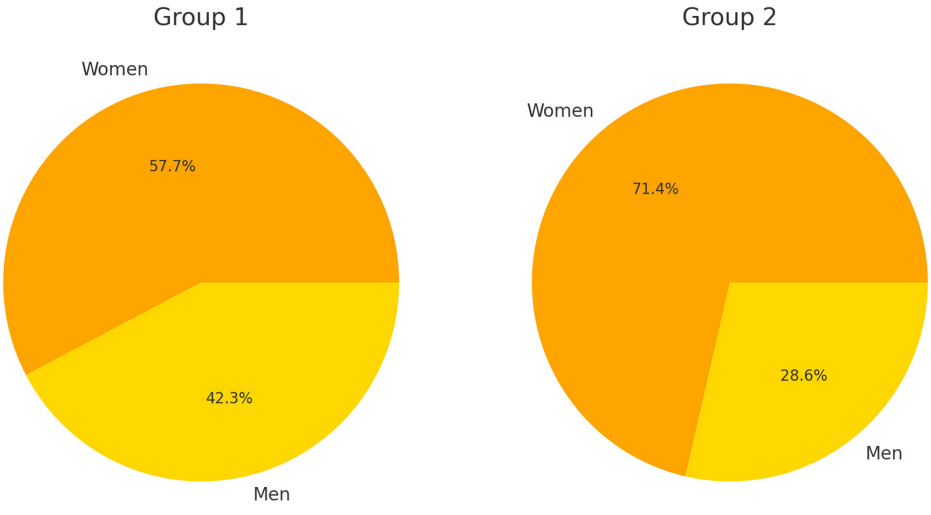

Fig. 1. Gender distribution

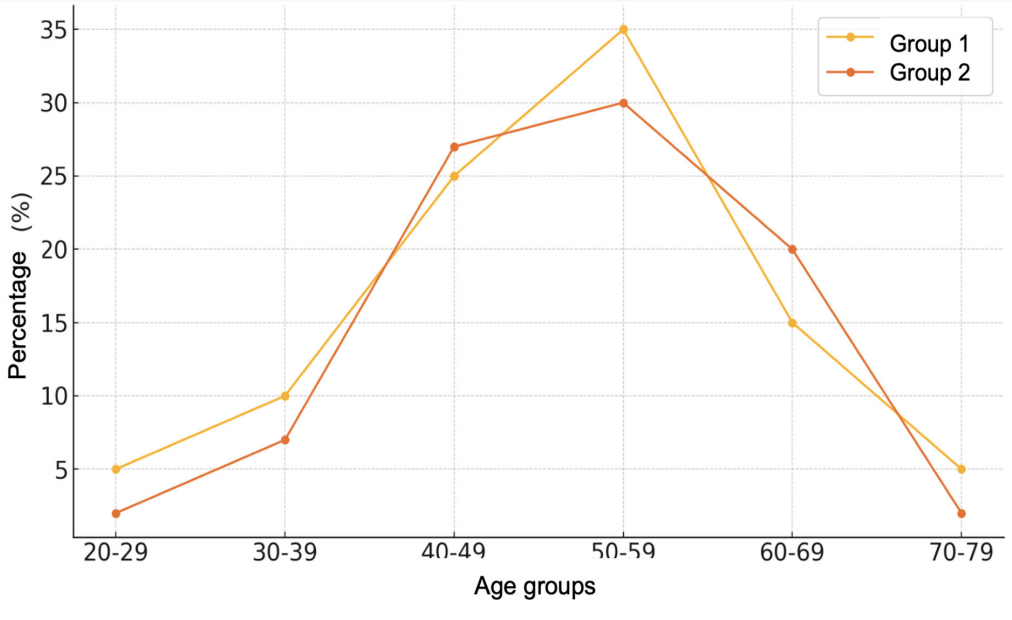

Fig. 2. Age distribution

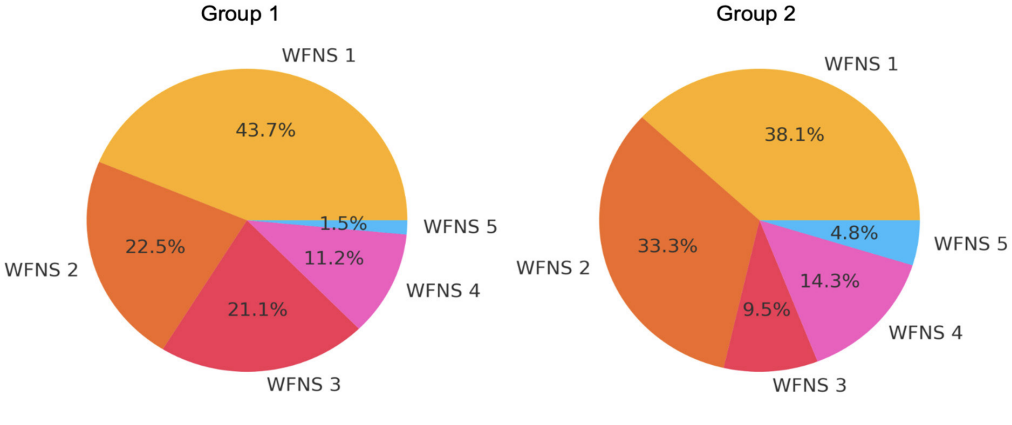

Fig. 3. Distribution of patients by WFNS scale at admission

Results and Discussion

Positive meningeal signs were identified in 88% of patients with MIA. No statistically significant differences were observed between the groups ***(Fig. 4)***.

Motor deficits at admission varied significantly between the groups. Paresis was observed in 77 patients (84%) in Group 1 and in only 2 patients (9.5%) in Group 2.

Vasospasm was detected in 47 patients (51.1%). The mortality rate among patients with vasospasm was 11.1%, compared to 19.1% in patients without vasospasm.

The patterns of hemorrhage distribution in patients with MIA are shown in ***Fig. 5 and 6***.

Intracranial complications were more frequent in Group 1, whereas extracranial septic complications were predominant in Group 2 ***(Fig. 7)***.

In Group 1, vasospasm occurred in 36 patients (50.8%), with clinical manifestations in 7 patients (9.9%), angiographically confirmed in 9 patients (12.7%), and delayed cerebral ischemia in 20 patients (28.2%). Mortality in patients with vasospasm was 19.4%, compared to 11.4% in those without vasospasm ***(Fig. 8)***.

Among women in Group 1, vasospasm was slightly less frequent than in men. Older patients (60–70 years) predominated in the non-vasospasm group, while vasospasm was evenly distributed across different age groups.

Comorbidities were present in 72 patients (78.3%). The proportion of patients with vasospasm and comorbidities was higher, indicating a potential link between comorbidities and an increased risk of vasospasm.

The most common hemorrhage type in both groups was SAH, but complex hemorrhages (e.g., combinations of SAH with ventricular and parenchymal hemorrhage) were more often associated with vasospasm.

In Group 2, comorbidities were observed in 53 patients (74.6%), with vasospasm detected in 11 patients (52.4%), of whom 2 had clinical manifestations (9.5%), 2 were angiographically confirmed (9.5%), and 7 developed delayed cerebral ischemia (33.3%). Mortality among patients with vasospasm was 18.2%, compared to 10.0% in those without vasospasm.

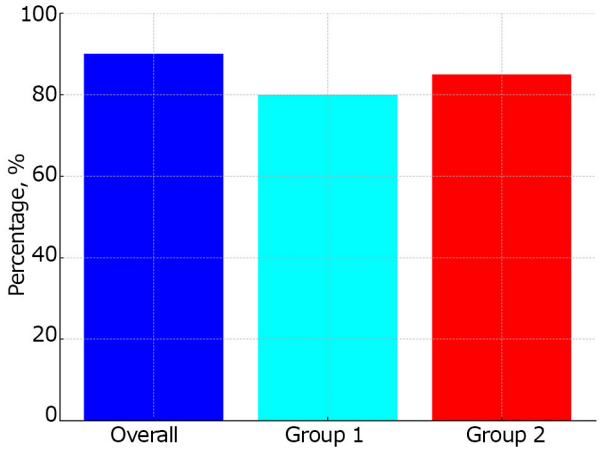

Fig. 4. Meningeal syndrome

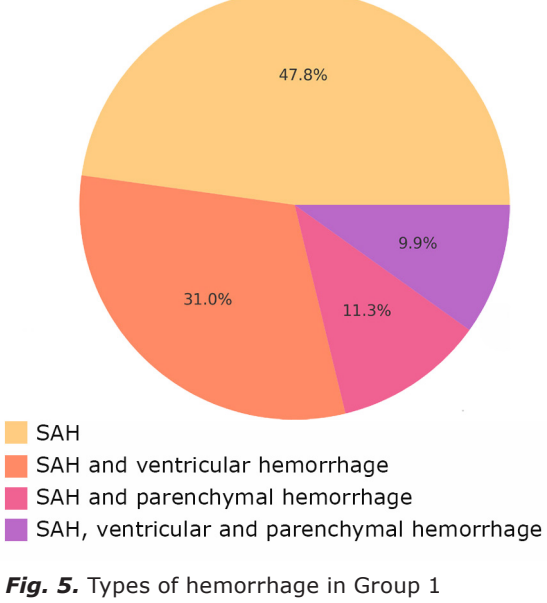

Fig. 5. Types of hemorrhage in Group 1

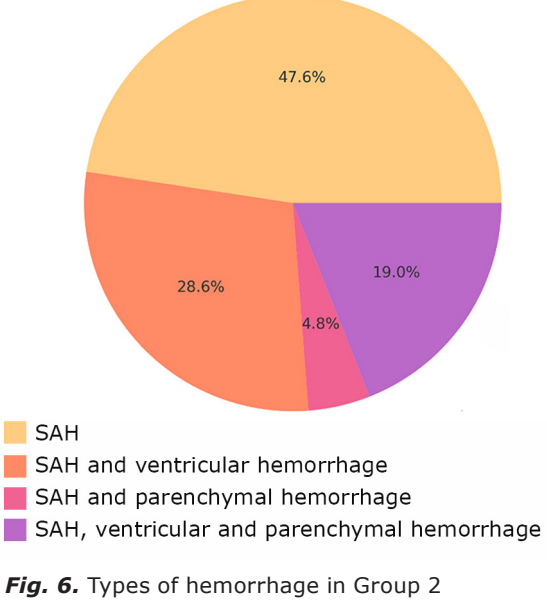

Fig. 6. Types of hemorrhage in Group 2

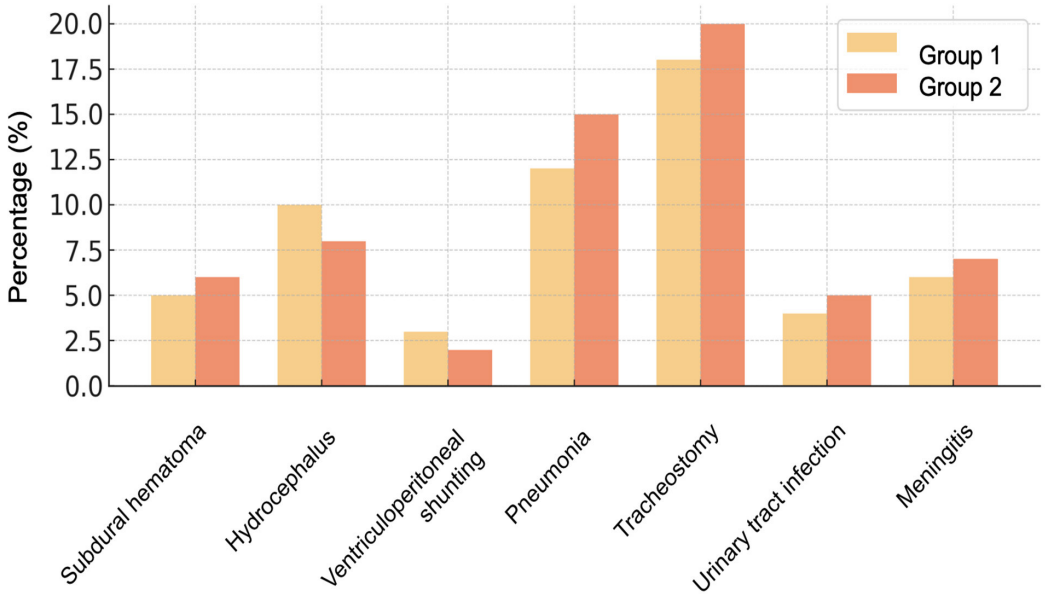

Fig.7. Complications

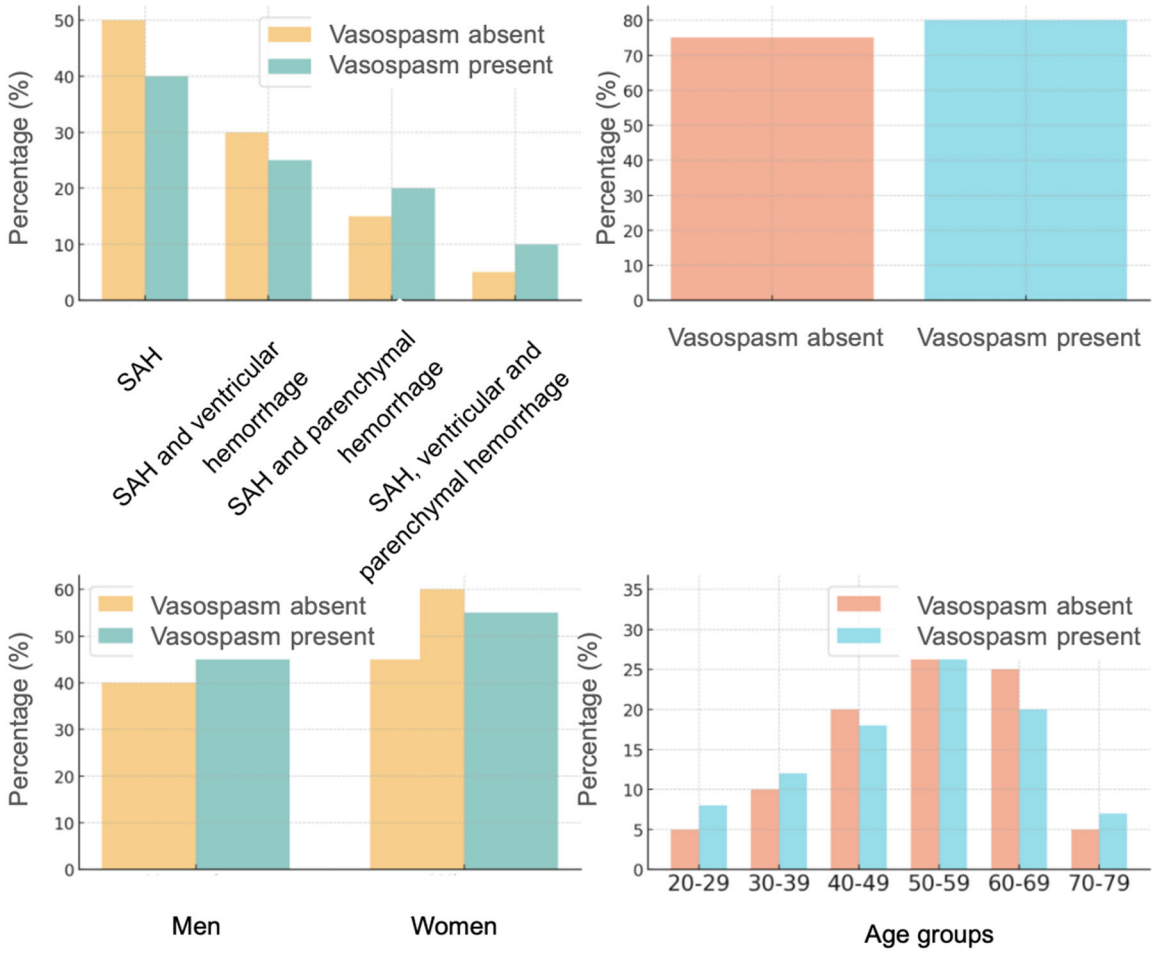

Fig. 8. Vasospasm by age, gender, comorbidities, and hemorrhage type in Group 1

Women with a higher number of MIA aneurysms had a slightly higher frequency of vasospasm compared to men.

In Group 2, significant differences were observed between age groups. Vasospasm occurred more frequently in the 45, 50, 55, and 70-year-old groups. In these age categories, vasospasm was more common, while other age groups demonstrated either a low frequency or absence of vasospasm.

The frequency of vasospasm was significantly higher in individuals with comorbidities compared to those without ***(Fig. 9)***.

More complex forms of hemorrhage, such as a combination of SAH with ventricular and parenchymal hemorrhages, were more often associated with the development of vasospasm.

An analysis of the presented results using binomial logistic regression revealed several trends and patterns that did not reach statistical significance but overall reflected the specific features of MIA progression. While statistical significance (e.g., $p < 0.05$) is considered a convenient indicator, the 0.05 threshold is conditional, and the p-value alone is not suitable for guiding clinical or scientific decisions. The p-value indicates (statistical) probability rather than (clinical) certainty, statistically characterizing individual comparisons but without clinical interpretation. A smaller sample size can substantially affect the p-value.

Multifactorial analysis indicates a statistically significant cumulative impact of the analyzed factors ($p = 0.023$). For example, the presence of comorbidities was 3.4 times more likely among patients with ≥3 aneurysms (OR = 3.4233, 95% CI 0.660–17.762, $p = 0.143$).

Patients in Group 2 were 1.9 times more likely to be admitted with a WFNS score of 2 ($p = 0.335$).

A WFNS score of 3 at admission was twice as frequently recorded in Group 1 ($p = 0.447$). Patients in Groups 1 and 2 were admitted equally often with a WFNS score of 4 ($p = 0.978$). The likelihood of being admitted with a WFNS score of 5 was 1.8 times higher for patients in Group 2 ($p = 0.830$) ***(Fig. 10)***.

The presence of meningeal syndrome increased the risk of having ≥3 aneurysms by more than four times (odds ratio (OR) = 4.41, 95% confidence interval (CI) 0.41–47.13, $p = 0.21$). The presence of motor impairments significantly reduced the risk of having ≥3 aneurysms (OR = 0.63, 95% CI 0.09–4.18, $p = 0.63$). Patients in Group 2 had a slightly higher probability of developing vasospasm (OR = 1.22, 95% CI 0.34–4.31, $p = 0.752$). The presence of comorbidities increased with the number of aneurysms (OR = 3.42, 95% CI 0.65–17.62, $p = 0.143$).

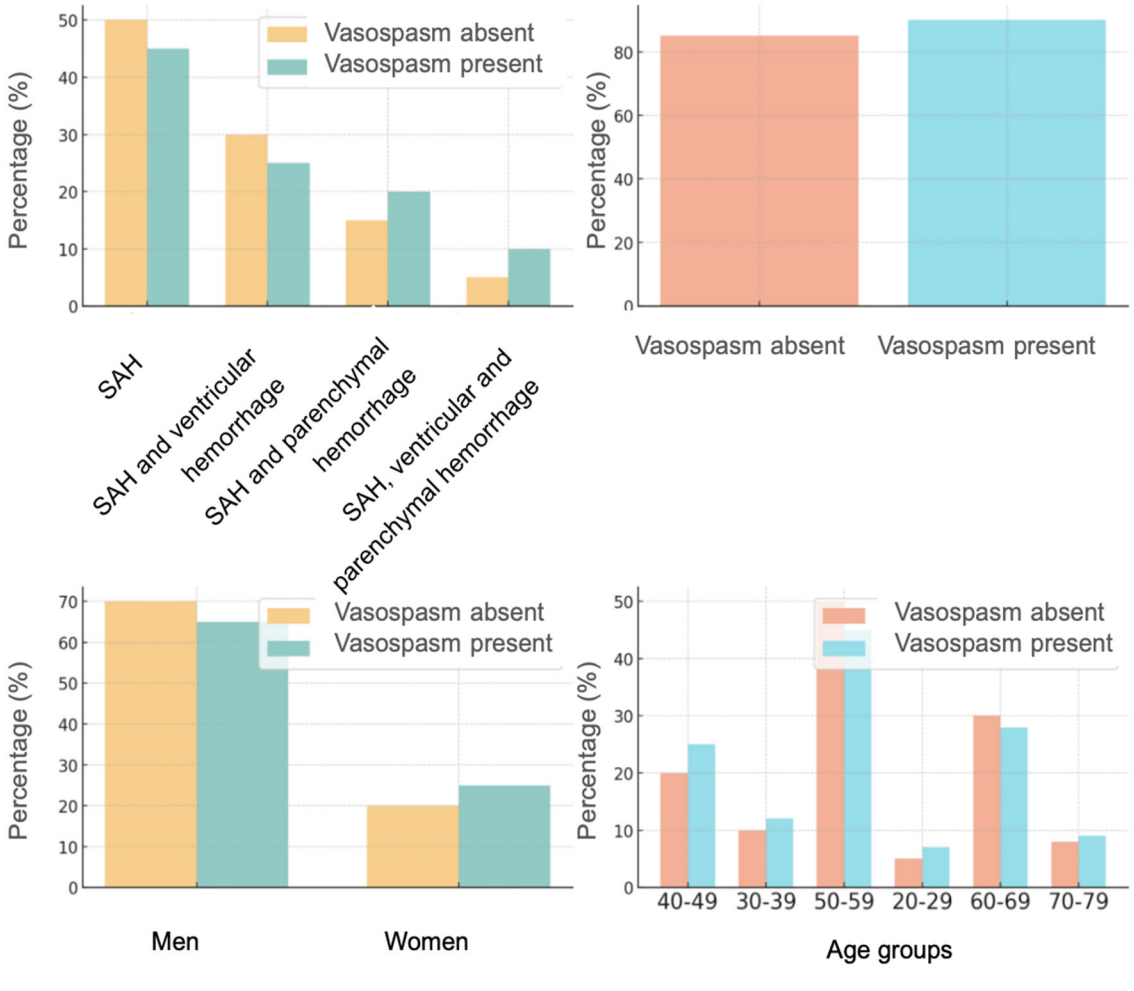

Fig. 9. Vasospasm by age, gender, comorbidities, and hemorrhage type in Group 2

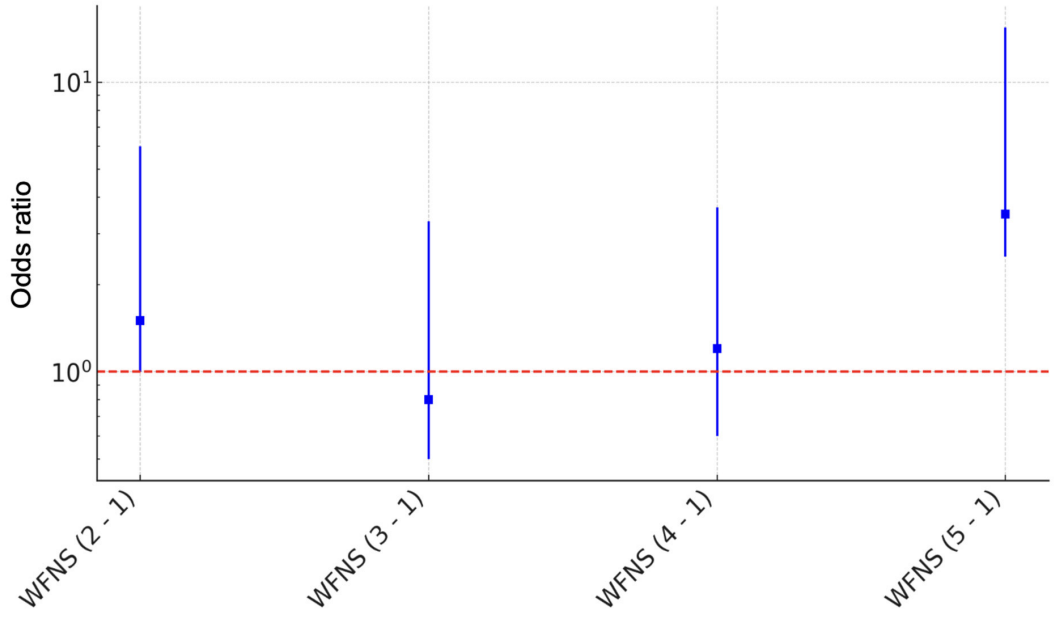

Fig. 10. Logistic regression plot with odds ratios and confidence intervals

Conclusions

Comorbidities increased the likelihood of ≥3 aneurysms by over threefold. Patients with fewer aneurysms were twice as likely to present in a milder condition (WFNS score 2). The likelihood of motor deficits decreased 4.4 times with an increased number of aneurysms. Vasospasm risk slightly increased with the number of aneurysms.

The probability of WFNS severity 5 on admission to hospital for group 2 patients was 1.8 times higher than for group 1 patients. The probability of motor deficits decreased 4.4 times with the number of aneurysms. The probability of vasospasm development slightly increased with the number of aneurysms.

Disclosure

Conflict of Interest

The authors declare no conflict of interest.

Ethical Standards

All procedures performed on patients during the study adhered to the ethical standards of the institutional and national ethics committees, as well as the 1964 Helsinki Declaration and its subsequent amendments or comparable ethical standards.

Informed Consent

Written informed consent was obtained from all patients.

Funding

The study was not sponsored.

References

1. Li Y, Bai X, Tu H, Zou Z, Huang Y, Cai J. Multiple intracranial enlarging dissecting aneurysms: a case report. BMC Neurol. 2023 Jul 12;23(1):265. doi: 10.1186/s12883-023-03303-6
2. Deniwar MA. Management of multiple and unruptured cerebral aneurysms. Egypt J Neurosurg. 2022;37:26. doi: 10.1186/s41984-022-00170-0
3. Bakker MK, Ruigrok YM. Genetics of Intracranial Aneurysms. Stroke. 2021 Aug;52(9):3004-3012. doi: 10.1161/STROKEAHA.120.032621
4. Schilling AM, Heidenreich JO, Oldenburg AC, Pietilä T, Stendel R, Wolf KJ. Multiple cerebral aneurysms in factor VII deficiency. AJNR Am J Neuroradiol. 2004 May;25(5):784-6.
5. Wang S, Wang J, Niu Z, Zhang K, Yang T, Hou S, Lin N. Causal relationship between mitochondrial-associated proteins and cerebral aneurysms: a Mendelian randomization study. Front Neurol. 2024 Jul 17;15:1405086. doi: 10.3389/fneur.2024.1405086
6. Grochowski C, Litak J, Kulesza B, et al. Size and location correlations with higher rupture risk of intracranial aneurysms. J Clin Neurosci. 2017; S0967586817314479. doi:10.1016/j.jocn.2017.10.064
7. Sato T, Matsushige T, Chen B, Gembruch O, Dammann P, Jabbarli R, Forsting M, Junker A, Maderwald S, Quick HH, Ladd ME, Sure U, Wrede KH. Correlation Between Thrombus Signal Intensity and Aneurysm Wall Thickness in Partially Thrombosed Intracranial Aneurysms Using 7T Magnetization-Prepared Rapid Acquisition Gradient Echo Magnetic Resonance Imaging. Front Neurol. 2022 Feb 18;13:758126. doi: 10.3389/fneur.2022.758126
8. Jiang H, Weng YX, Zhu Y, Shen J, Pan JW, Zhan RY. Patient and aneurysm characteristics associated with rupture risk of multiple intracranial aneurysms in the anterior circulation system. Acta Neurochir (Wien). 2016 Jul;158(7):1367-75. doi: 10.1007/s00701-016-2826-0

Original article

Ukr Neurosurg J. 2024;30(4):30-42
doi: 10.25305/unj.310430

The rat's sciatic nerve functional index dynamics after its transection and recovery by means of epineural neurorrhaphy

Ziia K. Melikov, Volodymyr V. Medvediev

Department of Neurosurgery, Bogomolets National Medical University, Kyiv, Ukraine

Received: 29 August 2024
Accepted: 27 September 2024

Address for correspondence:
Ziia K. Melikov, Department of Neurosurgery, Bogomolets National Medical University, 32 Platona Mayborody st., Kyiv, 04050, Ukraine, e-mail: melikov_ziya@ukr.net

Introduction. Peripheral nerve injury (PNI) is a common wartime pathology, the presence of which significantly complicates the course and treatment of combat injuries to the limbs. The development of new methods of treatment of PNI is impossible without validating existing models of PNI and clarifying the dynamics of the recovery process in this type of injury over long periods of observation. In this paper, the dynamics of the sciatic functional index (SFI) after transection and immediate suturing of the sciatic nerve of an adult rat during 24 weeks of observation was analyzed in detail.

Objective: to analyze the dynamics of SFI after transection, as well as after transection and immediate suturing of the sciatic nerve of an adult rat for 24 weeks and compare the obtained results with the data of other authors under similar experimental conditions.

Materials and Methods. The study was performed on 76 white adult outbred male rats, adhering to bioethical norms. In animals of the Sham group (n=24) an access to the sciatic nerve was performed, in animals of the Sect group (n=29) — the sciatic nerve was transected, and Raph group (n=23) — transection and immediate epineural suturing of the sciatic nerve was performed. A certain number of animals were removed from each group 4, 8, and 12 weeks after surgery for electrophysiological and morphological studies, and for the rest of the animals, the experiment was completed 24 weeks after the start of observation. SFI was determined before animals were removed, for all animals in each group at 4, 8, 12, 16, 20 and 24 weeks according to the Bain-Mackinnon-Hunter formula. Processing of digital data was carried out by various means of mathematical statistics.

Results. In animals of the Sham group, which were observed throughout the entire 24 weeks of the experiment (n=7), the average value of SFI one month after the injury simulation was -8.9 points and did not change significantly until the end of the experiment. In animals of the Sect group, which were observed throughout the entire 24 weeks of the experiment (n=8), one month after the injury, the mean SFI value was –84.7 points, significantly increasing to –67.0 points at the end of the 16th week, and subsequently significantly decreasing to –96.5 points. In animals of the Raph group, which were observed throughout the entire 24 weeks of the experiment (n=7), the average value of SFI after one month was -64.4 points, and its increase to -45.4 points at the end of week 24 should be considered relatively reliable. Pairwise comparison of the averaged for all animals SFI values in the Sham and Sect, Sham and Raph, and Sect and Raph groups revealed significant differences at 4, 8, 12, 20, and 24 weeks after simulated injury. At 16 weeks post-intervention, the SFI values in the Sect and Raph groups were significantly different from those in the Sham group, but were not different from each other.

Conclusions. The method of determining the function of the paretic limb after sciatic nerve injury in rats using SFI has a number of technical limitations, which are the reason for significant variability in experimental results among different research groups. The reliable biphasic SFI dynamics that was discovered after sciatic nerve transection, as well as the insignificant (*according to this data*) fluctuations in SFI after sciatic nerve transection and neurorrhaphy, require independent verification, pathophysiological interpretation, and should be taken into account when evaluating rehabilitation methods using such an experimental model of peripheral nerve injury.

Keywords: *peripheral nerve injury; sciatic nerve transection, neurorrhaphy, sciatic nerve functional index, temporal dynamics of the indicator*

Introduction

Peripheral nerve injury (PNI) is a common injury that often results in disability. Its prevalence, according to various sources, is approximately 3% of all injuries during peacetime [1-9] and around 5% when accounting for specific cases of plexus and spinal root injuries [8]. This translates to an incidence of 1–2 cases per 10,000 people annually [10-13], with even higher rates in developing countries [10]. During wartime, PNI frequently occurs as part of blast and gunshot injuries to the limbs, often accompanied by vascular and bone damage ([14–17] for peacetime gunshot PNIs, [18] - for peacetime PNIs in general, [19] - for wartime PNIs) significantly complicating the clinical course of this type of trauma.

PNI is generally considered the mildest form of nervous system injury but is characterized by a combination of prolonged sensory, motor, trophic, and pain disorders [1-8]. It also incurs substantial direct and indirect financial costs [4-7, 11, 20-26], which continue to rise annually [27]. Some studies have observed a decline in the proportion of PNI among peacetime injuries over the past 30 years [9]. Observational studies of patients with peripheral neuropathy indicate an increased risk of premature death [28]. However, it is unclear whether this is true for patients with post-traumatic neuropathy or if a direct link exists between PNI and mortality.

This type of trauma demonstrates age (average age 36–39 years [9, 11, 12, 27]) and sex specificity, occurring twice [11-13], three times [11, 18, 27, 29], or even four times [9] more often in men. The most common injuries involve the nerves of the upper limbs, particularly the wrist and hand [11-13, 18, 25, 27]. Left-sided injuries are reportedly more frequent [18, 25]. Treatment for PNI is primarily surgical [9, 12, 13], often performed urgently and typically involves direct anatomical repair of the nerve through neurorrhaphy [13].

Despite the relatively high regenerative potential of the peripheral nervous system, the plasticity of its central counterpart, and significant advances in PNI treatment, clinical outcomes remain suboptimal. Improvement is possible through a comprehensive approach targeting the injury site, the central nervous system, and paretic muscles [30]. Developing such methods requires experimental studies and standardization of PNI models [31-35].

The model of complete transection of the sciatic nerve is considered one of the most convenient for testing implant-based treatment approaches [31]. However, despite its relative simplicity, the reproducibility of results with this model is unsatisfactory, necessitating its validation. Moreover, there is limited information in the available literature on this model's behavior over periods exceeding 90 days [36-40]. Similarly, data on the statistical analysis of temporal changes in the functional-anatomical indicator, the sciatic functional index (SFI), following nerve transection or segment excision in rats, are scarce [41, 42].

Objective: To analyze the dynamics of SFI following transection and immediate suturing of the sciatic nerve in adult rat over a 24-week observation period and compare the results with data from other authors under similar experimental conditions.

Materials and Methods

Experimental animals and groups

The study was conducted on 76 white outbred rats aged 4–6 months, weighing 280–380 g, sourced from the vivarium of the Romodanov Institute of Neurosurgery of the National Academy of Medical Sciences of Ukraine. The animals were housed under natural light conditions, with standard temperature and humidity levels, and fed a balanced combined diet *ad libitum*. During the study, principles of bioethics and humane treatment of animals were followed in accordance with the EU Council Directive 86/609/EEC on the approximation of laws, regulations and administrative provisions of the Member States regarding the protection of animals used for experimental and other scientific purposes (1986), the European Convention for the Protection of Vertebrate Animals Used for Experimental and Other Scientific Purposes (1986), and the Law of Ukraine No. 3447-IV "On the Protection of Animals from Cruelty" (2006). Approval for the study was obtained from the Bioethics and Ethics Commission for Scientific Research of Bogomolets National Medical University (minutes No. 155, dated January 31, 2022) and the Bioethics Committee of the Romodanov Institute of Neurosurgery of the National Academy of Medical Sciences of Ukraine (minutes No. 39, dated May 18, 2022).

Three experimental groups were formed: 1) a group of sham-operated animals that underwent only surgical access to the sciatic nerve (Sham; n=24); 2) a group of modelling a complete section of the sciatic nerve in the middle third (Sect; n=29); 3) a group of modelling a complete transection of the sciatic nerve in the middle third and its immediate epineural neurorrhaphy (Raph; n=23). A certain number of animals were removed from each group 4, 8 and 12 weeks after the surgical intervention for electrophysiological and morphological studies ***(Table 1)***. The remaining animals completed the experiment 24 weeks after the start of the observation period.

Table 1. Composition of experimental groups and the time course of animal removal from the experiment

Term of animals withdrawal from the experiment; weeks after the surgical intervention	**The initial number of animals in each group (given in the title of each column) and the number of animals in the group withdrawed from the experiment at each of the indicated observation time points (given in the cells of the table)**		
	Sham (n=24)	**Sect (n=29)**	**Raph (n=23)**
4	5	8	5
8	6	6	5
12	6	7	6
24	7	8	7

This article contains some figures that are displayed in color online but in black and white in the print edition.

Surgical Procedures

The surgical procedures were performed under general anesthesia, induced via intraperitoneal injection of a mixture of xylazine hydrochloride (15 mg/kg, «Biowet», Poland) and ketamine hydrochloride (75 mg/kg, «Farmak», Ukraine). The adequacy of anesthesia was verified by the following criteria: absence of the corneal reflex, no withdrawal of the hind paw upon firm pressure on the foot, absence of whisker movements synchronized with the respiratory cycle, shallow rhythmic respiratory movements, and noticeable exophthalmos. Once these indicators were confirmed, the animal was positioned in a standard physiological posture (prone), with the limbs secured to the edges of the surgical table using cords. The skin on the posterolateral surface of the left thigh was shaved with scissors and treated with an antiseptic povidone-iodine solution («EGIS», Hungary). In moderately aseptic conditions, an incision was made along the line of the most superficial lateral surface of the femur. The attachment site of the tendon of the short head of the *biceps femoris muscle* was visualized, and a linear incision was made along the bone. The mobilized head of the muscle was retracted to the side ***(Figure 1, A)***. In the exposed pocket between the mobilized muscle head, bone, and other intact thigh muscles, the sciatic nerve trunk was identified and separated from surrounding tissues from the point where it exits the pelvic cavity to its bifurcation into main branches ***(Figure 1, B)***. In the Sham group, the surgical procedure ended at this stage by closing in layers of the dissected edge of the short head of the *biceps femoris muscle* and the tendinous portion of the *vastus lateralis muscle* at its attachment to the femur, followed by suturing of the skin edges with interrupted sutures (suture material No. 3-0, «Ethicon», USA). In the Sect group, the mobilized sciatic nerve trunk was transected using ophthalmic scissors, observing rapid retraction of the proximal stump ***(Figure 1, C)***. After ensuring hemostasis, the surgical procedure was completed as described above. In the Raph group, the stumps of the transected sciatic nerve were reconnected in an end-to-end manner using 3–6 (depending on nerve thickness) epineural interrupted sutures with moderate axial tension, performed with monofilament sutures (8.0–10.0, «Ethicon», USA) under 10–14x magnification of a surgical microscope ***(Figure 1, D)***. The procedure was completed as described above.

In all cases, the skin of the surgical wound was treated with povidone-iodine solution («Betadine®», «EGIS», Hungary). To prevent infectious complications, a solution of bicillin-5 («Arterium», Ukraine) was administered subcutaneously in the posterior cervical area at a dose of 1 million IU per 1 kg body weight. Anti-inflammatory and analgesic therapy included intraperitoneal administration of dexamethasone (*«KRKA»,* Slovenia) at a dose of 6 mg/kg body weight. After the described manipulations, the animals were kept in a room with an elevated air temperature for 2–4 hours until their behavioral activity resumed. Subsequently, they were housed under standard conditions in cages measuring 55 × 33 × 20 cm (length, width, height), with 3–6 animals per cage.

Determination of the sciatic functional index (SFI)

The SFI was measured in all experimental groups at 4, 8, 12, 16, 20, and 24 weeks post-operation. Testing was mandatory for animals at the specified time points before their removal from the experiment. The minimum testing period was set due to the unreliability of SFI measurements during the first 3 weeks following sciatic nerve injury in rats [43,44]. Differences between groups were identified for the 4th (4% of the observation period), 8th (11%), 12th (5%), and 24th (1%) weeks of observation. Footprints required for SFI calculation were obtained on a paper strip covering the floor of a tunneled horizontal runway [45–47]. Before testing, each animal was trained to move through the tunnel. After applying gouache to the plantar surface of the hind paws, the rat was released into the tunnel, which led to a cage. On the continuous, unidirectional gait footprints obtained, the distances between major anatomical points of the paw were measured, and SFI was calculated using the Bain–Mackinnon–Hunter formula [46]:

$$SFI = -38{,}3 \cdot \frac{PL_E - PL_N}{PL_N} + 109{,}5 \cdot \frac{TS_E - TS_N}{TS_N} + 13{,}3 \cdot \frac{IT_E - IT_N}{IT_N} - 8{,}8,$$

where E — injured limb; N — intact limb;
PL — distance from the heel to the longest toe;
TS — distance between the 1st and 5th toes;
IT — distance between the 2nd and 4th toes.

The SFI ranges from –100 points (reflecting footprints indicating a complete loss of sciatic nerve function) to 0 points (reflecting normal sciatic nerve function).

Exclusion Criteria

Animals showing signs of purulent-inflammatory complications, trophic ulcers on the paretic limb or adjacent areas, and/or signs of autophagy were removed from the experiment through chemical euthanasia (one animal from the Sect group on the 18th day post-operation).

In total, 16 animals died during the first 2 days after surgery due to unspecified reasons (6 animals from the Sham group, 6 from the Sect group, and 4 from the Raph group). Additionally, 3 animals died later (1 from the Sect group in the 5th month of observation and 2 from the Sect group during the 1st week of observation).

These animals, excluded from the experiment, were not included in the previously stated total number of experimental animals (76).

Statistical data analysis

Statistical analysis was performed using the EZR software package (*R*-Statistics), which is freely available online (https://www.softpedia.com/get/Science-CAD/EZR.shtml). The mean SFI values were presented as M±SD for samples with a normal distribution, where M (mean) represents the arithmetic mean, and SD (standard deviation) indicates the standard error of the mean. For samples without a normal distribution, data were presented as Me (Q_I-Q_{III}), where Me (median) is the median, and QI–QIII are the first and third quartiles, respectively. The distribution type was determined using the Shapiro–Wilk test.

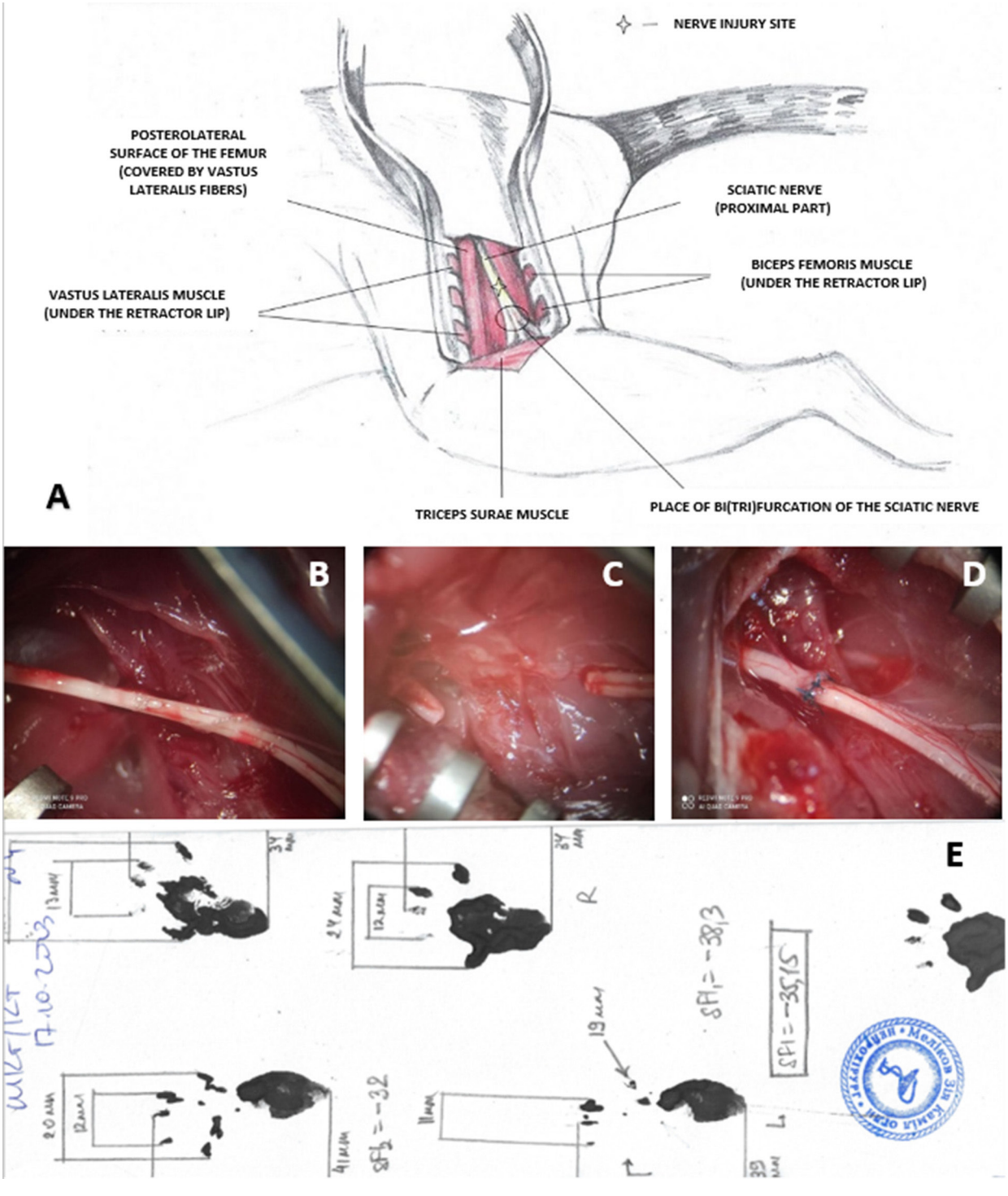

Fig. 1. Features of sciatic nerve injury modeling and SFI calculation in experimental animals:
A — Schematic representation of the surgical approach to the left sciatic nerve in a rat;
B–D — Intraoperative microphotographs of the surgical site after the main intervention stage:
B — Sciatic nerve trunk isolated from surrounding tissues (Sham group);
C — Sciatic nerve after transection, showing retraction and a gap between the proximal and distal stumps (Sect group);
D — Sciatic nerve after transection and immediate reconnection of the stumps with five end-to-end epineural interrupted sutures. Magnification ×14;
E — Example of SFI calculation using rat paw prints from the Raph group 12 weeks post-surgery. SFI –35.15.

For animals observed over all 24 weeks, differences in SFI values at different observation time-points were analyzed using the Friedman test (for non-normally distributed SFI values) or repeated-measures ANOVA (rANOVA) with Bonferroni correction for multiple comparisons (for normally distributed SFI values). If in this way significant differences were detected within a group, additional pairwise comparisons between SFI values at different observation time-points were performed using the Student's t-test (for normally distributed data) or the Wilcoxon rank-sum test (for non-normal distributions).

To assess correlations between SFI values and observation time in animals, which were observed throughout the entire 24 weeks of the experiment, the Spearman rank correlation test was used for non-normally distributed SFI values (distribution of observation duration values was always non-normal), while Pearson's test was applied for normally distributed SFI values. Bonferroni correction was applied for multiple comparisons.

To evaluate significant differences in SFI values between groups at specific time points, the normality of distribution was assessed using the Shapiro–Wilk test. If at least one sample deviated from a normal distribution, the Kruskal–Wallis test was used to assess group differences, followed by Steel–Dwass post hoc comparisons. For normally distributed SFI values, Bartlett's test was applied to compare variance homogeneity. If variances were non-normally distributed, the Kruskal–Wallis test and Steel–Dwass post hoc test were used. For normally distributed variances, ANOVA with Tukey's post hoc test was applied to compare samples.

In all cases, a result was considered statistically significant if the probability of the null hypothesis was less than 0,05 ($p < 0,05$).

Results

The group-averaged values for animals observed throughout the 24 weeks of the experiment are presented in Table 2 and analyzed for significance of changes over time ***(Table 2, Fig. 2)***.

In the Sham group (n=7), the mean SFI value one month after injury modeling was –8,93 points (–16,7; –8,81) and did not significantly change throughout the experiment ($p > 0.05$, Friedman test with Bonferroni correction) ***(Table 2)***. This is supported by the absence of a correlation between SFI values and the duration of observation in this group ($r_S = 0,28$, $p > 0,05$) ***(Fig. 2)***.

Table 2. Averaged SFI values in experimental groups obtained from the results of testing animals observed throughout all 24 weeks of the experiment

Observation period, week	Experimental groups		
	Sham (n = 7)	**Sect (n = 8)**	**Raph (n = 7)**
	Me (Q_I–Q_{III})	**Me (Q_I–Q_{III})**	**Me (Q_I–Q_{III})**
4	–8,93 (–16,7;–8,81)	–84,68 (–93,67;–72,87) *	–64,4 (–77,65;–56,52)
8	–11,35 (–15,38;–9,07)	–80,98 (–85,75;–73,9) *	–61,55 (–68,96;–48,01)
12	–4 (–7,61;–3,81)	–76,15 (–81,63;–73,01) *	–63,38 (–74,84;–60,21)
16	–7,89 (–9,29;–6,71)	–66,95 (–72,32;–64,52) *†	–52,37 (–58,11;–51,21)
20	–11,2 (–15,46;–5,4)	–76,91 (–83,32;–70,44)	–56,3 (–60,59;–47,67)
24	–6,4 (–9,08;–4,37)	–96,48 (–100,0;–79,08) †	–45,4 (–58,7;–37,35)

Note: *SFI values in the Sect group significantly differ from the values in this group at 16 weeks of observation; † The difference in SFI values in the Sect group between 16 and 24 weeks of observation is statistically significant.

In the Sect group (n=8), the mean SFI value one month after injury modeling was –84,68 points (–93,67; –72,87). By the end of week 16, it increased to –66,95 points (–72,32; –64,52) ($p < 0,05$, Student's t-test for pairwise comparisons with values at weeks 4, 8, and 12). However, it decreased again to –96,48 points (–100,0; –79,08) by the end of the experiment ($p < 0,01$, Wilcoxon T-test for pairwise comparisons between weeks 16 and 24) ***(Table 2)***. Thus, no significant correlation was found between SFI values and observation duration in this group ($r = –0,06$, 95% CI –0,34 to +0,22, $p = 0,67$). If two sub-periods, 4-16 and 16-24 weeks, are distinguished in the total follow-up period in the Sect group, a statistically significant average strength of association between SFI values and duration of follow-up was found for each of them ***(Fig. 2)***: positive correlation (r=0,43, 95% CI +0,1 to +0,7, p<0,05) and negative correlation (r=–0,58, 95% CI –0,8 to –0,2, p<0,01), respectively.

In the Raph group (n=7), the mean SFI value one month after injury modeling was –64,4 points (–77,65; –56,52), which non-significantly increased to –45,4 points (–58,7; –37,35) by the end of the experiment (Friedman test with Bonferroni correction, $p > 0,05$ for comparisons across observation periods) ***(Table 2)***. However, the presence of a moderate positive correlation between SFI values and observation duration ($r = 0,45$, 95% CI +0,2 to +0,7, $p < 0,05$) indicates the significance of this SFI dynamic ***(Fig. 2)***.

Pairwise intergoup comparisons of SFI values of all animals revealed statistically significant differences for all three group pairs (Sham and Sect, Sham and Raph, and Sect and Raph) at weeks 4, 8, 12, 20, and 24 after injury modeling ($p < 0,05$, Kruskal–Wallis test and Steel–Dwass post hoc comparisons) ***(Table 3; Fig. 3)***. At week 16 post-injury, SFI values in the Sect and Raph groups were significantly different from the Sham group ($p < 0,05$, ANOVA and Tukey's post hoc test) but not from each other ($p > 0,05$, ANOVA and Tukey's post hoc test) ***(Table 3; Fig. 3)***.

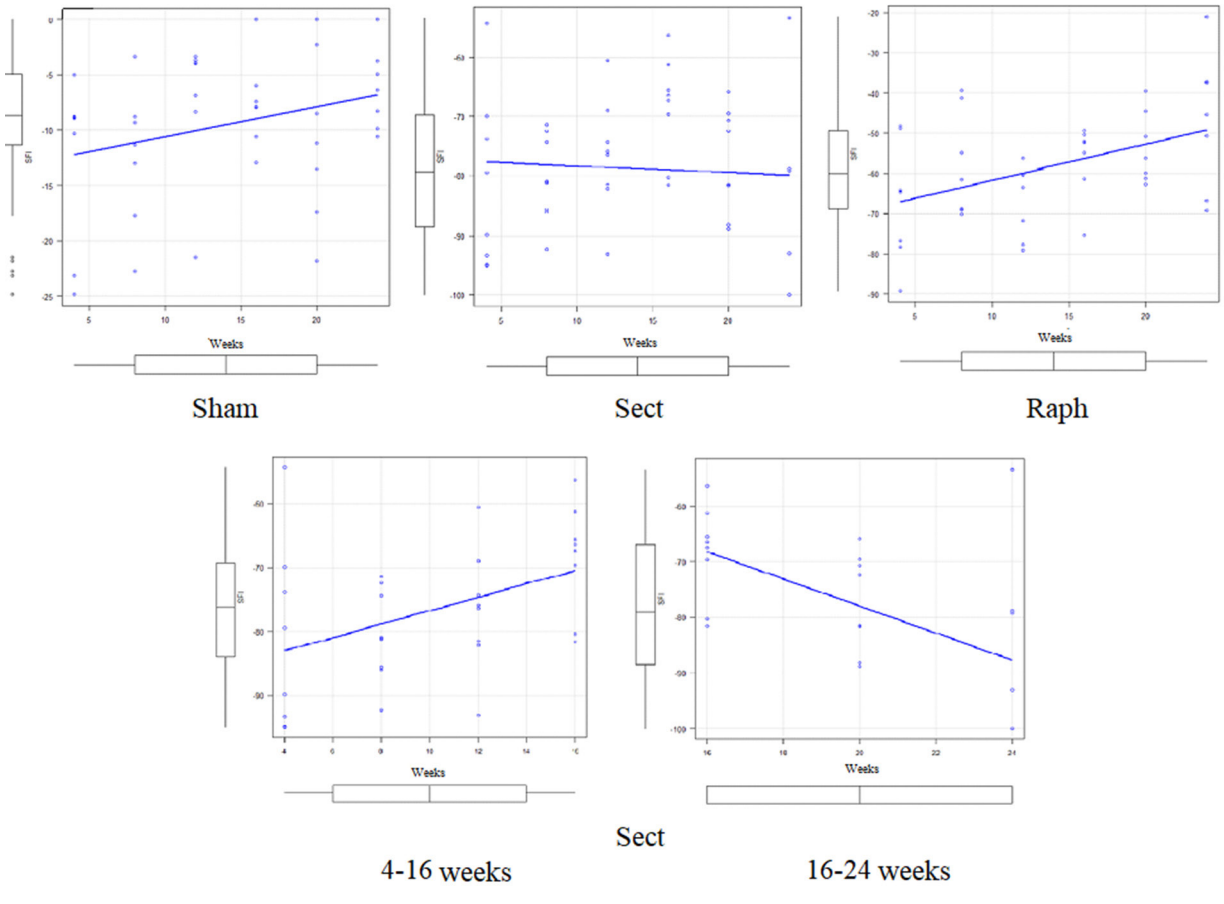

Fig. 2. Correlation between SFI values and the duration of observation in experimental groups (Sham — n=7, Sect — n=8, Raph — n=7; see Table 2). Upper row from left to right: Sham group — $r_S = 0,28$ (Spearman rank correlation test, p=0,07); Sect group — r=–0,06, 95% CI –0,34…+0,22 (Pearson's test, p=0,67); Raph group — r=0,45, 95% CI +0,2... +0,7 (Pearson's test, p<0,05). Lower row from left to right: Sect group, 4, 8, 12, and 16 weeks of observation — r=0,43, 95% CI +0,1… +0,7 (Pearson's test, p=0,015); Sect group, 16, 20, and 24 weeks of observation — r=–0,58, 95% CI –0,8…–0,2 (Pearson's test, p=0,003).

Table 3. Averaged SFI values of the experimental groups (obtained from the results of testing all animals) and their differences at each observation period

Observation period, week	Experimental groups (the number of animals tested at each time point of the experiment is indicated in each corresponding cell of the table)		
	Sham	**Sect**	**Raph**
4	Me (Q_I–Q_{III}), n=24	Me (Q_I–Q_{III}), n=29	Me (Q_I–Q_{III}), n=24
	–7,6 (–13,91;–4,09)	–79,9 (–89,85;–73,85)	–70,41 (–77,42;–58,57)
8	M±SD, n=19	M±SD, n=21	M±SD, n=19
	–11,36±5,18	–77,15±10,1	–51,99±20,63
12	M±SD, n=13	M±SD, n=15	M±SD, n=14
	–7,62±6,29	–78,49±8,64	–60,38±12,95
16	M±SD, n=7	M±SD, n=8	M±SD, n=8
	–7,54±4,03	–68,58±8,67 •	–58,39±10,01 •
20	M±SD, n=7	M±SD, n=8	M±SD, n=7
	–10,67±7,81	–77,34±8,82	–53,57±8,93
24	Me (Q_I–Q_{III}), n=7	Me (Q_I–Q_{III}), n=8	Me (Q_I–Q_{III}), n=7
	–6,4 (–9,08;–4,37)	–96,48 (–100,0;–79,08)	–45,4 (–66,7;–37,2)

Note. • The difference in SFI values between the Sect and Raph groups is statistically insignificant; the difference in SFI values when comparing all pairs at all other observation time points is statistically significant.

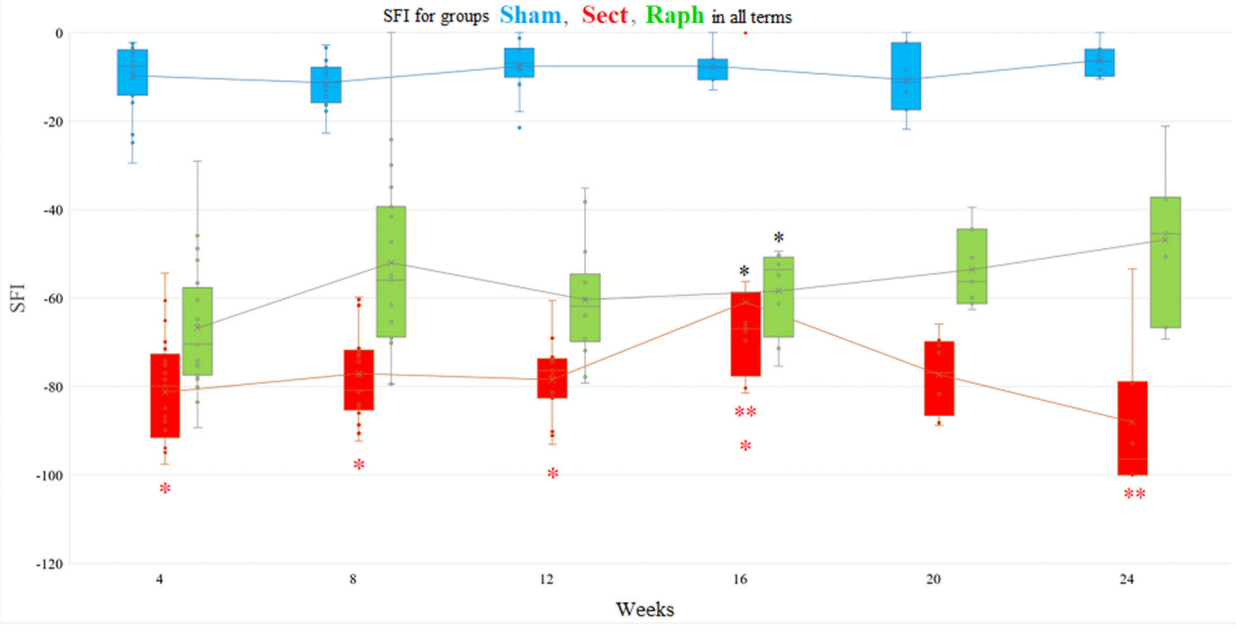

Fig. 3. Actual SFI values of all experimental animals (points; see Table 3), their medians (horizontal lines within the rectangles), the boundaries of the I and III quartiles (parts of the colored bar located below and above the median, respectively, at each time point), mean values (x), standard deviations (distance between the mean value marker and the lower or upper edge of the bar), and the degree of dispersion (variance) beyond the upper and lower quartiles (horizontal whisker bars) of the three experimental groups at all observation time points. The mean values at different observation time points for each group are connected by a solid line of the corresponding color, which only conditionally reflects the temporal dynamics, since in all groups at the same time points a certain number of rats were removed, reducing the number of animals in the group:
*(black, located on top) — the difference in SFI values between the Sect and Raph groups after 16 weeks of observation is statistically insignificant;
*(red, located below) — the difference in SFI values in the Sect group at 4, 8, and 12 weeks of observation compared to the value at 16 weeks of observation is statistically significant;
**(red, located below) — the difference in SFI values in the Sect group at 16 and 24 weeks of observation is statistically significant.

Discussion

Limitations of the method for determining the state of the paretic limb using SFI

The study of the effectiveness of any new method for restoring the function of an injured nerve is carried out under experimental conditions using various models of this pathology. Probably, the most common model today is the injury of the sciatic nerve of an adult rat, specifically its complete transection [31–35, 48]. However, a significant number of questions remain unresolved (standardization of the surgical component, means of verifying nerve regeneration, clinical translation of the obtained results) [44].

Despite the mixed type of the sciatic nerve and the important role of somatosensory signaling in locomotion [49], researchers' attention is focused on monitoring the correlates of the integral motor capability of the paretic limb against the background of sciatic nerve injury. The most common of these is SFI, which reflects the anatomical features of the paretic foot under the condition of its loading during the free unidirectional locomotion of the animal. From this perspective, the index is a functional-anatomical indicator. The method of calculating SFI was proposed and algorithmized by L. De Medinaceli et al. (1982, 1984) [41, 50], subsequently modified and tested [46, 51]. Today, it can be stated that some studies indicate the absence of correlation between SFI values and morphometric indicators of the sciatic nerve in some models of its injury (reviewed [46]), while others demonstrate such a correlation ([42, 52], reviewed [43]). Importantly, SFI values correlate [51] with a more complex and subjective [53, 54] indicator of motor activity of the rat's hind limb, proposed by D.M. Basso, M.S. Beattie, J.C. Bresnahan for assessing motor deficit in animals against the background of spinal cord injury [54, 55]. This indicator may prove to be more sensitive for detecting residual motor deficit after certain types of sciatic nerve injury [51, 56, 57].

Despite the widespread use of SFI, it is important to remember a number of technical limitations of this method for determining the state of the paretic limb [46, 56]: 1) obtaining quality prints is possible only at a moderate speed of the animal passing through the track, 2) the increase in the animal's mass during the experiment changes the characteristics of the prints and can affect the result of the SFI calculation, 3) the clarity of the prints can be significantly distorted due to deformation and positioning of the paretic foot caused by contractures, as well as due to the consequences of autophagic or automutilative disruption of the foot's anatomy. For example, autophagy of the phalanges of the denervated foot [58] usually occurs starting from the third week after injury, is accompanied by infection, regional edema, and dystrophic changes in the foot tissue, and is considered a manifestation of post-traumatic complex regional pain syndrome [58, 59]. Obviously, dystrophic changes in the denervated foot can distort its prints, and chronic pain can cause protective locomotion to limit mechanical irritation, which also affects the prints, including those of the intact foot due to its compensatory overloading [46].

Given the mentioned factors, the relevance of the methodology for assessing the function of the rat's sciatic nerve using SFI is probably satisfactory only after 3 weeks of observation [43]. The individual variability of SFI values, characteristic of any study mentioned here, remains unexplained; its probable causes, among other things, may be individual differences in the segmental sources of nerve fibers of the sciatic nerve [60], and therefore, the muscles innervated by this nerve, as well as the disregard for the high branching of the nerve into branches [61].

Another feature of the modern variant of SFI calculation is the impossibility of its accurate determination in intact animals. For this reason, in the Sham group, the recovery of the SFI value to zero points was not registered. One of the explanations is the peculiarity of the SFI calculation formula, according to which, with complete symmetry of the prints of the hind feet of an intact animal, all members of the formula turn to zero except for the last term, so SFI under such conditions should be –8.8 points. The motivation of Bain, Mackinnon, and Hunter regarding this feature is not clarified due to the inaccessibility of their publication. However, according to E.F. Oliveira et al. (2001) [52], the fact that SFI in healthy intact animals with such a calculation does not equal zero may indicate the limited ability of this method to determine the state of the paretic limb.

Long-term monitoring of consequences is a key requirement from the perspective of quality and safety control of any new treatment method. Paradoxically, there is an extremely limited number of works in which, on the model of sciatic nerve transection and its immediate reconstruction, the state of the neuromuscular apparatus was assessed for more than 3 months, i.e., more than 12-13 weeks or 90 days ([36] — 14 weeks, [37] — 32 weeks, [40] — 24 weeks, [38] — 52 weeks, [39] — 5 months). In some of these works [37], there is no assessment of the motor activity of the paretic limb, at least using SFI.

Comparison of obtained data with results from other research groups

Given the mentioned reservations, it is necessary to compare the data we obtained with the results from other groups. A distinctive feature of the SFI value dynamics we observed is its multiphase nature: in the Sect group, the maximum value occurs at the 16th week of observation, while in the Raph group, it occurs at the 8th and 24th weeks. The phasic nature of SFI dynamics in similar experimental models has been noted in many available studies. For example, in the case of modeling the transection and immediate suturing of the sciatic nerve in rats, L. De Medinaceli et al. (1982) [41] found an increase in the SFI index (calculated using their primary formula) from less than –100 points to approximately –90 points on the 11th day of observation, followed by a decrease to approximately –100 points on the 32nd day. It is not known whether these temporal changes in SFI were statistically significant.

A similar dynamic with a peak on the 10th day of observation (approximately –75 points) was observed by A. Ganguly et al. (2017) [62] after complete transection of the sciatic nerve without neurosuturing in adult male Long Evans rats. In other strains under similar conditions and instruments, they recorded a decrease and stabilization of SFI values (from approximately –75 to –100 points, Wistar strain), a consistently low value

(approximately –100 points, Sprague Dawley strain), a decrease by the 14th day and a gradual increase (from approximately –75 to approximately –100 points, Lewis and Fischer strains). The total observation period in this study was only 35 days. The authors did not perform any statistical verification of the described features of SFI dynamics. Notably, according to the same data, with digital registration and analysis of prints, SFI values were higher than with conventional (analog) methods.

In adult male Sprague Dawley rats, Y. Jung and colleagues (2014) [63], by analysing hind feet prints obtained by the analogue method, recorded an increase in the average SFI value from approximately –100 to about -75 points during the first week after a simulation of complete transection and immediate sciatic nerve suturing similar to ours, a decrease during the 2nd week and a gradual increase to approximately -60 points at the 12th week of the experiment.

According to J.K. Terzis and K.J. Smith (1987) [64], after transection and immediate suturing of the sciatic nerve in adult male Sprague Dawley rats, a biphasic dynamics of SFI (calculated using the primary method [41]) was recorded: from approximately –90 points in the 1st week to approximately –70 points in the 7th week and approximately –90 points in the 12th week of observation. The authors did not perform statistical verification of this dynamics. However, P.J. Evans et al. (1991) [36] under similar experimental conditions noted an increase in the SFI value to approximately –80 points by the end of the first month, a decrease over the next 2 weeks, a repeated increase to approximately –65 points by the end of the 10th week, a decrease by the end of the 12th week, and an increase to –40 points by the 14th week of observation. It is not known whether these changes were statistically significant.

After modeling complete transection and immediate suturing of the sciatic nerve in adult male Sprague Dawley rats, M. Sakuma et al. (2016) [65] detected two peaks in SFI values using digital print registration tools: a narrow peak at the beginning of the second month (approximately 6 weeks after injury modeling, approximately –100 points with an initial value of approximately –130 points) and around the 70th day (10 weeks after injury modeling, approximately –100 points with a value on the 90th day of approximately –120 points). Thus, under these experimental conditions, the authors did not find any signs of SFI recovery over a 3-month observation period. Strangely, the registration and analysis of prints using the same instrument after modeling complete transection of the sciatic nerve even without neurorrhaphy, according to A. Ganguly et al. (2017) [62] for the Sprague Dawley strain, yielded a much higher SFI value on the 35th day—approximately –40 points compared to approximately –120 points [65].

Therefore, after complete transection and immediate suturing of the sciatic nerve in adult male rats, some authors did not find signs of SFI recovery at the beginning of the second month [41] or up to the 12th [64] or 13th week [65], while others recorded it only after 12 weeks [63] or 14 weeks [36]. We were unable to find results from longer studies of SFI levels under these experimental conditions.

Significant discrepancies in SFI monitoring results are also characteristic of: 1) the model of sciatic nerve transection without neurorrhaphy performed on different rat strains [62], 2) obtaining SFI by conventional and digital methods [62], 3) obtaining prints and calculating SFI using the same system, but after sciatic nerve transection without neurorrhaphy (better results — [62]) and with immediate neurorrhaphy (worse results — [65]).

In the study by V.Y. Molotkovets et al. (2020) [39], following isolated transection of the sciatic nerve in adult male rats, the SFI value changed from –(79,3±3,8) points after 1 month post-injury to –(75,0±2,9) points at the end of the 3rd month, and to –(73,2±5,4) points at the end of the 5th month. In the case of immediate neurorrhaphy (we provide corrected data due to the presence of an editorial error [39]), the values changed from –(41,6±3,7) points at the end of the first month to –(33,2±4,4) points at the end of the 3rd month, and to –(21,3±1,2) points at the end of the 5th month of observation, which significantly differs from our data and the data of other authors.

Under similar experimental conditions, O. Goncharuk et al. (2020) [66] found that during the first month after isolated transection of the sciatic nerve in adult male rats, the SFI values were approximately –70 points. In the case of immediate suturing, the values gradually increased, almost linearly, from approximately –70 points 1 week post-injury to approximately –35 points after 4 weeks of observation.

Therefore, our data on SFI recovery following transection and immediate suturing of the rat's sciatic nerve (approximately –60 points at the 12th week) are consistent with the data of Y. Jung et al. (2014) [63] and P.J. Evans et al. (1991) [36], while the results of O. Goncharuk et al. (2020) [66] and V.Y. Molotkovets et al. (2020) [39] indicate much better SFI recovery outcomes.

Heterogeneous dynamics of SFI values can also be observed in the case of autoplasty of the transected sciatic nerve. For example, in a model of excising an 8-millimeter segment of the sciatic nerve and immediately closing the resulting defect with the same fragment in Fischer rats, T. Meder et al. (2021) [40] describe a biphasic dynamics of SFI—an increase from approximately –80 points at the 2nd week of observation to approximately –50 points at the 7th week, a slight decrease by the 10th week, a stable value until the 20th week, and an increase to approximately –50 points by the 24th week of observation. The authors did not determine the statistical significance of all these changes.

The statistical significance of SFI dynamics after sciatic nerve injury remains unexplored. Only one study contains an analysis of the reliability of temporal changes in SFI [42], but in this study, the observation of the injury lasted only 6 weeks. A crush injury, rather than transection of the rat's sciatic nerve, was reproduced. This issue is tangentially addressed in the model of sciatic nerve injury and immediate suturing in rats by L. De Medinaceli et al. (1982) [41], as well as by J.M. Shenaq et al. (1989) in a model of excision and immediate repair of a one-centimeter defect of the rat's sciatic nerve [67]. Attempts to analyze the statistical significance of differences in SFI values at three observation time points (1, 3, and 5 months) after transection or transection and immediate suturing of the rat's sciatic nerve were also made by V.Y. Molotkovets et al. (2020) [39], but the results of this analysis are not provided in the cited

publication. Moreover, the limited number of time points does not reveal all the features of the recovery process dynamics. However, the authors found a statistically significant difference between SFI values at the end of the 3rd and 5th months, but not between the values at the end of the 1st and 3rd months. This observation is consistent with the data of other authors [36] and, to some extent, with our data, which indicate that in the case of transection and immediate suturing of the adult rat's sciatic nerve, a large increase in SFI values (irreversible until the end of observation in each of these experiments) occurs in the late period of the injury, no earlier than the 4th month.

Pathophysiological assumptions and speculative interpretation of the obtained data

It is known that regenerative growth of nerve fibers through the injury zone begins as early as the fourth day after transection and immediate suturing of the sciatic nerve in adult male Sprague Dawley rats. This growth occurs at a rate of 3,2 mm/day, as determined for sensory fibers by studying mechanical sensitivity along the exposed nerve trunk ("pinch test") [68]. Regenerative growth of motor fibers into the portion of the sciatic nerve distal to the crush zone in animals of a similar strain, sex, and age was observed starting from the third day. This was identified through the accumulation of radioactive-labeled (^{3}H) proline in growth cones, previously stereotactically introduced into the anterior horn of the corresponding spinal cord segment. The growth rate of motor fibers ranged from 3,0 to 4,4 mm/day [69]. In mice, the regeneration of large fibers (motor and sensory) starts later and is generally less effective than the regeneration of small, autonomic, and pain fibers [70]. According to these data, knowing the distance from the injury site to the innervation zone, it can be stated that the first fibers will reach the innervation zone of the corresponding muscles after injury and immediate neurorrhaphy of the sciatic nerve in adult rats between the third or fourth day and the end of the first month.

Overall, in our opinion, interpreting the dynamics of the sciatic functional index (SFI) during the first month after sciatic nerve injury should consider the following factors: the rate of regenerative nerve fiber growth, sprouting reinnervation of paretic muscles by fibers from the intact femoral nerve, plasticity at various levels of the motor system, the potential development of pain syndrome, functional compensation of weight-bearing by the intact hind limb, immunogenic demyelination, and remyelination of nerve fibers (reviewed in [30, 44]), alongside the low reliability of the SFI during the first three weeks of observation. For instance, the peak SFI values recorded in some studies [41, 62, 63] during the second week of observation may indicate temporary compensation due to either preserved innervation of the paretic limb muscles for various reasons or additional loading of the intact limb. The rapid decline in SFI may be related to the exhaustion of this compensatory mechanism.

During the second month, the active establishment of functionally significant contacts between regenerating nerve fibers and muscles likely continues (see [37]), which is assumed to influence changes in the SFI. There is evidence that the regeneration of small autonomic and pain fibers begins earlier and yields greater functional outcomes (regarding their respective functions) than the regeneration of large-caliber fibers (motor and sensory) [69]. At this stage and beyond, plasticity processes in both central and peripheral parts of the motor system, including muscles and neuromuscular synapses, play a significant role (reviewed in [30, 44]). Additionally, the dynamics of the trauma zone's organization process may be relevant. Scar consolidation could theoretically contribute to demyelination, reduced conduction velocity, complete or partial action potential blockage, or even the death of individual nerve fibers. The exhaustion of motor neurons overloaded by primary compensatory activity redistribution, which maintained or initially restored connections with the paretic limb muscles, is also possible. If such motor neurons die, it will result in a decrease in the SFI, as observed in the Raph group during the third month. In the Sect group, similar dynamics were observed later, suggesting that processes characteristic of the Raph group in the second and third months may occur in the Sect group during the fourth and fifth months.

The near-linear increase in SFI after sciatic nerve transection and immediate suturing ([39]—over the first five months, [66]—over the first month) or for certain rat strains after sciatic nerve crush modeling ([62]—during the second and third weeks) could be explained by a linear increase in the number of motor fibers reinnervating damaged muscles during the specified period. This would involve a "wedge-shaped" growth front of these fiber groups at a uniform speed but with varying onset times for individual fiber growth. This scenario would resemble one of the mechanisms of ontogenetic growth in nerve fiber bundles, with leaders and followers among them [71, 72]. However, it is doubtful that the sensitivity of the SFI allows for such fine detection of changes in muscle innervation volume.

In general, it can be stated that identifying the role of each of these pathophysiological components in SFI dynamics is currently impossible due to limited knowledge about the molecular and cellular mechanisms of nerve regeneration and the inability to simultaneously monitor each component in real-time. Therefore, the most promising research designs should include not only SFI monitoring but also molecular-genetic, electrophysiological, morphological, and other modern methods applied concurrently.

Conclusions

Despite the relative simplicity of modeling, PNI remains poorly studied. One of the most common models of PNI is the transection of the sciatic nerve in adult rats. The most widely used and currently irreplaceable method for assessing the function of the paretic limb under these experimental conditions is the calculation of the SFI. However, literature data on the behavior of this parameter in this type of PNI vary significantly, are mostly limited to the first three months of observation, and often fail to reveal the reliability of SFI dynamics. According to our findings, in the case of sciatic nerve transection in adult rats, SFI values change in a biphasic manner, with a statistically significant peak at the 16th week of observation. In contrast, in the case of transection followed by immediate suturing, the SFI

dynamics differ significantly, showing two statistically insignificant peaks at the 8th and 24th weeks of the experiment.

A comparison of our data with the results of other groups highlights the limitations of the methodology for studying sciatic nerve injury using SFI. We believe that improving this methodology should involve not only the development of more precise methods of lifetime monitoring of paretic limb function—combined with molecular-genetic, electrophysiological, and morphological analysis—but also the application of relevant statistical methods to assess the significance of temporal changes in the identified parameters over extended observation periods.

Disclosure

Conflict of Interest

The authors declare no conflicts of interest.

Ethical Standards

All procedures performed on experimental animals during the study complied with ethical standards and were approved by the ethics committee of the scientific institution where the research was conducted.

Funding

The study received no external sponsorship.

References

1. Kouyoumdjian JA. Peripheral nerve injuries: a retrospective survey of 456 cases. Muscle Nerve. 2006 Dec;34(6):785-8. doi: 10.1002/mus.20624
2. Taylor CA, Braza D, Rice JB, Dillingham T. The incidence of peripheral nerve injury in extremity trauma. Am J Phys Med Rehabil. 2008 May;87(5):381-5. doi: 10.1097/PHM.0b013e31815e6370
3. Scholz T, Krichevsky A, Sumarto A, Jaffurs D, Wirth GA, Paydar K, Evans GR. Peripheral nerve injuries: an international survey of current treatments and future perspectives. J Reconstr Microsurg. 2009 Jul;25(6):339-44. doi: 10.1055/s- 0029-1215529
4. Antoniadis G, Kretschmer T, Pedro MT, König RW, Heinen CP, Richter HP. Iatrogenic nerve injuries: prevalence, diagnosis and treatment. Dtsch Arztebl Int. 2014 Apr 18;111(16):273-9. doi: 10.3238/arztebl.2014.0273
5. Castillo-Galván ML, Martínez-Ruiz FM, de la Garza-Castro O, Elizondo-Omaña RE, Guzmán-López S. [Study of peripheral nerve injury in trauma patients]. Gac Med Mex. 2014 NovDec;150(6):527-32. Spanish
6. Missios S, Bekelis K, Spinner RJ. Traumatic peripheral nerve injuries in children: epidemiology and socioeconomics. J Neurosurg Pediatr. 2014 Dec;14(6):688-94. doi: 10.3171/2014.8.PEDS14112
7. Bekelis K, Missios S, Spinner RJ. Falls and peripheral nerve injuries: an age-dependent relationship. J Neurosurg. 2015 Nov;123(5):1223-9. doi: 10.3171/2014.11.JNS142111
8. Dalamagkas K, Tsintou M, Seifalian A. Advances in peripheral nervous system regenerative therapeutic strategies: A biomaterials approach. Mater Sci Eng C Mater Biol Appl. 2016 Aug 1;65:425-32. doi: 10.1016/j.msec.2016.04.048
9. Zaidman M, Novak CB, Midha R, Dengler J. Epidemiology of peripheral nerve and brachial plexus injuries in a trauma population. Can J Surg. 2024 Jun 26;67(3):E261-E268. doi: 10.1503/cjs.002424
10. Jiang L, Jones S, Jia X. Stem Cell Transplantation for Peripheral Nerve Regeneration: Current Options and Opportunities. Int J Mol Sci. 2017 Jan 5;18(1). pii: E94. doi: 10.3390/ijms18010094
11. Tapp M, Wenzinger E, Tarabishy S, Ricci J, Herrera FA. The Epidemiology of Upper Extremity Nerve Injuries and Associated Cost in the US Emergency Departments. Ann Plast Surg. 2019 Dec;83(6):676-680. doi: 10.1097/SAP.0000000000002083
12. Kim SJ, Kwon YM, Ahn SM, Lee JH, Lee CH. Epidemiology of upper extremity peripheral nerve injury in South Korea, 2008 to 2018. Medicine (Baltimore). 2022 Dec 2;101(48):e31655. doi: 10.1097/MD.0000000000031655
13. Murphy RNA, de Schoulepnikoff C, Chen JHC, Columb MO, Bedford J, Wong JK, Reid AJ. The incidence and management of peripheral nerve injury in England (2005-2020). J Plast Reconstr Aesthet Surg. 2023 May;80:75-85. doi: 10.1016/j.bjps.2023.02.017
14. Omid R, Stone MA, Zalavras CG, Marecek GS. Gunshot Wounds to the Upper Extremity. J Am Acad Orthop Surg. 2019 Apr 1;27(7):e301-e310. doi: 10.5435/JAAOS-D-17-00676
15. Baker HP, Straszewski AJ, Dahm JS, Dickherber JL, Krishnan P, Dillman DB, Strelzow JA. Gunshot-related lower extremity nerve injuries. Eur J Orthop Surg Traumatol. 2023 May;33(4):851-856. doi: 10.1007/s00590-022-03220-3
16. Dugom PM, Jester MP, Archie WH, Huynh DM, Scarcella JF, Guo Y. Outcomes in Ballistic Injuries to the Hand: Fractures and Nerve/Tendon Damage as Predictors of Poor Outcomes. Hand (N Y). 2024 May;19(3):382-386. doi: 10.1177/15589447221092111
17. Muss TE, Hu S, Bauder AR, Lin IC. The Epidemiology, Management, and Outcomes of Civilian Gunshot Wounds to the Upper Extremity at an Urban Trauma Center. Plast Reconstr Surg Glob Open. 2024 Apr 17;12(4):e5753. doi: 10.1097/GOX.0000000000005753
18. Aman M, Zimmermann KS, Thielen M, Thomas B, Daeschler S, Boecker AH, Stolle A, Bigdeli AK, Kneser U, Harhaus L. An Epidemiological and Etiological Analysis of 5026 Peripheral Nerve Lesions from a European Level I Trauma Center. J Pers Med. 2022 Oct 8;12(10):1673. doi: 10.3390/jpm12101673
19. Shaprynskyi Y, Lypkan V. Treatment of patients with gunshot traumatic amputations of the lower limbs due to explosive injury in the conditions of today's war in Ukraine. Reports of Vinnytsia National Medical University. 2023;27:581-585. 10.31393/reports-vnmedical-2023-27(4)-08
20. Rosberg HE, Carlsson KS, Höjgård S, Lindgren B, Lundborg G, Dahlin LB. Injury to the human median and ulnar nerves in the forearm--analysis of costs for treatment and rehabilitation of 69 patients in southern Sweden. J Hand Surg Br. 2005 Feb;30(1):35-9. doi: 10.1016/j.jhsb.2004.09.003
21. Immerman I, Price AE, Alfonso I, Grossman JA. Lower extremity nerve trauma. Bull Hosp Jt Dis (2013). 2014;72(1):43-52.
22. Wali AR, Park CC, Brown JM, Mandeville R. Analyzing costeffectiveness of ulnar and median nerve transfers to regain forearm flexion. Neurosurg Focus. 2017 Mar;42(3):E11. doi: 10.3171/2016.12.FOCUS16469
23. Foster CH, Karsy M, Jensen MR, Guan J, Eli I, Mahan MA. Trends and Cost-Analysis of Lower Extremity Nerve Injury Using the National Inpatient Sample. Neurosurgery. 2019 Aug 1;85(2):250-256. doi: 10.1093/neuros/nyy265
24. Khalifeh JM, Dibble CF, Dy CJ, Ray WZ. Cost-Effectiveness Analysis of Combined Dual Motor Nerve Transfers versus Alternative Surgical and Nonsurgical Management Strategies to Restore Shoulder Function Following Upper Brachial Plexus Injury. Neurosurgery. 2019 Feb 1;84(2):362-377. doi: 10.1093/neuros/nyy015
25. Bergmeister KD, Große-Hartlage L, Daeschler SC, Rhodius P, Böcker A, Beyersdorff M, Kern AO, Kneser U, Harhaus L. Acute and long-term costs of 268 peripheral nerve injuries in the upper extremity. PLoS One. 2020 Apr 6;15(4):e0229530. doi: 10.1371/journal.pone.0229530
26. Raizman NM, Endress RD, Styron JF, Emont SL, Cao Z, Park LI, Greenberg JA. Procedure Costs of Peripheral Nerve Graft Reconstruction. Plast Reconstr Surg Glob Open. 2023 Apr 10;11(4):e4908. doi: 10.1097/GOX.0000000000004908
27. Karsy M, Watkins R, Jensen MR, Guan J, Brock AA, Mahan MA. Trends and Cost Analysis of Upper Extremity Nerve Injury Using the National (Nationwide) Inpatient Sample. World Neurosurg. 2019 Mar;123:e488-e500. doi: 10.1016/j.wneu.2018.11.192
28. Hicks CW, Wang D, Matsushita K, Windham BG, Selvin E. Peripheral Neuropathy and All-Cause and Cardiovascular

Mortality in U.S. Adults : A Prospective Cohort Study. Ann Intern Med. 2021 Feb;174(2):167-174. doi: 10.7326/M20-1340
29. Trehan SK, Model Z, Lee SK. Nerve Repair and Nerve Grafting. Hand Clin. 2016 May;32(2):119-25. doi: 10.1016/j.hcl.2015.12.002
30. Melikov ZK, Medvediev VV. Peripheral nerve injury: molecular pathophysiology and prospects for restorative treatment by means of cell transplantation: a literature review. Ukr Neurosurg J. 2023Dec.26;29(4):3-12. doi: 10.25305/unj.288785
31. Geuna S. The sciatic nerve injury model in pre-clinical research. J Neurosci Methods. 2015 Mar 30;243:39-46. doi: 10.1016/j.jneumeth.2015.01.021
32. Gordon T, Borschel GH. The use of the rat as a model for studying peripheral nerve regeneration and sprouting after complete and partial nerve injuries. Exp Neurol. 2017 Jan;287(Pt 3):331-347. doi: 10.1016/j.expneurol.2016.01.014
33. Vela FJ, Martínez-Chacón G, Ballestín A, Campos JL, Sánchez-Margallo FM, Abellán E. Animal models used to study direct peripheral nerve repair: a systematic review. Neural Regen Res. 2020 Mar;15(3):491-502. doi: 10.4103/1673-5374.266068
34. Li A, Pereira C, Hill EE, Vukcevich O, Wang A. In Vitro, In Vivo and Ex Vivo Models for Peripheral Nerve Injury and Regeneration. Curr Neuropharmacol. 2022;20(2):344-361. doi: 10.2174/1570159X19666210407155543
35. Varier P, Raju G, Madhusudanan P, Jerard C, Shankarappa SA. A brief review of in vitro models for injury and regeneration in the peripheral nervous system. International Journal of Molecular Sciences. 2022 Jan 13;23(2):816. doi: 10.3390/ijms23020816
36. Evans PJ, Bain JR, Mackinnon SE, Makino AP, Hunter DA. Selective reinnervation: a comparison of recovery following microsuture and conduit nerve repair. Brain Res. 1991 Sep 20;559(2):315-21. doi: 10.1016/0006-8993(91)90018-q
37. Meyer RS, Abrams RA, Botte MJ, Davey JP, Bodine-Fowler SC. Functional recovery following neurorrhaphy of the rat sciatic nerve by epineurial repair compared with tubulization. J Orthop Res. 1997 Sep;15(5):664-9. doi: 10.1002/jor.1100150506
38. Meek MF, Den Dunnen WF, Schakenraad JM, Robinson PH. Long-term evaluation of functional nerve recovery after reconstruction with a thin-walled biodegradable poly (DL-lactide-epsilon-caprolactone) nerve guide, using walking track analysis and electrostimulation tests. Microsurgery. 1999;19(5):247-53. doi: 10.1002/(sici)1098-2752(1999)19:5<247::aid-micr7>3.0.co;2-e
39. Molotkovets VY, Medvediev VV, Korsak AV, Chaikovsky YuB, Tsymbaliuk VI. Restoration of the Integrity of a Transected Peripheral Nerve with the Use of an Electric Welding Technology. Neurophysiology. 2020;52, 31–42. doi: 10.1007/s11062-020-09848-3
40. Meder T, Prest T, Skillen C, Marchal L, Yupanqui VT, Soletti L, Gardner P, Cheetham J, Brown BN. Nerve-specific extracellular matrix hydrogel promotes functional regeneration following nerve gap injury. NPJ Regen Med. 2021 Oct 25;6(1):69. doi: 10.1038/s41536-021-00174-8
41. de Medinaceli L, Freed WJ, Wyatt RJ. An index of the functional condition of rat sciatic nerve based on measurements made from walking tracks. Exp Neurol. 1982 Sep;77(3):634-43. doi: 10.1016/0014-4886(82)90234-5
42. Wang T, Ito A, Aoyama T, Nakahara R, Nakahata A, Ji X, Zhang J, Kawai H, Kuroki H. Functional evaluation outcomes correlate with histomorphometric changes in the rat sciatic nerve crush injury model: A comparison between sciatic functional index and kinematic analysis. PLoS One. 2018 Dec 12;13(12):e0208985. doi: 10.1371/journal.pone.0208985
43. Monte-Raso VV, Barbieri CH, Mazzer N, Yamasita AC, Barbieri G. Is the Sciatic Functional Index always reliable and reproducible? Journal of Neuroscience Methods. 2008;170(2):255-61. doi: 10.1016/j.jneumeth.2008.01.022
44. Tsymbaliuk VI, Medvediev VV, Ivanchov PV, Molotkovets VY, Chaikovsky YB, Korsak AV. [Electrical welding technology in restoring the integrity of the injured peripheral nerve: review of literature and own experimental research]. Ukr Neurosurg J. 2020;26(2):24-33 Ukrainian. doi: 10.25305/unj.199507
45. Dellon ES, Dellon AL. Functional assessment of neurologic impairment: track analysis in diabetic and compression neuropathies. Plast Reconstr Surg. 1991 Oct;88(4):686-94. PubMed PMID: 1896540
46. Varejão AS, Meek MF, Ferreira AJ, Patrício JA, Cabrita AM. Functional evaluation of peripheral nerve regeneration in the rat: walking track analysis. J Neurosci Methods. 2001 Jul 15;108(1):1-9. Review. PubMed PMID: 11459612
47. Tsymbalyuk VI, Petriv TI, Molotkovets VY, Medvedev VV, Luzan BM, inventors; Bogomolets National Medical University, assignee. The device for conducting the "walk on the track" test. Patent of Ukraine 118157. 2017 July 27.
48. Rigoni M, Montecucco C. Animal models for studying motor axon terminal paralysis and recovery. Journal of Neurochemistry. 2017;142:122-9. doi: 10.1111/jnc.13956
49. Frigon A, Akay T, Prilutsky BI. Control of Mammalian Locomotion by Somatosensory Feedback. Compr Physiol. 2021 Dec 29;12(1):2877-2947. doi: 10.1002/cphy.c210020
50. de Medinaceli L, DeRenzo E, Wyatt RJ. Rat sciatic functional index data management system with digitized input. Comput Biomed Res. 1984 Apr;17(2):185-92. doi: 10.1016/0010-4809(84)90031-4
51. Schiaveto de Souza A, da Silva CA, Del Bel EA. Methodological evaluation to analyze functional recovery after sciatic nerve injury. J Neurotrauma. 2004 May;21(5):627-35. doi: 10.1089/089771504774129955
52. Oliveira EF, Mazzer N, Barbieri CH, Selli M. Correlation between functional index and morphometry to evaluate recovery of the rat sciatic nerve following crush injury: experimental study. J Reconstr Microsurg. 2001 Jan;17(1):69-75. doi: 10.1055/s-2001-12691
53. Abdallah I, Medvediev V, Draguntsova N, Voitenko N, Tsymbaliuk V. Dependence of the restorative effect of Macroporous poly(N-[2-Hydroxypropyl]-methacrylamide hydrogel on the severity of experimental lacerative spinal cord injury. USMYJ. 2021 Dec. 26;127(4):8-21. doi: 10.32345/USMYJ.127(4).2021.8-21
54. Medvediev VV, Abdallah IM, Draguntsova NG, Savosko SI, Vaslovych VV, Tsymbaliuk VI, Voitenko NV. Model of spinal cord lateral hemi-excision at the lower thoracic level for the tasks of reconstructive and experimental neurosurgery. Ukr Neurosurg J. 2021Sep.27;27(3):33-5. doi: 10.25305/unj.234154
55. Basso DM, Beattie MS, Bresnahan JC. A sensitive and reliable locomotor rating scale for open field testing in rats. J Neurotrauma. 1995 Feb;12(1):1-21. doi: 10.1089/neu.1995.12.1
56. Dinh P, Hazel A, Palispis W, Suryadevara S, Gupta R. Functional assessment after sciatic nerve injury in a rat model. Microsurgery. 2009;29(8):644-9. doi: 10.1002/micr.20685
57. Amniattalab A, Mohammadi R. Functional, Histopathological and Immunohistichemical Assessments of Cyclosporine A on Sciatic Nerve Regeneration Using Allografts: A Rat Sciatic Nerve Model. Bull Emerg Trauma. 2017 Jul;5(3):152-159.
58. Wall PD, Devor M, Inbal R, Scadding JW, Schonfeld D, Seltzer Z, Tomkiewicz MM. Autotomy following peripheral nerve lesions: experimental anaesthesia dolorosa. Pain. 1979 Oct;7(2):103-11. doi: 10.1016/0304-3959(79)90002-2
59. Coderre TJ, Grimes RW, Melzack R. Autotomy following sciatic and saphenous nerve sections - sparing of the medial toes after treatment of the sciatic-nerve with capsaicin. Experimental Neurology. 1986;91(2):355-65. DOI: 10.1016/0014-4886(86)90075-0
60. Asato F, Butler M, Blomberg H, Gordh T. Variation in rat sciatic nerve anatomy: implications for a rat model of neuropathic pain. J Peripher Nerv Syst. 2000 Mar;5(1):19-21. doi: 10.1046/j.1529-8027.2000.00155.x
61. Rupp A, Schmahl W, Lederer W, Matiasek K. Strain differences in the branching of the sciatic nerve in rats. Anat Histol Embryol. 2007 Jun;36(3):202-8. doi: 10.1111/j.1439-0264.2007.00751.x
62. Ganguly A, McEwen C, Troy EL, Colburn RW, Caggiano AO, Schallert TJ, Parry TJ. Recovery of sensorimotor function following sciatic nerve injury across multiple rat strains. J

Neurosci Methods. 2017 Jan 1;275:25-32. doi: 10.1016/j.jneumeth.2016.10.018
63. Jung Y, Ng JH, Keating CP, Senthil-Kumar P, Zhao J, Randolph MA, Winograd JM, Evans CL. Comprehensive evaluation of peripheral nerve regeneration in the acute healing phase using tissue clearing and optical microscopy in a rodent model. PLoS One. 2014 Apr 8;9(4):e94054. doi: 10.1371/journal.pone.0094054
64. Terzis JK, Smith KJ. Repair of severed peripheral nerves: comparison of the "de Medinaceli" and standard microsuture methods. Exp Neurol. 1987 Jun;96(3):672-80. doi: 10.1016/0014-4886(87)90228-7
65. Sakuma M, Gorski G, Sheu SH, Lee S, Barrett LB, Singh B, Omura T, Latremoliere A, Woolf CJ. Lack of motor recovery after prolonged denervation of the neuromuscular junction is not due to regenerative failure. Eur J Neurosci. 2016 Feb;43(3):451-62. doi: 10.1111/ejn.13059
66. Goncharuk O, Savosko S, Petriv T, Tatarchuk M, Medvediev V, Tsymbaliuk V. Epineurial sutures, polyethylene glycol hydrogel and fibrin glue in the sciatic nerve repair in rats: functional and morphological assessments in experiment. Georgian Med News. 2020 Dec;(309):124-131.
67. Shenaq JM, Shenaq SM, Spira M. Reliability of sciatic function index in assessing nerve regeneration across a 1 cm gap. Microsurgery. 1989;10(3):214-9. doi: 10.1002/micr.1920100315
68. Forman DS, Wood DK, DeSilva S. Rate of regeneration of sensory axons in transected rat sciatic nerve repaired with epineurial sutures. J Neurol Sci. 1979 Dec;44(1):55-9. doi: 10.1016/0022-510x(79)90222-3
69. Forman DS, Berenberg RA. Regeneration of motor axons in the rat sciatic nerve studied by labeling with axonally transported radioactive proteins. Brain Res. 1978 Nov 10;156(2):213-25. doi: 10.1016/0006-8993(78)90504-8
70. Navarro X, Verdú E, Butí M. Comparison of regenerative and reinnervating capabilities of different functional types of nerve fibers. Exp Neurol. 1994 Oct;129(2):217-24. doi: 10.1006/exnr.1994.1163
71. Tessier-Lavigne M, Goodman CS. The molecular biology of axon guidance. Science. 1996 Nov 15;274(5290):1123-33. doi: 10.1126/science.274.5290.1123
72. Breau MA, Trembleau A. Chemical and mechanical control of axon fasciculation and defasciculation. Semin Cell Dev Biol. 2023 May 15;140:72-81. doi: 10.1016/j.semcdb.2022.06.014

Original article

Ukr Neurosurg J. 2024;30(4):43-50
doi: 10.25305/unj.310254

Evaluation of the structures of the optic nerve and chiasm in patients with skull base tumors using high-resolution MRI

Ekaterina S. Egorova [1], Valeriia V. Musulevska [2], Mykola O. Guk [2], Oksana Y. Skobska [3]

[1] Group of Neurophthalmology, Romodanov Neurosurgery Institute, Kyiv, Ukraine
[2] Endonasal Skull Base Surgery, Department Romodanov Neurosurgery Institute, Kyiv, Ukraine
[3] Group of Otoneurology, Romodanov Neurosurgery Institute, Kyiv, Ukraine

Received: 20 August 2024
Accepted: 21 October 2024

Address for correspondence:
Valeriia V. Musulevska, Group of Neurophthalmology, Romodanov Neurosurgery Institute, 32 Platona Mayborody st., Kyiv, 04050, Ukraine, e-mail: musulevskaria@gmail.com

Objective: To investigate the effectiveness of radiological methods for diagnosing optic nerve and chiasm atrophy in compressive optic neuropathy caused by tumors of the chiasmal-sellar region (CSR).

Material and methods: The diagnostic and treatment outcomes of 50 patients (100 eyes) with CSR tumors were analyzed. These patients were treated at the A.P. Romodanov Institute of Neurosurgery of the National Academy of Medical Sciences of Ukraine from 2021 to 2023. The study group of patients (50 patie:nts) was divided into two subgroups: Group I – restoration of visual functions (26 patients, 52%, 52 eyes); Group II – no restoration of visual functions (24 patients, 48%, 48 eyes). Clinical-neurological, ophthalmological, and otoneurological examinations were performed. MRI of the brain was conducted on all patients using high-field scanners (1.5 and 3.0 Tesla), and measurements of the optic nerve (ON) diameter in the intraorbital and intracranial parts, as well as the height and width of the chiasm.

Results: The morphometric parameters of the ON diameter in the intraorbital part and the height of the chiasm did not significantly differ between the studied groups ($p>0.05$). The morphometric parameters of Group I did not differ from the control group ($p>0.05$). In Group II the average diameter of the intracranial part of the ON (2.31±0.26 mm) and the average width of the chiasm (11.39±0.31 mm) were statistically significantly different from the control group values: 2.97±0.2 mm and 13.69±0.57 mm, respectively, $p<0.05$. Despite significant variability in individual characteristics, the parameters of the intracranial part of the ON ≤ 2.31 mm and the chiasm width of ≤ 11.39 mm indicate irreversible atrophic changes and can be used to predict ophthalmological outcomes in patients with CSR tumors.

Conclusions: Measuring the thickness of the chiasm and the diameter of the intracranial part of the optic nerve using high-resolution MRI is a convenient and effective method for diagnosing optic nerve atrophy (ONA) and predicting ophthalmological outcomes after decompression of the optochiasmal complex.

Keywords: *chiasmal-sellar region tumors; high-resolution MRI; compressive optic neuropathy; optic nerve atrophy*

Introduction

The optic chiasm is a crucial neuroanatomical structure in the brain where the optic nerves converge and partially cross. It is located above the area of the tuberculum sellae. Above the chiasm lies the floor of the third ventricle with the *recessus opticus*, as well as the anterior cerebral and anterior communicating arteries, while below, it borders the diaphragm of the tuberculum sellae. The internal carotid arteries are located laterally to the chiasm [1-3] ***(Fig. 1)***.

The total length of the optic nerve (ON) ranges from 35 to 55 mm. It consists of intraorbital, intracanalicular, and intracranial sections. The intracranial section is the most variable, measuring 4–17 mm [4]. Studies using histological methods and magnetic resonance imaging (MRI) at 1.5 Tesla have shown a reduction in the normal diameter of the ON along the intraorbital segment from (3.99±0.04) mm immediately behind the eyeball to (3.50±0.04) mm at a distance of 10 mm from the posterior pole of the eyeball [5]. S. Mncube

and M. Goodier (2019) conducted a study using high-resolution MRI (>1.5 Tesla) and reported a range of normal ON diameters: the intraorbital section at 5 mm from the posterior pole of the eyeball measured 2.52 mm (1.53–3.69 mm), at 10 mm from the posterior pole 2.37 mm (1.44–3.63 mm), and the intracranial section 4.27 mm (2.46–5.19 mm) [6]. According to M. Prairie et al. (2024), an ON diameter of ≤2.3 mm at 10 mm from the posterior pole of the eyeball is a highly sensitive and specific indicator of optic nerve atrophy (ONA) [7]. B. Zhao et al. (2019) found that an ON area of ≤4.0 mm² measured by MRI is both highly sensitive and specific for predicting the presence of ONA [8].

Studies using high-resolution MRI have reported that the average area of the chiasm is between 27.07 and 43.7 mm², with an average length of 5–12 mm, average width of 12.23–15.0 mm, and average height of 1.93–3.5 mm [6, 9, 10]. According to J. Parravano et al. (1993), a chiasm width of <13.5 mm is a marker of optic nerve atrophy (ONA) [11].

The morphometric parameters of the optic nerve (ON) and chiasm reported in the literature vary, but most researchers agree that the width of the chiasm and the diameter of the intracranial portion of the ON are reliable measurement indicators [6].

Assessing the morphometric parameters of the ON and chiasm with MRI can provide additional information for diagnosing ONA and predicting ophthalmological outcomes following the removal of tumors in the chiasmal-sellar region (CSR). However, there are few reports on average chiasm sizes based on MRI in the healthy population, and existing data are inconsistent. Given the individual variability in chiasm size and ON thickness, identifying parameters that could supplement objective ophthalmological data on atrophic changes in the visual pathway is relevant.

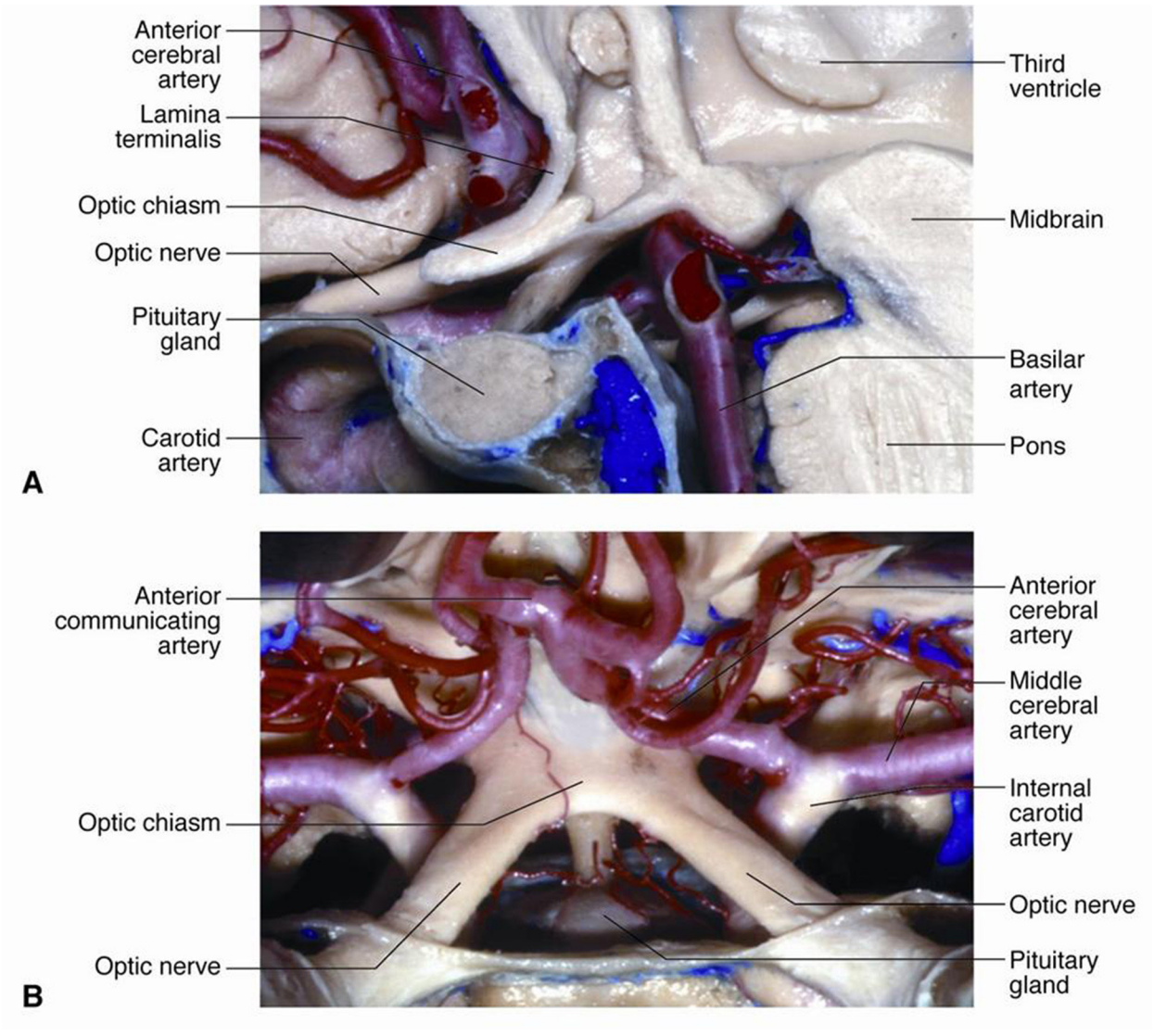

Fig. 1. Anatomy of the chiasmal-sellar region: A – sagittal section; B – horizontal section. The intracranial part of the optic nerves is shown [1]

This article contains some figures that are displayed in color online but in black and white in the print edition.

Objective: To analyze the effectiveness of radiological methods for diagnosing optic nerve and chiasm atrophy in compressive optic neuropathy caused by tumors in the chiasmal-sellar region.

Materials and Methods

Study participants

The diagnostic and treatment outcomes of 50 patients (100 eyes) with chiasmal syndrome caused by CSR tumors—pituitary adenomas in 26 patients (52%) and tuberculum sellae meningiomas in 24 patients (48%)—were analyzed. These patients received treatment at the A.P. Romodanov Institute of Neurosurgery, National Academy of Medical Sciences of Ukraine, from 2021 to 2023 (study group). The study group included 25 women (50%) and 25 men (50%), with an average age of 50.50±10.21 years.

The study was conducted in compliance with bioethics principles, including the provisions of the Declaration of Helsinki on human rights, and was approved by the Ethics Committee of the A.P. Romodanov Institute of Neurosurgery, National Academy of Medical Sciences of Ukraine (minutes No. 5, dated 13.12.2019). All patients provided informed and voluntary written consent to participate in the study and for data publication.

Inclusion criteria

The inclusion criteria were: pituitary adenomas and tuberculum sellae meningiomas without optic nerve canal involvement, presence of chiasmal syndrome, and a follow-up period of at least 12 months.

Exclusion criteria included progressive tumor growth, supradiaphragmatic craniopharyngiomas and other CSR tumors with cystic components, patients with signs of intracranial hypertension, prior radiation therapy or surgery, and concurrent ophthalmological diseases. Craniopharyngiomas were excluded from the study as the visual impairment in these cases is caused not only by optic nerve atrophy (ONA) but also by tumor invasion into the ON and/or chiasm. Assessing the extent of visual function restoration is challenging due to potential intraoperative devascularization of the visual apparatus, which significantly affects postoperative visual acuity.

Group characteristics

Based on ophthalmological outcomes following CSR tumor removal, patients were divided into two subgroups: Group I, with restoration of visual functions (26 patients, 52%, 52 eyes), and Group II, without restoration of visual functions (24 patients, 48%, 48 eyes). The control group consisted of 20 healthy adults (40 eyes) with no ophthalmological or neurosurgical pathology.

Study Design

The patients underwent clinical-neurological, ophthalmological, and otoneurological examinations using instrumental and laboratory diagnostic methods.

All patients underwent MRI of the brain using high-field scanners (1.5 and 3.0 Tesla) in native mode and with contrast enhancement in three projections. Standard brain imaging protocols included T1WI and T2WI T2WI slices. MRI was performed at least two weeks prior to surgery. The ON diameter was measured at two points: the intraorbital section (10 mm from the posterior pole of the eyeball) and the intracranial section (5–6 mm from the chiasm) in the axial projection ***(Fig. 2)***. The height of the chiasm was measured in the frontal (coronal) projection, and the width of the chiasm in the axial projection ***(Fig. 3)***.

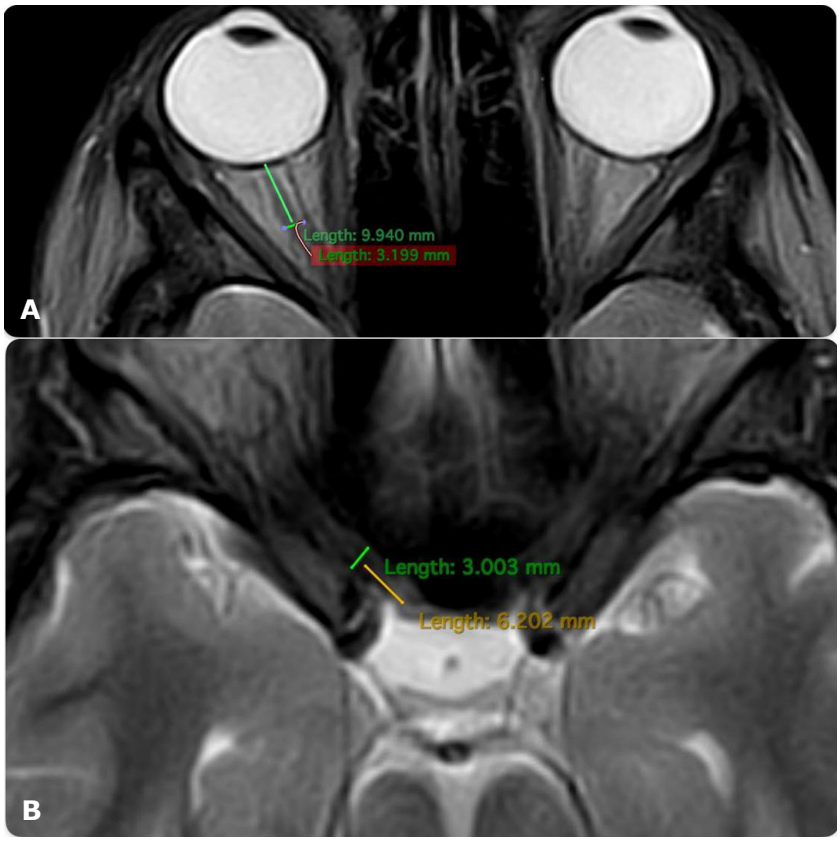

Fig. 2. Technique for measuring the diameter of the optic nerve (brain MRI, axial projection, T1-weighted images):
A – intraorbital part;
B – intracranial part

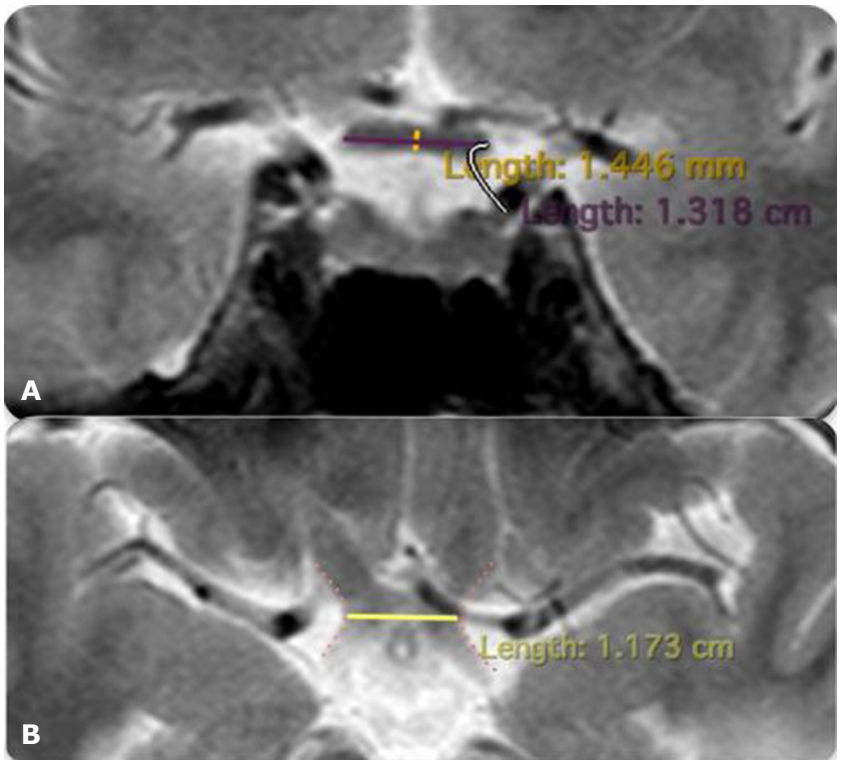

Fig. 3. Technique for measuring chiasm parameters:
A – height (brain MRI, coronal projection T1WI-weighted images), marked by a yellow line;
B – width (brain MRI, axial projection T1WI-weighted images), marked by a yellow line

The ophthalmological examination included visometry, biomicroscopy, perimetry (both kinetic and static), and ophthalmoscopy (both direct and indirect). The first examination was performed on the 1st–2nd day after hospital admission, the second on the 5th–7th day of the postoperative period (early postoperative period), and follow-ups were conducted at 1, 3, and 6 months, as well as at 1 year. Examinations continued throughout the year if delayed (late) visual function recovery was observed.

Visual acuity was tested with optimal correction. The visual field was assessed using the Centerfield 2 perimeter (Germany) with the "Threshold test neuro - 30-2" and "Neuro screening" programs, focusing on defect localization and the mean deviation (MD) indicator of total light sensitivity loss.

Visual function recovery was defined as an improvement in visual acuity to ≥1.0, elimination of visual field defects, and MD < -2 dB in both eyes.

Statistical Analysis

Data were entered into Excel and analyzed using the "Statistica 6.0" software. Results are presented as the mean ± standard deviation (M±SD). To assess the significance of differences (p-value) between independent groups, Student's t-test for paired samples was applied. A p-value < 0.05 was considered statistically significant. Pearson's χ^2 test or Fisher's exact test was used to evaluate the distribution frequency for traits when the sample size was small.

Results and Discussion

The results of the morphometric measurements of the ON and chiasm are presented in ***Tables 1*** and ***2***.

A uniform age distribution was found across both groups (p > 0.05). Patients in the study groups demonstrated reduced visual acuity and visual field defects in the form of bitemporal heteronymous hemianopia (complete or partial) ***(Figures 4*** and ***5)***.

It was established that the average visual acuity values (Group I – 0.66±0.31, Group II – 0.55±0.32) and the average total light sensitivity loss before surgery (group I – 13.81±0.82 dB, group II – 15.32±0.71 dB) did not differ significantly (p>0.05). However, the duration of visual impairments was significantly different (Group I – 5.35±4.38 months, Group II – 21.80±0.32 months, p<0.05).

The diameter of the ON in the intraorbital part and the chiasm height did not differ significantly between groups (p>0.05). There was also no statistically significant difference in morphometric parameters between group I and the control group (p>0.05). In group II, the average diameter of the intracranial part of the optic nerve (2.31±0.26 mm) and the average chiasm width (11.39±0.31 mm) were significantly smaller than in the control group (2.97±0.20 mm and 13.69±0.57 mm, respectively, p<0.05). The diameter of the intraorbital part of the optic nerve and the chiasm height in group II tended to decrease, though the difference was not statistically significant (p>0.05).

In healthy individuals, the average optic nerve diameter was: intraorbital part – 3.08±0.25 mm, intracranial part – 2.97±0.20 mm, consistent with values reported by S.S. Mncube and M.D. Goodier (2019) [6], at 2.52 mm (1.53–3.69 mm) and 4.27 mm (2.46–5.19 mm), and the average chiasm width (13.69±0.57 mm) aligns with findings from S.S. Mncube and M.D. Goodier (2019), – 13.63 mm (11.13–16.92 mm), and is only slightly different from values reported by S.O. Polat et al. (2020) – 12.82±1.27 mm and V. Juenger et al. (2020) – 12.23±1.15 mm [9, 10].

According to the literature [6, 9, 10], the chiasm height in healthy individuals varies from 1.93 to 3.5 mm, which is consistent with our findings of 2.01±0.35 mm. The lack of a statistically significant difference in chiasm height across the studied groups suggests low diagnostic value for this parameter in diagnosing optic nerve atrophy (ONA), likely due to the difficulty of measuring small structures under chiasmal compression.

An intracranial optic nerve diameter of ≤2.31 mm and a chiasm width of ≤11.39 mm indicate irreversible atrophic changes and may be used to predict ophthalmic outcomes in patients with skull base tumors. These findings align with the conclusion by M. Prairie et al. (2024) that an intracranial optic nerve diameter of ≤2.3 mm is a highly sensitive and specific marker for ONA [7]. According to J. Parravano et al. (1993), a chiasm width of <13.5 mm is a sign of ONA. Such conflicting conclusions may stem from technical challenges in using low-resolution MRI to measure small structures in the visual pathway [11].

The results obtained suggest that a reduction in chiasm width and intracranial optic nerve diameter occurs earlier than reductions in chiasm height and the diameter of the intraorbital part of the ON.

Table 1. Clinical and morphometric characteristics of the study groups

Clinical data	Group I n=26	Group II n=24	Student's t-test value, p
Age, years	51,50±11,38	50,4±9,5	t=0,07 p>0,05
Visual Acuity	0,66±0,31	0,55±0,32	t=0,25 p>0,05
MD, dB	13,81±0,82	15,32±0,71	t=1,39 p>0,05
Disease duration, months	5,35±4,38	21,80±0,32	t=3,75* p<0,05
Diameter of intraorbital part of ON, mm	2,99±0,16	2,88±0,26	t=0,36 p>0,05
Diameter of intracranial part of ON, mm	2,84±0,25	2,31±0,26	t=0,64 p>0,05
Chiasm Height, mm	2,13±0,35	1,97±0,24	t=0,38 p>0,05
Chiasm Width, mm	12,86±0,32	11,39±0,31	t=3,3* p<0,05

Note: * – The difference in values is statistically significant.

Table 2. Average morphometric parameters of the optic nerve and chiasm, mm

Group	Diameter of intraorbital part of ON	Diameter of intracranial part of ON	Chiasm height	Chiasm width
Control Group, n=20	3,08±0,25	2,97±0,20	2,01±0,35	13,69±0,57
Group I, n=26	2,99±0,16	2,84±0,25	2,13±0,35	12,86±0,32
Group II, n=24	2,88±0,26	2,31±0,26*	1,97±0,24	11,39±0,31*

Note: * – The difference in values is statistically significant.

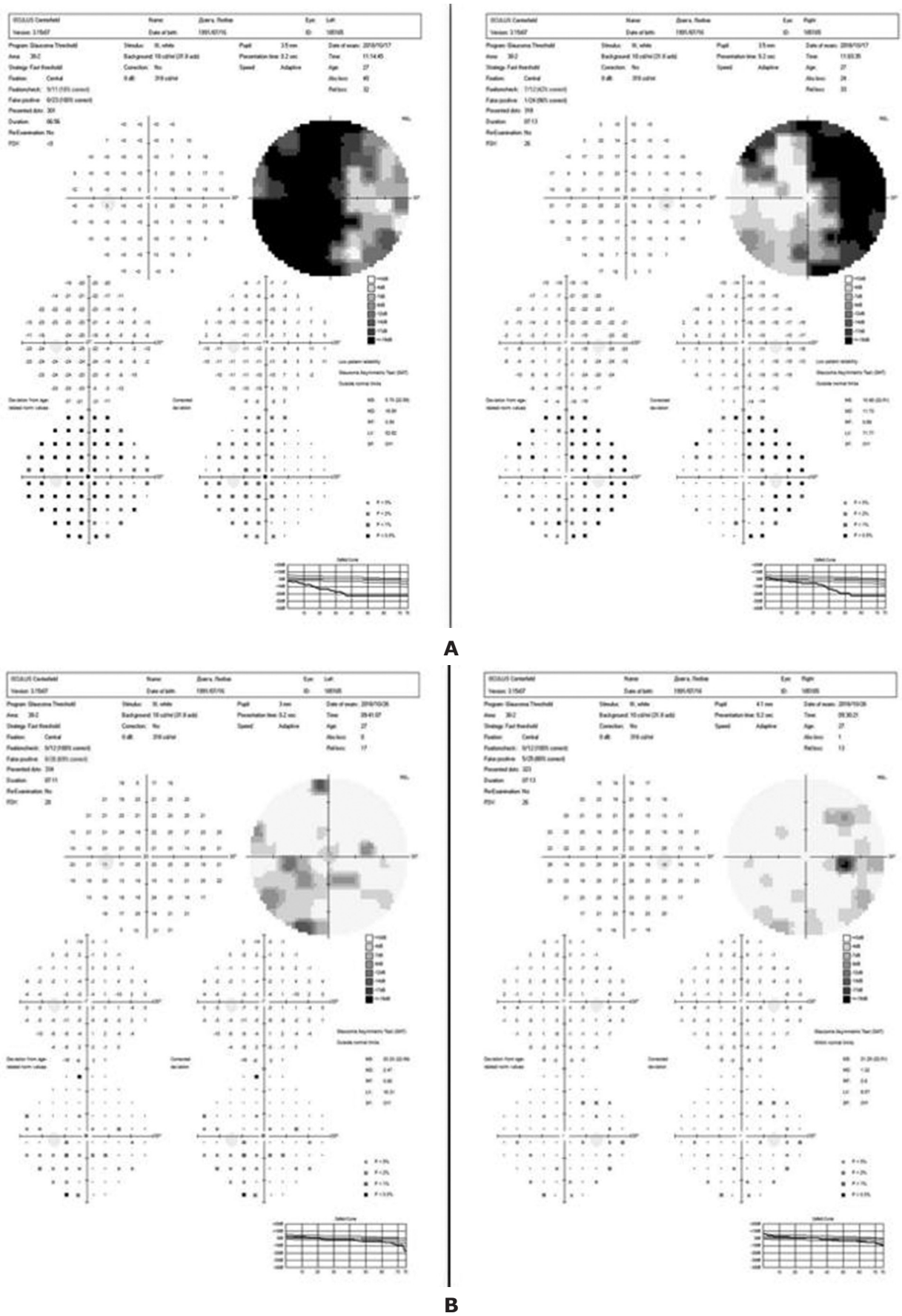

Fig. 4. Automated static perimetry of a patient from group I: A – before surgery; B – after surgery

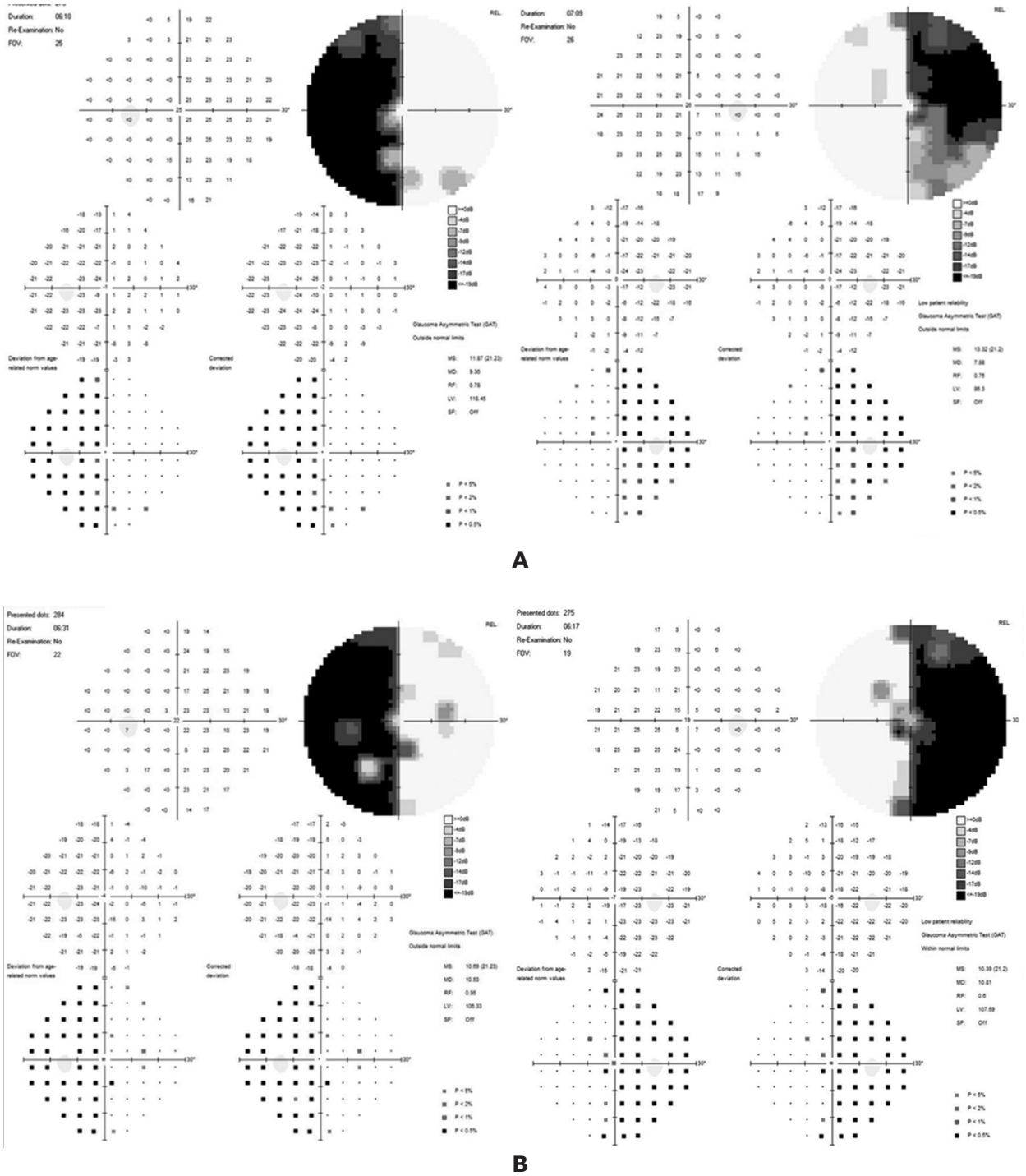

A

B

Fig. 5. Automated static perimetry of a patient from Group II: A – before surgery; B – after surgery.

Conclusions

High-resolution MRI enables informative visualization of the structures of the visual pathway and the characteristics of CSR.

In cases of compressive optic neuropathy, an intracranial optic nerve diameter of ≤2.31 mm and a chiasm width of ≤11.39 mm indicate atrophic changes, which can serve as a convenient supplementary diagnostic tool for optic nerve atrophy (ONA). These indicators can be used to predict visual recovery outcomes in the surgical treatment of certain chiasmal-sellar region.

Disclosure

Conflict of Interest

The authors declare no conflict of interest.

Ethical Standards

All procedures performed on patients during the study adhered to the ethical standards of the institutional and national ethics committees and to the 1964 Declaration of Helsinki and its later amendments or comparable ethical standards.

Informed Consent

Informed consent was obtained from all patients.

Funding

The study received no sponsorship or financial support.

References

1. Rhoton AL Jr. The sellar region. Neurosurgery. 2002 Oct;51(4 Suppl):S335-74. doi: 10.1097/00006123-200210001-00009
2. Danesh-Meyer HV, Yoon JJ, Lawlor M, Savino PJ. Visual loss and recovery in chiasmal compression. Prog Retin Eye Res. 2019 Nov;73:100765. doi: 10.1016/j.preteyeres.2019.06.001
3. Gupta M, Ireland AC, Bordoni B. Neuroanatomy, Visual Pathway. 2022 Dec 19. In: StatPearls. Treasure Island (FL): StatPearls Publishing; 2024 Jan–.
4. Kiernan JA, Barr ML. Barr's the human nervous system: an anatomical viewpoint. Lippincott Williams & Wilkins; 2014.
5. Karim S, Clark RA, Poukens V, Demer JL. Demonstration of systematic variation in human intraorbital optic nerve size by quantitative magnetic resonance imaging and histology. Invest Ophthalmol Vis Sci. 2004 Apr;45(4):1047-51. doi: 10.1167/iovs.03-1246
6. Mncube SS, Goodier MD. Normal measurements of the optic nerve, optic nerve sheath and optic chiasm in the adult population. SA J Radiol. 2019 Nov 5;23(1):1772. doi: 10.4102/sajr.v23i1.1772
7. Prairie ML, Gencturk M, McClelland CM, Marka NA, Jiang Z, Folkertsma M, Lee MS. Establishing Optic Nerve Diameter Threshold Sensitive and Specific for Optic Atrophy Diagnosis. Clin Neuroradiol. 2024 Jun;34(2):373-378. doi: 10.1007/s00062-023-01369-w
8. Zhao B, Torun N, Elsayed M, Cheng AD, Brook A, Chang YM, Bhadelia RA. Diagnostic Utility of Optic Nerve Measurements with MRI in Patients with Optic Nerve Atrophy. AJNR Am J Neuroradiol. 2019 Mar;40(3):558-561. doi: 10.3174/ajnr.A5975
9. Polat SÖ, Öksüzler FY, Öksüzler M, Uygur AG, Yücel AH. The determination of the pituitary gland, optic chiasm, and intercavernous distance measurements in healthy subjects according to age and gender. Folia Morphol (Warsz). 2020;79(1):28-35. doi: 10.5603/FM.a2019.0058
10. Juenger V, Cooper G, Chien C, Chikermane M, Oertel FC, Zimmermann H, Ruprecht K, Jarius S, Siebert N, Kuchling J, Papadopoulou A, Asseyer S, Bellmann-Strobl J, Paul F, Brandt AU, Scheel M. Optic chiasm measurements may be useful markers of anterior optic pathway degeneration in neuromyelitis optica spectrum disorders. Eur Radiol. 2020 Sep;30(9):5048-5058. doi: 10.1007/s00330-020-06859-w
11. Parravano JG, Toledo A, Kucharczyk W. Dimensions of the optic nerves, chiasm, and tracts: MR quantitative comparison between patients with optic atrophy and normals. J Comput Assist Tomogr. 1993 Sep-Oct;17(5):688-90. doi: 10.1097/00004728-199309000-00003

Original article

Ukr Neurosurg J. 2024;30(4):51-56
doi: 10.25305/unj.312398

Surgical treatment of meningiomas invading the superior sagittal sinus

Mykhaylo S. Kvasha, Anatoliy V. Spiridonov

Extracerebral Tumor Department, Romodanov Neurosurgery Institute, Kyiv, Ukraine

Received: 29 September 2024
Accepted: 04 November 2024

Address for correspondence:
Anatoliy V. Spiridonov, Extracerebral Tumor Department, Romodanov Neurosurgery Institute, 32 Platona Mayborody st., Kyiv, 04050, Ukraine, e-mail: av.spiridonov0202@gmail.com

Objective: To investigate the impact of the degree of invasion of the superior sagittal sinus by meningiomas on the radicality of removal and to assess the risks of complications during surgical intervention for superior sagittal sinus meningiomas.

Materials and Methods: The study included 82 patients who underwent surgery at the Romodanov Neurosurgery Institute over the past 10 years (from 2013 to 2023). The cohort comprised 53 women and 29 men, with an average age of 43.4±1.7 years. Inclusion criteria are: a histologically confirmed diagnosis of meningioma and evidence of superior sagittal sinus invasion based on neuroimaging (MRI with intravenous contrast enhancement, MSCT angiography).

Results: A total of 84 surgical procedures were performed on 82 patients. Among these, 71 were primary cases (84.5%), and 13 were secondary cases (15.5%). In 7 out of 13 secondary surgeries, superior sagittal sinus invasion was first detected through neuroimaging and confirmed intraoperatively. Postoperative hemiparesis of varying degrees was observed in 41 patients (50%), with 10 cases showing an increase in neurological deficits due to surgical intervention. Motor deficits completely regressed within 3-6 months post-surgery in 28 out of 41 patients. Tumor recurrence was identified in 4 patients (4.9%) within 2.5-6 years after the primary surgery. Among these, 3 were morphologically confirmed as "anaplastic meningioma Grade III," and 1 as "atypical meningioma Grade II".

Conclusions: Meningiomas originating from the arachnoid membrane constitute a significant proportion of primary intracranial tumors, with varying degrees of venous sinus invasion. Surgical planning for meningiomas invading the superior sagittal sinus should consider the radiological classification of invasion degrees, which aids in determining the treatment strategy. MRI with intravenous contrast and MSCT angiography are crucial for identifying collateral blood flow and assessing the degree of venous sinus invasion before surgical intervention.

Keywords: *meningioma; superior sagittal sinus; angiography; hemiparesis*

Introduction

Meningiomas are benign tumors originating from the arachnoid membrane and account for 14–19% of all primary intracranial neoplasms [1]. Neurosurgical treatment of meningiomas that invade the sagittal sinus and cause partial or complete occlusion is a challenging task [2]. One aspect of the diagnostic problem for meningiomas in the sagittal sinus region is the preoperative determination of their relationship with the major brain arteries and the dura mater sinuses. Neuroimaging techniques, such as contrast-enhanced magnetic resonance imaging (MRI) ***(Fig. 1)*** and multislice computed tomography (MSCT) angiography ***(Fig. 2)***, enable the assessment of the tumor's relationship with the major arteries and venous sinuses.

A retrospective comparison of angiographic data with intraoperative and pathological findings has identified a number of characteristic radiological features that allow the determination of the relationship between meningiomas in the sagittal sinus region and the major brain arteries and venous sinuses in the preoperative period. This issue is also complicated by the frequent involvement of draining veins in the tumor, whose injury can lead to the appearance or worsening of neurological deficits in patients. Aggressive removal of these tumors may result in sinus thrombosis, leading to venous infarction and worsening neurological symptoms depending on the location of the meningioma.

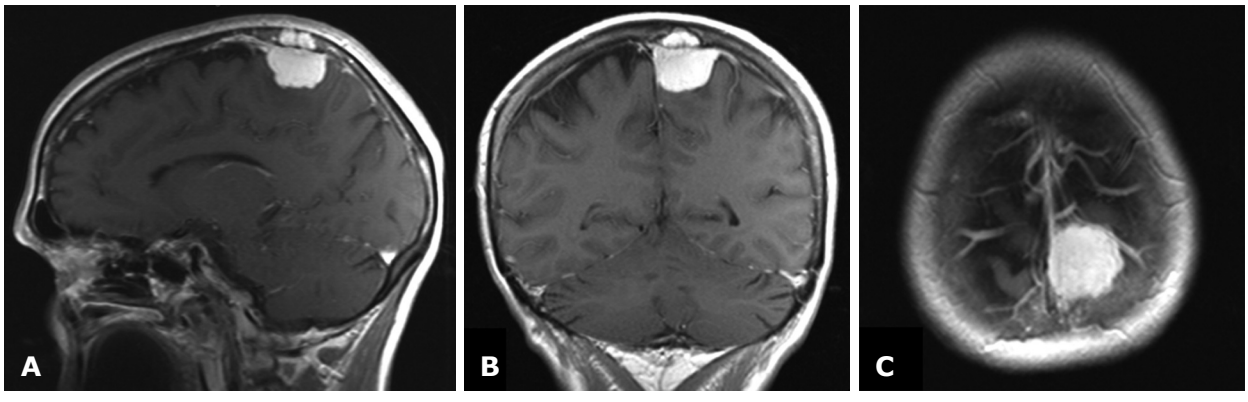

Fig. 1. Brain MRI. Meningiomas of the mid-posterior third of the superior SSS in T1-weighted contrast-enhanced mode: A - sagittal projection, B - frontal projection, C - axial projection

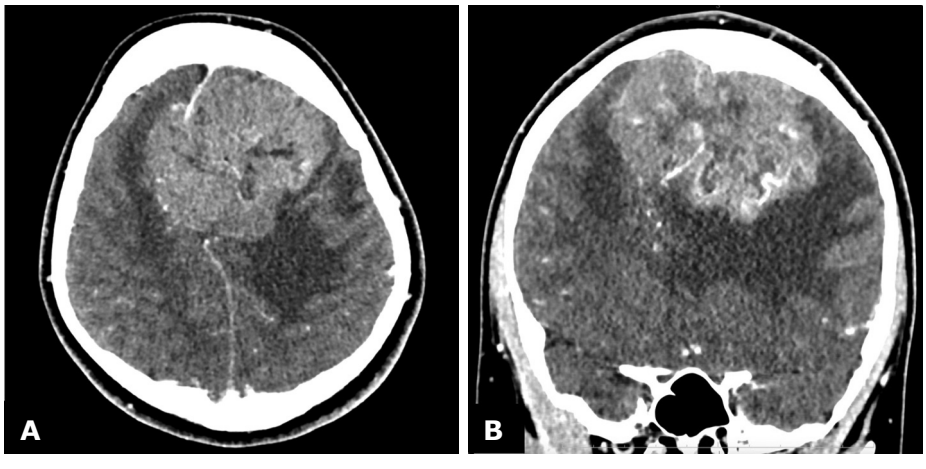

Fig. 2. MSCT - angiography. Giant meningioma of the anterior and middle third of the SSS with total occlusion of the superior sagittal sinus in the venous phase: A - axial projection; B - frontal projection

Materials and Methods

Study participants

The study included 82 patients operated on at the Romodanov Neurosurgery Institute during the last 10 years (2013–2023). There were 53 women, and 29 men. The mean age of the patients was (43.4±1.7) years.

The study was approved by the ethics and bioethics committee of the Romodanov Institute of Neurosurgery, National Academy of Medical Sciences of Ukraine (minutes No. 3 dated December 16, 2020). All participants provided informed and voluntary written consent for participation in the study and publication of data.

Inclusion Criteria

1) A histologically confirmed diagnosis of meningioma.

2) Evidence of invasion into the superior sagittal sinus (SSS) based on neuroimaging data (contrast-enhanced MRI, MSCT angiography).

3) Surgical intervention for a meningioma involving the superior sagittal sinus.

Group Characteristics

Type I invasion of meningioma of the superior sagittal sinus (SSS) by the classification of M.P. Sindou and J.E. Alvernia was detected in 50 (61.0%) patients, type II - in 9 (11.0%), type III - in 5 (6.0%), type IV - in 5 (6%), type V - in 6 (7.3%) and type VI - in 7 (8.7%).

Most meningiomas (71%) of the superior sagittal sinus site were located in the middle third of the sinus, corresponding to the segment from the coronal to the lambdoid suture, consistent with literature data (45.0–70.5%). Meningiomas in the anterior third of the sinus (from the crista galli to the coronal suture) accounted for 22% (18 patients), while those in the posterior third of the sinus accounted for 7% (6 patients).

In 68 cases (81%), a conservative approach was employed involving coagulation of the falx cerebri. In 16 cases (19%), an aggressive approach was taken, including resection of the affected portion of the falx cerebri, with resection of the affected SSS segment in 12 cases (75%).

Study Design

The study is retrospective.

Statistical Analysis

Data processing and analysis were performed using descriptive statistics, univariate and multivariate analysis, and survival assessment methods. The

This article contains some figures that are displayed in color online but in black and white in the print edition.

following software was used: Statistica v.10 (StatSoft® Inc., USA, license No. STA862D175437Q), SPSS 17.0 (IBM, USA), MedCalc (MedCalc Software Ltd, Ostend, Belgium; www.medcalc.org, trial versions 20.113 (2022) and 20.218 (2023)) The Shapiro-Wilk test was applied to verify the conformity of quantitative variables to a normal distribution. For normally distributed data, parametric statistics were used, including: mean (M), standard error of the mean (m), standard deviation (SD), comparisons were made using Student's t-tests for independent (t) and dependent (T) samples. The statistical significance of differences in categorical data was assessed using Pearson's χ^2 test.

Results

One of the critical factors to consider during surgical planning is the presence of collateral circulation developed during tumor growth [3]. In our practice, in addition to contrast-enhanced MRI, MR angiography or MSCT angiography was frequently employed for surgical planning. In 73% of patients, collateral blood flow was detected via magnetic resonance venography in cases of superior sagittal sinus occlusion.

Lesions of the SSS with complete lumen occlusion were identified in 6 cases via direct sinusography.

In 5 cases, a local filling defect of the SSS was recorded at the site of partial invasion of its lumen by the tumor. Indirect signs suggestive of potential tumor invasion into the SSS wall include the vascular shadow of the tumor in the sinus projection area [4]. Another diagnostic indicator is the outward deviation of the peripheral ascending branches of the callosomarginal artery. This sign indicates meningioma infiltration into the parasagittal angle, implying contact with the SSS wall. This is further supported by the displacement of the A4–A5 segments of the anterior cerebral artery across the midline.

Thus, careful examination of angiograms in patients with SSS meningiomas allows surgeons to preoperatively assess the degree of involvement of major brain vessels and dura mater sinuses in the tumor process.

Based on the obtained data, the following focal craniographic signs of intracranial meningiomas indicate the tumor's proximity to the bone: productive changes such as hyperostosis, bone thickening characterized by "swelling with irregular trabecular remodeling," and bone hypervascularization primarily due to the expansion and increased number of diploic channels. These features are diagnostically significant as they provide insights into both the localization and type of tumor. These signs are most commonly associated with meningiomas located on the convexity and, to a lesser extent, the basal surfaces of the cerebral hemispheres. It is important to note that hyperostosis (often diffuse) may sometimes be the only radiological sign of intraosseous or "en plaque" meningiomas [5].

Osteolytic changes such as thinning, protrusion, or erosion of the bone also suggest proximity to the tumor. However, these changes may also occur in other benign neoplasms. Bone resorption or osteoporosis, particularly in the convexity regions of the skull, can result not only from tumor effects but also from prolonged intracranial hypertension. Therefore, evaluating these signs requires considering clinical manifestations as well.

Radiological classification of venous sinus invasion:

Group 1 - partial sinus occlusion (<50%)

Group 2 - subtotal sinus occlusion (50–99%)

Group 3 - total venous sinus occlusion

To determine the degree of invasion using this classification, intravenous-enhanced MRI is used to assess meningioma spread, complemented by MSCT angiography ***(Table 1)***.

Patients were also classified according to the widely accepted classification by M.P. Sindou and J.E. Alvernia ***(Figs. 3 and 4)***.

The majority (71%) of SSS meningiomas were located in the middle third of the sinus, corresponding to the area between the coronal and lambdoid sutures, aligning with data from the literature (45.0–70.5%). Meningiomas of the anterior third of the sinus (from the crista galli to the coronal suture) accounted for 22% (18 patients), while those of the posterior third of the sinus made up 7% (6 patients) ***(Fig. 5)***.

The clinical symptoms in patients with SSS meningiomas included seizures (29.3%), headaches (89.0%), and varying degrees of hemiparesis (37.8%).

Surgical Treatment

Patients were positioned laterally in a park-bench position or supine with head fixation using a three-point Mayfield clamp. A horseshoe-shaped skin incision, based at the SSS, was made with particular attention to preserving the integrity of the periosteum for subsequent dura mater reconstruction. Craniotomy was performed, typically using two burr holes placed in the SSS projection based on MRI and MSCT angiography data. Bone flap craniotomy was extended across the midline. The next step involved incision and possible resection of the affected dura mater, devascularization of the tumor from the falx cerebri and SSS, piecemeal tumor resection, and removal. In 68 cases (81%), a conservative approach with coagulation of the falx cerebri was adopted, while in 16 cases (19%), an aggressive approach involving excision of the affected segment of the falx cerebri was employed, with SSS resection in 12 (75%) of these cases. The latter was predominantly observed in patients with type V and VI invasion as per M.P. Sindou and J.E. Alvernia's classification. All 12 patients underwent the SSS reconstruction of the dura mater using the periosteum, muscle, or "TachoComb" (Takeda, Austria). Dural defect repair was conducted with the periosteum or artificial dura to prevent postoperative cerebrospinal fluid (CSF) leakage.

Table 1. Distribution of patients by degree of superior sagittal sinus invasion in this study

Angiographic type	Degree of sinus invasion	Number of patients
Group 1	<50%	49 (59,8%)
Group 2	50–99%	11 (13,4%)
Group 3	Total	22 (26,8%)

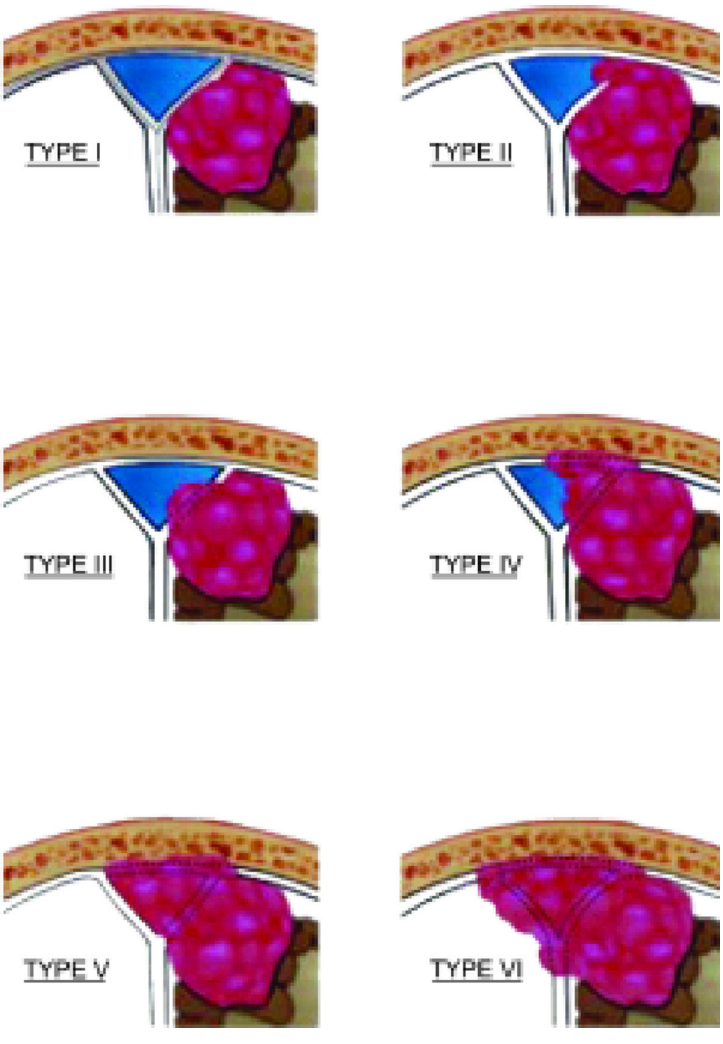

Fig. 3. Schematic representation of types of invasion of the SSS. Type I – the meningioma is adjacent to the outer wall of the sinus; type II – invasion into the lateral corner of the SSS; type III – invasion into the ipsilateral wall of the sinus; type IV – invasion into both the ipsilateral wall and roof of the sinus; type V – total occlusion of the sinus, but the contralateral wall remains intact; type VI – total invasion of the SSS involving all walls of the sinus

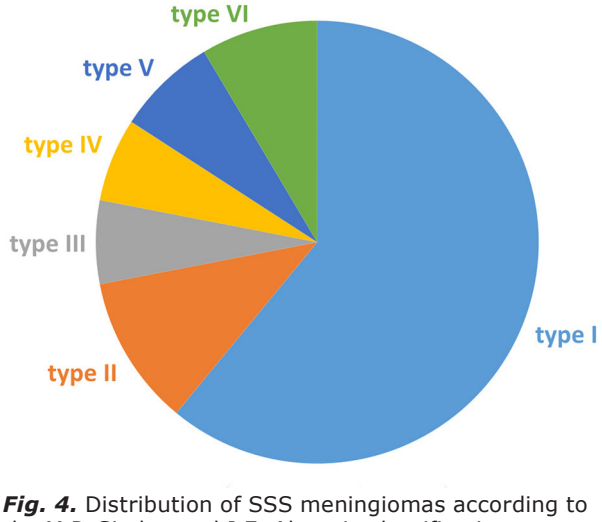

Fig. 4. Distribution of SSS meningiomas according to the M.P. Sindou and J.E. Alvernia classification

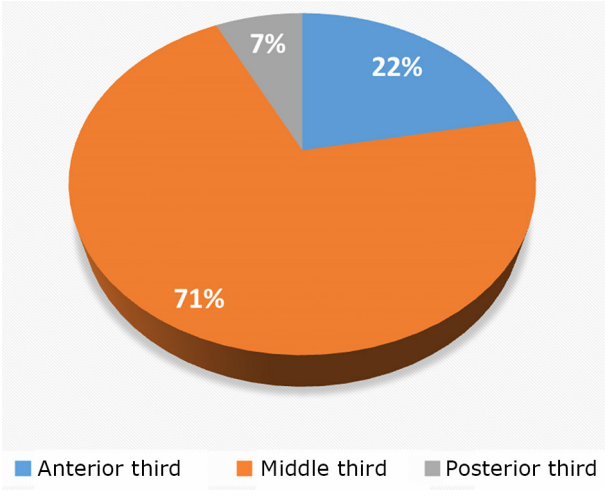

Fig. 5. Distribution of patients based on the "growth zone" of the tumor concerning the SSS

A total of 84 surgical procedures were performed on 82 patients, including 71 (84.5%) primary surgeries and 13 (15.5%) reoperations. Among the 13 reoperations, invasion into the SSS was newly detected in 7 cases based on neuroimaging and confirmed intraoperatively (p=0.001).

Two reoperations were necessitated by epidural hematoma due to low molecular weight heparin administration for SSS thrombosis prevention. Of the 68 subtotal tumor resections (Simpson III) [7], caused by residual tumor in the sinus cavity, 21 (30.9%) patients were elderly (>75 years), and in 42 (61.8%), the tumor involved the middle third of the SSS with venous drainage involvement.

Partial SSS thrombosis was diagnosed in 5 asymptomatic cases (6%) on postoperative MSCT angiography, correlating with type V-VI invasion according to M.P. Sindou and J.E. Alvernia (p=0.001).

Postoperative CSF leakage occurred in 3 (3.6%) cases, which were managed conservatively with lumbar drainage for 4–5 days and anti-edema therapy without requiring further surgery.

In the postoperative period, 41 (50.0%) patients experienced varying degrees of hemiparesis. Neurological deficits worsened in 10 patients due to surgery but fully regressed within 3–6 months in 28 cases.

Seizure control (Engel I: seizure-free) was achieved in 22 (91.7%) out of 24 patients with preoperative epilepsy after 3–6 months of follow-up [8].

Within 3 months after surgery, 27 (32.9%) patients complained of recurrent headache.

Persistent tumor growth was detected in 4 patients (4.9%) between 2.5–6.0 years postoperatively. Histological analysis confirmed "anaplastic meningioma Grade III" in 3 cases and "atypical meningioma Grade II" in 1 case [9]. All patients were referred for radiosurgical treatment, achieving remission consistent with the literature (p<0.05) [10].

Conclusions

Meningiomas originating from the arachnoid membrane represent a significant portion of primary intracranial tumors with varying degrees of venous sinus invasion. Surgical planning for SSS-invasive meningiomas should consider radiological invasion classifications to guide treatment strategy.

Preoperative MRI with intravenous contrast and MSCT angiography allow for identifying collateral blood flow and determining the degree of sinus invasion.

Recognizing angiographic vascularization features of meningiomas aids in surgical strategy. A clear understanding of the topography of afferent tumour vessels facilitates intraoperative identification and timely blockage of them to prevent excessive bleeding which complicates the performance of the planned volume of surgical intervention.

Postoperative monitoring of neurological status and complications remains critical for patients undergoing surgical treatment of SSS meningiomas.

Disclosure

Conflict of Interest

The authors declare no conflicts of interest.

Ethical Standards

All procedures performed on patients during the study adhered to the ethical standards of the institutional and national ethics committees, as well as the 1964 Helsinki Declaration and its subsequent amendments or comparable ethical standards.

Informed Consent

Informed consent was obtained from all patients.

Funding

The study was not supported by any sponsorship.

References

1. Aghi M, Barker Ii FG. Benign adult brain tumors: an evidence-based medicine review. Prog Neurol Surg. 2006;19:80-96. doi: 10.1159/000095184
2. Schmutzer M, Skrap B, Thorsteinsdottir J, Fürweger C, Muacevic A, Schichor C. Meningioma involving the superior sagittal sinus: long-term outcome after robotic radiosurgery in primary and recurrent situation. Front Oncol. 2023 Jul 11;13:1206059. doi: 10.3389/fonc.2023.1206059
3. Gatterbauer B, Gevsek S, Höftberger R, Lütgendorf-Caucig C, Ertl A, Mallouhi A, Kitz K, Knosp E, Frischer JM. Multimodal treatment of parasagittal meningiomas: a single-center experience. J Neurosurg. 2017 Dec;127(6):1249-1256. doi: 10.3171/2016.9.JNS161859
4. Gagliardi F, De Domenico P, Snider S, Pompeo E, Roncelli F, Barzaghi LR, Acerno S, Mortini P. Efficacy of radiotherapy and stereotactic radiosurgery as adjuvant or salvage treatment in atypical and anaplastic (WHO grade II and

III) meningiomas: a systematic review and meta-analysis. Neurosurg Rev. 2023 Mar 17;46(1):71. doi: 10.1007/s10143-023-01969-7
5. Gravbrot N, Rock CB, Weil CR, Rock CB, Burt LM, DeCesaris CM, Jensen RL, Shrieve DC, Cannon DM. Gross Tumor and Intracranial Control Benefits with Fractionated Radiotherapy Compared with Stereotactic Radiosurgery for Patients with WHO Grade 2 Meningioma. World Neurosurg. 2024 Aug;188:e259-e266. doi: 10.1016/j.wneu.2024.05.093
6. Sindou MP, Alvernia JE. Results of attempted radical tumor removal and venous repair in 100 consecutive meningiomas involving the major dural sinuses. J Neurosurg. 2006 Oct;105(4):514-25. doi: 10.3171/jns.2006.105.4.514
7. Simon M, Gousias K. Grading meningioma resections: the Simpson classification and beyond. Acta Neurochir (Wien). 2024 Jan 23;166(1):28. doi: 10.1007/s00701-024-05910-9
8. Fisher RS, van Emde Boas W, Blume W, Elger C, Genton P, Lee P, Engel J Jr. Epileptic seizures and epilepsy: definitions proposed by the International League Against Epilepsy (ILAE) and the International Bureau for Epilepsy (IBE). Epilepsia. 2005 Apr;46(4):470-2. doi: 10.1111/j.0013-9580.2005.66104.x
9. Torp SH, Solheim O, Skjulsvik AJ. The WHO 2021 Classification of Central Nervous System tumours: a practical update on what neurosurgeons need to know-a minireview. Acta Neurochir (Wien). 2022 Sep;164(9):2453-2464. doi: 10.1007/s00701-022-05301-y
10. Lubgan D, Rutzner S, Lambrecht U, Rössler K, Buchfelder M, Eyüpoglu I, Fietkau R, Semrau S. Stereotactic radiotherapy as primary definitive or postoperative treatment of intracranial meningioma of WHO grade II and III leads to better disease control than stereotactic radiotherapy of recurrent meningioma. J Neurooncol. 2017 Sep;134(2):407-416. doi: 10.1007/s11060-017-2540-7

Original article

Ukr Neurosurg J. 2024;30(4):57-63
doi: 10.25305/unj.313077

Minimizing skull defects in retrosigmoid approach: precision mapping of the sigmoid sinus with mastoid emissary vein canal

Artem V. Rozumenko, Mykola V. Yehorov, Vasyl V. Shust, Dmytro M. Tsiurupa, Anton M. Dubrovka, Petro M. Onishchenko, Volodymyr O. Fedirko

Department of Subtentorial Neuro-Oncology, Romodanov Neurosurgery Institute, Kyiv, Ukraine

Received: 10 October 2024
Accepted: 04 November 2024

Address for correspondence:
Artem V. Rozumenko, Department of Subtentorial Neuro-Oncology, Romodanov Neurosurgery Institute, 32 Platona Mayborody st., Kyiv, Ukraine, 04050, e-mail: dr.rozumenko@gmail.com

Objective. The retrosigmoid approach is a commonly used cranial approach to the cerebellopontine angle lesions, vascular and nerve pathologies. This study aims to develop a practical technique for intraoperative mapping of the sigmoid sinus using the topography of the mastoid emissary vein (MEV) canal to improve the accuracy of retrosigmoid craniotomy, and minimize postoperative adverse outcomes.

Materials and methods. Consecutive patients who underwent retrosigmoid approaches for cerebellopontine angle occupying lesions from October 2023 through August 2024 were included in the study. Perioperative computed tomography (CT) was performed with a slice thickness 0.5 mm in the axial plane. The projection of the internal opening of the MEV canal onto the external surface of the mastoid process was determined as the posterior border sigmoid sinus and anterior border for craniotomy. Comparative analyses were performed using t-test and Chi-square test.

Results. A total of 20 patients were operated for neoplasms occupying the cerebellopontine angle using retrosigmoid approach. The average measured distance from the external opening of the MEV canal to the projection of sigmoid sinus posterior border was 9.36 ± 2.17 mm (range 6.3–13.20 mm). The postoperative CT data showed statistically significant differences between the study and control groups in measures of bone window ($p = 0.057$) and surrounding cranial defect ($p < 0.001$). The size of bone flaps was slightly similar in all groups ($p = 0.114$). The mean cranial defect in the study group was almost twice smaller than in the control group 22.4% vs. 44.5% respectively.

Conclusions. This study confirms the utility of mastoid emissary vein canal topography in improving the accuracy of retrosigmoid craniotomy. By facilitating precise sigmoid sinus mapping, the technique reduces the extent of bone removal and minimizes postoperative cranial defect.

Keywords: *Mastoid emissary vein canal; retrosigmoid craniotomy; mastoid foramen; cranial topography*

Abreviations: MF – mastoid foramen; MEV – mastoid emissary vein; RSA – retrosigmoid approach; RSC – retrosigmoid craniotomy; CPA – cerebellopontine angle; SS – sigmoid sinus

Introduction

The retrosigmoid approach (RSA) is a well-established cranial approach to the cerebellopontine angle (CPA), commonly used for the resection of various neoplasms, vascular anomalies, and cranial nerve pathologies [1]. Existing external anatomical landmarks for RSA, such as the occipitomastoid suture, asterion and mastoid foramen (MF), are known to be highly variable [2, 3, 4]. In rural surgical practices, this variability often necessitates a two-step retrosigmoid craniotomy (RSC), where initial bone removal over the cerebellar hemisphere is followed by further bone drilling to expose the venous sinuses. Precise craniotomy planning and intraoperative orientation are crucial for minimizing unnecessary cranial defects and reducing the risk of inadvertent sinus exposure, which carries a high risk of laceration [5, 6, 7].

Previous anatomical studies have revealed topographic variations in the mastoid emissary vein (MEV) canal in cadaver specimens, which offer valuable insights for improving surgical mapping and reducing the risk of excessive bleeding or thromboembolic complications during RSA [2, 3, 4, 8]. Efforts to delineate the posterior border of sigmoid sinus (SS) using alternative external anatomical landmarks, such as the digastric point, have not consistently clarified the trajectory of the superior aspect of the SS [5, 6].

Other studies have evaluated the accuracy of 3D CT reconstruction and navigation techniques in identifying the junction of the transverse sinus and SS during

retrosigmoid craniotomies. These studies highlight the reliability of navigation based on anatomical landmarks while underscoring the limitations of using the asterion as a reference point [7, 8, 9, 10].

This study is aimed to develop practical technique of intraoperative sigmoid sinus posterior border mapping using topography of the MEV canal to facilitate precise maximally lateral craniotomy for cerebellar retraction and skull defect minimization.

Materials and Methods

Study Design

This study employed a prospective cohort design to investigate the efficacy and outcomes of SS mapping technique in RSA surgery. The study adhered to ethical guidelines of the Declaration of Helsinki and institutional review board approval.

Patient Selection

Consecutive patients who underwent retrosigmoid approaches for CPA occupying lesions from October 2023 through August 2024 were included in the study. Informed consent was obtained from all patients before surgery.

Imaging

Perioperative CT was performed on Aquilion ONE (Toshiba, Japan) with a slice thickness of 0.5 mm in the axial plane and a 0.25 mm slice reconstruction interval.

Image processing

The CT data were processed using Horos 3.3.6 (Horos Project, GNU Lesser General Public License, Version 3). The data series were visualized in 3D MPR mode with a CT bone window regime (WL 300, W 1500).

The MF (external opening of MEV canal) was identified using axial scans in the horizontal plane. Subsequently, the angle of the horizontal plane was adjusted by manipulating the horizontal axis on sagittal images to align with the internal opening of the MEV canal. This maneuver allowed visualization of nearly the entire MEV canal length, clarifying its direction within the bone and its inclination angle.

The projection of the internal opening of the MEV canal onto the external surface of the mastoid process was determined by constructing a perpendicular line to the external mastoid surface. The distance between the projection points and the MF was measured ***(Fig. 1)***.

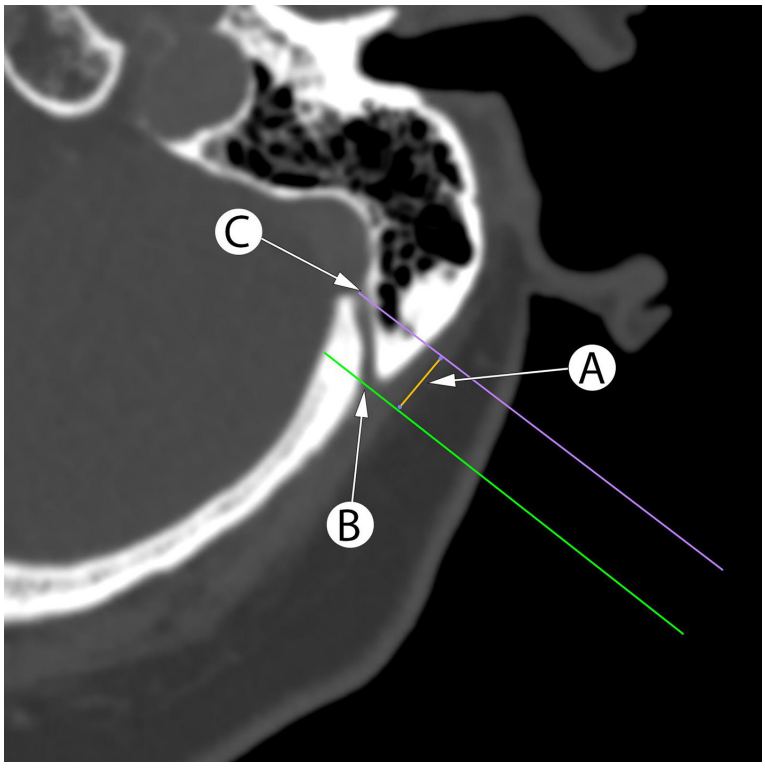

Fig. 1. Planning the retrosigmoid craniotomy using axial CT scans with measurement of the distance (A) between perpendicular lines to mastoid surface between the mastoid foramen (B) and internal opening of the MEV canal (C) projection corresponds to projection of the sigmoid sinus posterior border

This article contains some figures that are displayed in color online but in black and white in the print edition.

Surgical procedure

The RSA was performed in the park bench position with rigid head fixation. We used standard retroauricular slightly C-shaped skin incision with further periosteal dissection forming one soft tissue flap. After coagulation of MEV, the MF was sealed with bone wax. The posterior border projection of the SS at the level of MF was identified according to preoperative calculations. The line "A" connecting calculated point with digastric point was recognized as posterior border SS and anterior border for the craniotomy. The asterion was always selected as the upper border of planned craniotomy. The initial burr hole was placed over the cerebral hemisphere at the medial lower part of the surgical wound. After blunt dura separation, the bone cutting was performed with high-speed drill including asterion, MF and digastric groove in one or two step maneuvers without additional use of rongeurs to widen the craniotomy.

Data Collection

Patient demographics, short-term postoperative complications, and outcomes were documented. All clinical and neuroimaging data were stored in a local hospital database.

Statistical Analysis

Descriptive statistics were used to summarize patient characteristics, and outcomes were presented as frequencies and percentages. Continuous variables were reported as means with standard deviations or medians with interquartile ranges, as appropriate. Comparative analyses were performed using Chi-square test for categorical variables, and the two-sample t-test was applied for comparing continuous variables. P-value < 0.05 was considered statistically significant.

Results

A total of 20 patients were operated on for CPA lesions using the RSA. The study group consisted of 10 patients where craniotomy was performed with MEV topography data ***(Tab. 1)***, other 10 patients were in the control cohort.

The MEV canal was presented in all cases of study group on CT as hypodense straight structure passing close to the Frankfort Horizontal Plane with one or two external openings ***(Fig. 2A and 2B)***. In our series only in 2 cases the MEV canal had curved "S" like form in axial or sagittal plane ***(Fig. 2C and 2D)***. The medium distance between external and internal MEV canal opening was 11.90 ± 1.18 mm (range 9.40–14.10 mm). The medium measured distance "A" from the external opening of the MEV canal to the projection of SS posterior border was 9.36 ± 2.17 mm (range 6.3–13.20 mm).

Intraoperatively in all cases of study group the MEV was found on the retromastoid area as a thin-walled vessel with intact circulation. The intraoperative anatomy was consistent with the preoperative CT findings. The MEV was managed in standard fashion, dissected and coagulated followed by waxing of MF.

The postoperative CT data ***(Fig. 3)*** showed statistically significant differences between study and control groups in measures of bone window (p = 0.057) and surrounding cranial defect (p < 0.001). The size of bone flaps was slightly similar in all groups (p = 0.114). The data of calculations are presented in ***Table 2***.

The mean cranial defect in the study group was almost twice smaller than in the control group (22.4% vs. 44.5%). Additionally, the maximal cranial defect in the study group was smaller than the minimal defect in the control group (31.4% vs. 34.4%).

Table 1. Clinical and anatomical data of patients in the MEV topography study group

Case	Side	Age	MEV canal length, mm	MEV canal shape	MF external opening, n	Bone thickness, mm	Distance to sagittal sinus, mm	Bone flap square, cm2	Window square, cm2	Cranial defect, % to the whole craniotomy
1	L	28	11.60	S	2	6.9	9.30	7.50	9.70	22.68
2	L	53	13.60	S	1	11.8	11.80	7.40	10.30	28.16
3	R	72	12.30	C	1	12.17	10.50	5.90	8.60	31.40
4	L	59	11.10	S	1	7.34	8.70	6.50	8.50	23.53
5	L	56	14.10	S	2	7.61	10.60	5.30	7.30	27.40
6	R	39	9.40	S	1	6.32	7.10	8.70	10.50	17.14
7	L	63	11.30	S	1	12.74	8.10	6.80	9.20	26.09
8	L	37	11,5	S	2	8.76	8.20	5.90	7.20	18.06
9	L	26	14.10	C	2	11.79	13.20	10.62	12.06	11.94
10	L	34	9.6	S	2	8.77	6.13	6.95	8.40	17.26

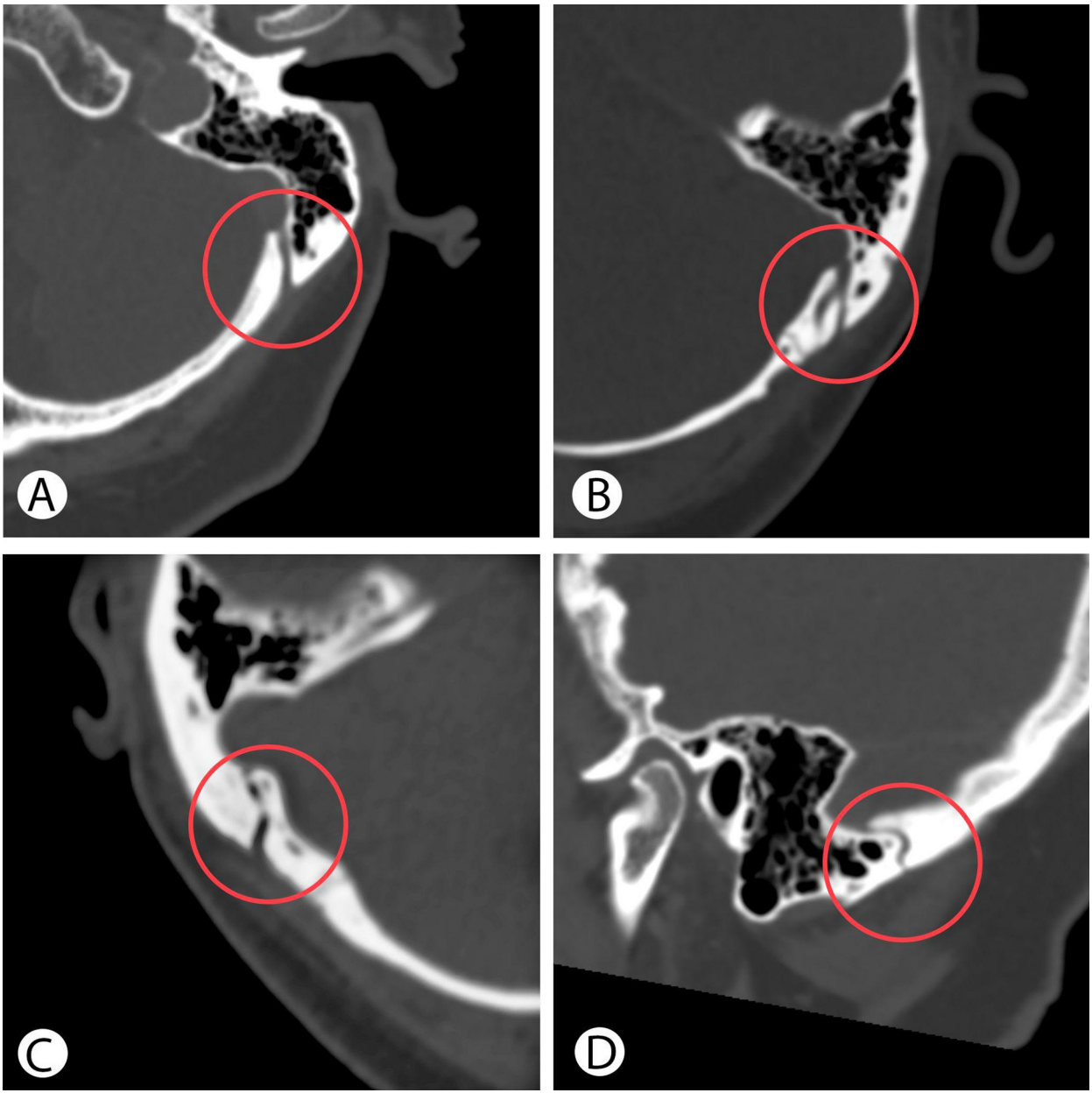

Fig. 2. Preoperative CT reveals the straight shape of the MEV canal in axial plane (A), with two external openings (B), a curved shape in axial (C) and sagittal plane (D).

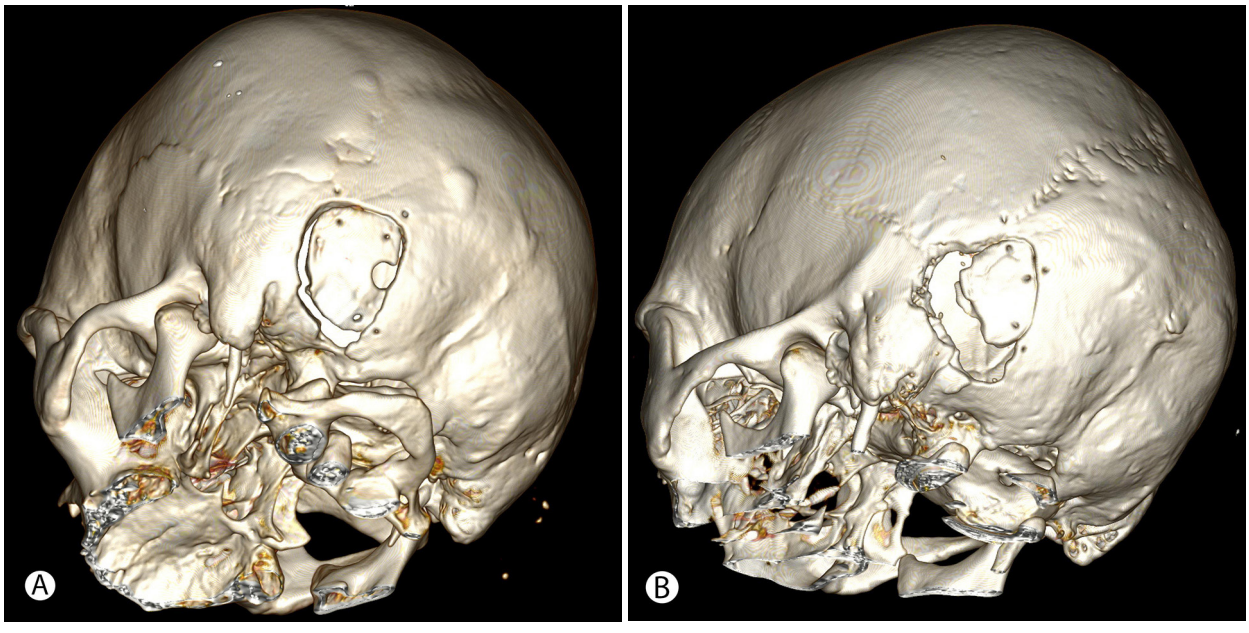

Fig. 3. Postoperative CT after retrosigmoid approach with the use of MEV topography shows minimal linear cranial defect (A), compared to a wide retromastoid defect due to additional bone removal after initially insufficient craniotomy (B)

Table 2. Comparison of demographic parameters and surgical outcomes between study and control groups

Descriptives	Study group	Control group	P–value
Number of patients, n	10	10	–
Median age, yrs	47	54	0.236
Age range, yrs	26–72	33–72	
Mean bone flap ± m, cm2	7.16 ± 1.55	6.05 ± 1.41	0.114
Bone flap range, cm2	5.30–10.62	4.10–8.30	
Mean bone window ± m, cm2	9.18 ± 1.51	10.93 ± 2.27	0.057
Bone window range, cm2	7.20–12.06	7.30–14.70	
Mean cranial defect ± m, %	22.26 ± 6.11	44.47 ± 7.21	< 0.001
Cranial defect range, %	11.94–31.40	34.38–55.96	

Discussion

The retrosigmoid approach plays a crucial role in neurosurgery, providing access to the posterior fossa for various pathologies at CPA. Enhanced visualization on all CPA levels implies following the classical rule for exposition of the posterior margin of the SS as a lateral border of the RSC. The SS projection has an individual relation with external bone landmarks [3, 4, 8]. This fact provoked the profound study of regional anatomy of most prominent bone structures such as asterion, mastoid sulcus and mastoid foramen (MF) with its emissary vein to find the topographical patterns and prevent the complications caused by local venous system interruption [5, 6, 11, 13].

Tubbs et al. (2009) [8] performed a study aimed to enhance the precision of the RSC by investigating external bony landmarks on 100 adult skulls. The authors' technique included both side skull drilling from inside at the transverse-sigmoid sinus junction area. The position of the burr hole was measured from a well-defined horizontal zygomatic line and vertical mastoid line. The results indicated consistent patterns for left and right sides, but revealed variability of measured distances with a standard deviation of 8.35 mm for zygomatic line and 7.25 mm for mastoid line. These findings emphasize the significance of refining landmark data for accurate external localization of the area near the transverse-sigmoid sinuses for RSA planning.

The study of Hampl et al. (2018) [4], involving 295 skulls, comprehensively evaluated both quantitative and qualitative parameters of the MF. The MEV passing through the MF holds crucial neurosurgical significance due to its variable presence near the occipitomastoid suture, posing a risk of bleeding in surgical approaches through the mastoid process, particularly in RSA. The work reveals that expecting a variable location and number of mastoid emissary veins (MEVs), often with two external openings (41.2%). Internal openings predominantly occur as a single foramen (76%) with a median length of the MEV canal 9,3 mm. The work focuses on the prevention of dyshemic complications associated with venous system disorders and the need for preoperative neuroimaging to prevent predictable situations in the surgical field. However, the technical part of performing RSA, taking into account data on the individual anatomy of the MEV canal, was beyond the scope of these and other predominantly anatomical studies [2, 3, 11].

Neuronavigation supports transverse and SS mapping and helps in planning and performing RSA. The group of 30 patients was analyzed by da Silva et al. [9] showed prevalence of image-guidance over anatomical surface landmarks. In an even smaller group of patients, Hamasaki et al. [7] demonstrated the advantage of 3D reconstruction of CT data and the establishment of a topographic relations of the sinus projection to external bony landmarks without neuronavigation.

In 2021, Kubo et al. [6] proposed a line that is an extension of the digastric groove to determine the position of the initial burr hole for RSA. The aim of the study was to determine the safe zone of skull perforation outside the sinus passage in trigeminal neuralgia. Although the authors do not mention the use of neuroimaging methods to create access and perform a precise craniotomy. However, on the detailed diagram they show the significant variability in the location of external landmarks such as the asterion relative to the projection of the adjacent sinuses.

The study of Rosen et al. [12] focuses on the CT morphometric features of MEV. Through the evaluation of 100 consecutive patients with vestibular schwannomas, the research highlights notable anatomical variations in the number, size, and intraosseous length of MEVs, emphasizing the necessity of thin-slice CT for accurate preoperative planning. The detection rate of MEVs in thin-slice CT scans was significantly different from standard CT scans. Using thin-slice CT data the MEVs localization and diameter could be predicted to prevent surgical injuries.

The following studies by Hu et al. [10] proposed the use of a coordinate system based on 3D reconstruction of CT data. Several landmarks except asterion were identified and marked on the outer surface of the skull: the midpoint of the posterior edge of the external auditory canal, the apex of the mastoid process and the digastric groove apex. To locate the key point for burr hole above the sinus, the ratio of segments of the transected lines was calculated, instead of absolute values.

The publication of Hall [13] in 2019 summarized the results of previous morphometric studies. Eight methods of key point localisation were used on 50 models of 3D skulls. The authors prefer methods that allow the use of bone landmarks directly within the surgical field to reduce the possible errors due to the surgical draping and soft tissues. Although the selected techniques operate with the indents that are indicated in absolute numbers, the burr hole enhances surgical effectiveness while reducing the risk of complications linked to excessive exposure of venous sinuses or the creation of oversized bony defects.

The present study focused on clinical implementation of previously described cranial landmarks to develop a simple technique of precise RSA to avoid time-consuming bone removal, tearing of the sinus wall, and postoperative cranial defect. The distance between MF and projection point of the MEV confluence into SS, its most posterior border, allows one to choose the optimal position of the RSC.

Additionally, besides sinus mapping, our study considers that the modified RSC technique proposed by Choque-Velasquez and Hernesniemi [14] is less harmful and risky. According to the authors, for RSA a single burr hole is placed on the occipital squama over the cerebellar hemisphere at medio-caudal part of the planned bone window. This location of burr hole is simple to perform due to thinner bone and safer due to plain dura mater layers beneath. When classic RSA implies key hole drilling at the asterion area with thick bone and high risk of sinus wall perforation. If necessary, the basal extension of RSA to the condylar region was performed by craniotome forming a single bone flap to avoid additional bone removal in close to the sinuses.

The evolution of RSA went from rejection of bone flap removal in all cases for posterior fossa decompression to maximal preservation of surrounding tissue layers for better consolidation of surgical wound [2, 14, 1]. Further development of reliable and simple techniques for intraoperative orientation would have impact on surgery related risks levels and facilitate fast patient postoperative recovery.

Conclusion

This study confirms the utility of mastoid emissary vein canal topography in improving the accuracy of retrosigmoid craniotomy. By facilitating precise sigmoid sinus mapping, the technique reduces the extent of bone removal and minimizes postoperative cranial defect. These findings highlight the potential of this approach to enhance surgical safety and efficiency in cerebellopontine angle procedures.

References

1. Sepehrnia A, Knopp U. Osteoplastic lateral suboccipital approach for acoustic neuroma surgery. Neurosurgery. 2001;48(1):229-30; discussion 230-1. doi:10.1097/00006123-200101000-00046
2. Zhou W, Di G, Rong J, Hu Z, Tan M, Duan K, Jiang X. Clinical applications of the mastoid emissary vein. Surg Radiol Anat. 2023 Jan;45(1):55-63. doi: 10.1007/s00276-022-03060-0
3. Chaiyamoon A, Schneider K, Iwanaga J, Donofrio CA, Badaloni F, Fioravanti A, Tubbs RS. Anatomical study of the mastoid foramina and mastoid emissary veins: classification and application to localizing the sigmoid sinus. Neurosurg Rev. 2023 Dec 19;47(1):16. doi: 10.1007/s10143-023-02229-4
4. Hampl M, Kachlik D, Kikalova K, Riemer R, Halaj M, Novak V, Stejskal P, Vaverka M, Hrabalek L, Krahulik D, Nanka

O. Mastoid foramen, mastoid emissary vein and clinical implications in neurosurgery. Acta Neurochir (Wien). 2018 Jul;160(7):1473-1482. doi: 10.1007/s00701-018-3564-2
5. Raso JL, Gusmão SN. A new landmark for finding the sigmoid sinus in suboccipital craniotomies. Neurosurgery. 2011 Mar;68(1 Suppl Operative):1-6; discussion 6. doi: 10.1227/NEU.0b013e3182082afc
6. Kubo M, Mizutani T, Shimizu K, Matsumoto M, Iizuka K. New methods for determination of the keyhole position in the lateral suboccipital approach to avoid transverse-sigmoid sinus injury: Proposition of the groove line as a new surgical landmark. Neurochirurgie. 2021 Jul;67(4):325-329. doi: 10.1016/j.neuchi.2020.12.009
7. Hamasaki T, Morioka M, Nakamura H, Yano S, Hirai T, Kuratsu J. A 3-dimensional computed tomographic procedure for planning retrosigmoid craniotomy. Neurosurgery. 2009 May;64(5 Suppl 2):241-5; discussion 245-6. doi: 10.1227/01.NEU.0000336763.90656.2B
8. Tubbs RS, Loukas M, Shoja MM, Bellew MP, Cohen-Gadol AA. Surface landmarks for the junction between the transverse and sigmoid sinuses: application of the "strategic" burr hole for suboccipital craniotomy. Neurosurgery. 2009 Dec;65(6 Suppl):37-41; discussion 41. doi: 10.1227/01.NEU.0000341517.65174.63
9. da Silva EB Jr, Leal AG, Milano JB, da Silva LF Jr, Clemente RS, Ramina R. Image-guided surgical planning using anatomical landmarks in the retrosigmoid approach. Acta Neurochir (Wien). 2010 May;152(5):905-10. doi: 10.1007/s00701-009-0553-5
10. Hu W, Zhou J, Liu ZM, Li Y, Cai QF, Hu XM, Yu YB. Computed Tomography Study of the Retrosigmoid Craniotomy Keyhole Approach Using Surface Landmarks. Int J Clin Pract. 2023 Mar 1;2023:5407912. doi: 10.1155/2023/5407912
11. Reis CV, Deshmukh V, Zabramski JM, Crusius M, Desmukh P, Spetzler RF, Preul MC. Anatomy of the mastoid emissary vein and venous system of the posterior neck region: neurosurgical implications. Neurosurgery. 2007 Nov;61(5 Suppl 2):193-200; discussion 200-1. doi: 10.1227/01.neu.0000303217.53607.d9
12. Roser F, Ebner FH, Ernemann U, Tatagiba M, Ramina K. Improved CT Imaging for Mastoid Emissary Vein Visualization Prior to Posterior Fossa Approaches. J Neurol Surg A Cent Eur Neurosurg. 2016 Nov;77(6):511-514. doi: 10.1055/s-0036-1584208
13. Hall S, Peter Gan YC. Anatomical localization of the transverse-sigmoid sinus junction: Comparison of existing techniques. Surg Neurol Int. 2019 Sep 27;10:186. doi: 10.25259/SNI_366_2019
14. Choque-Velasquez J, Hernesniemi J. One burr-hole craniotomy: Upper retrosigmoid approach in helsinki neurosurgery. Surg Neurol Int. 2018 Aug 14;9:163. doi: 10.4103/sni.sni_186_18

Case Report

Ukr Neurosurg J. 2024;30(4):64-67
doi: 10.25305/unj.311488

A multiple suture craniosynostosis with fusion of sagittal, metopic, and bilateral coronal sutures: Case report

Ozan Baskurt[1], Hidayet Ş. Çine[2], Ece Uysal[3], Tufan Hicdonmez[1]

[1] Department of Neurosurgery, Istinye University Faculty of Medicine, Liv Hospital Vadistanbul, Istanbul, Türkiye
[2] Department of Neurosurgery, İstanbul Medeniyet University, Prof. Dr. Süleyman Yalçın City Hospital, Istanbul, Türkiye
[3] Department of Neurosurgery, University of Health Sciences, Prof. Dr. Cemil Taşcıoğlu City Hospital, Istanbul, Türkiye

Received: 13 September 2024
Accepted: 11 October 2024

Address for correspondence:
Ozan Baskurt, M.D., Department of Neurosurgery, Istinye University Faculty of Medicine, Emirgan mah. Camlar sok. No:23 Cam Palas Apt Daire:6 Sariyer, Istanbul, Türkiye, e-mail: ozanbskrt@gmail.com

Multisutural synostosis, characterized by the fusion of multiple cranial sutures without a clear underlying syndrome, represents a rare subtype of craniosynostosis. Particularly uncommon is the simultaneous fusion of the sagittal, metopic, and bilateral coronal sutures. This report details the case of a 50-month-old boy, who had an abnormal head shape due to the simultaneous fusion of four sutures. The closure of the sagittal, metopic, and bilateral coronal sutures has led to a distinct head shape marked by flattening of the forehead and anterior skull, contrasting with the typical Mercedes-Benz pattern observed in craniosynostosis cases. Surgical intervention involved osteotomy with symmetrical barrel staves in the parietal and frontal regions, resulting in improved forehead contour.

Key Words: *brachicephaly; craniosynostosis; multisutural craniosynostosis; nonsyndromic craniosynostosis; scaphocephaly; trigonocephaly*

Abbreviations: C - coronal, L - lambdoid, M - metopic, S - sagittal

Introduction:

Craniosynostosis refers to the premature fusion of one or more cranial sutures, resulting in an abnormal head shape [1]. Typically, it manifests as an isolated fusion affecting a single suture and is not commonly associated with an identifiable genetic syndrome [2]. In contrast, syndromic synostoses, though less prevalent, often involve multiple sutures, including at least both coronal (C) sutures [3].

Apart from these syndromic cases, a small subset of patients exhibits a complex pattern of synostosis without an easily identifiable underlying syndrome. Involvement of the metopic (M) and sagittal (S) sutures, followed by the S and bilateral lambdoid (2L) sutures, represents the most common types of this multisutural, nonsyndromic craniosynostosis [4]. Simultaneous fusion of the S, M, and bilateral coronal (2C) sutures is exceptionally rare.

This report presents a case of complex nonsyndromic craniosynostosis where four sutures (S, M and 2C sutures) were fused simultaneously and its surgical management.

Case Presentation:

A 50-month-old boy was admitted to the neurosurgery department with an abnormally shaped head since early infancy. He had an uneventful delivery at 30 weeks via C-section due to a breech-presenting twin. After lying in an incubator for 3 weeks, he always lagged behind his peers in terms of head circumference, height and weight. According to the parents, his development was normal within the typical developmental milestones. His head circumference was between the 10th and 25th percentile for his age group. The patient was examined for the syndrome before admission to our clinic, but no pathology was found.

He presented with an unusual cranial shape characterized by distinctive frontal flattening of the cranium as the main feature of this rare form of craniosynostosis. Three-dimensional computed tomography revealed the fusion of the S, M, and 2C sutures. Radiological sign of increased intracranial pressure was also noted via the copper beaten skull appearance ***(Fig. 1A)***. Fundoscopic examination was normal.

The child underwent surgery. After a bicoronal skin incision, bilateral paramedian parietal bony incision using a high speed craniotome along the fused S suture was made. The middline S bone left in place. The craniotomy was extended beyond the closed cranial suture along the M suture. Then bilateral barrel-stave osteotomies were performed bilaterally and extended to the contiguous frontal bone with bilateral removal of fused C sutures ***(Fig. 1B)***. The postoperative course was uneventful. Postoperative assessments noted improvement in forehead flattening, with further enhancement observed fifteen months post-surgery. Radiologic evaluation showed resolution of the increased intracranial pressure on the cranial bone with widened biparietal diameter ***(Fig. 1C)***.

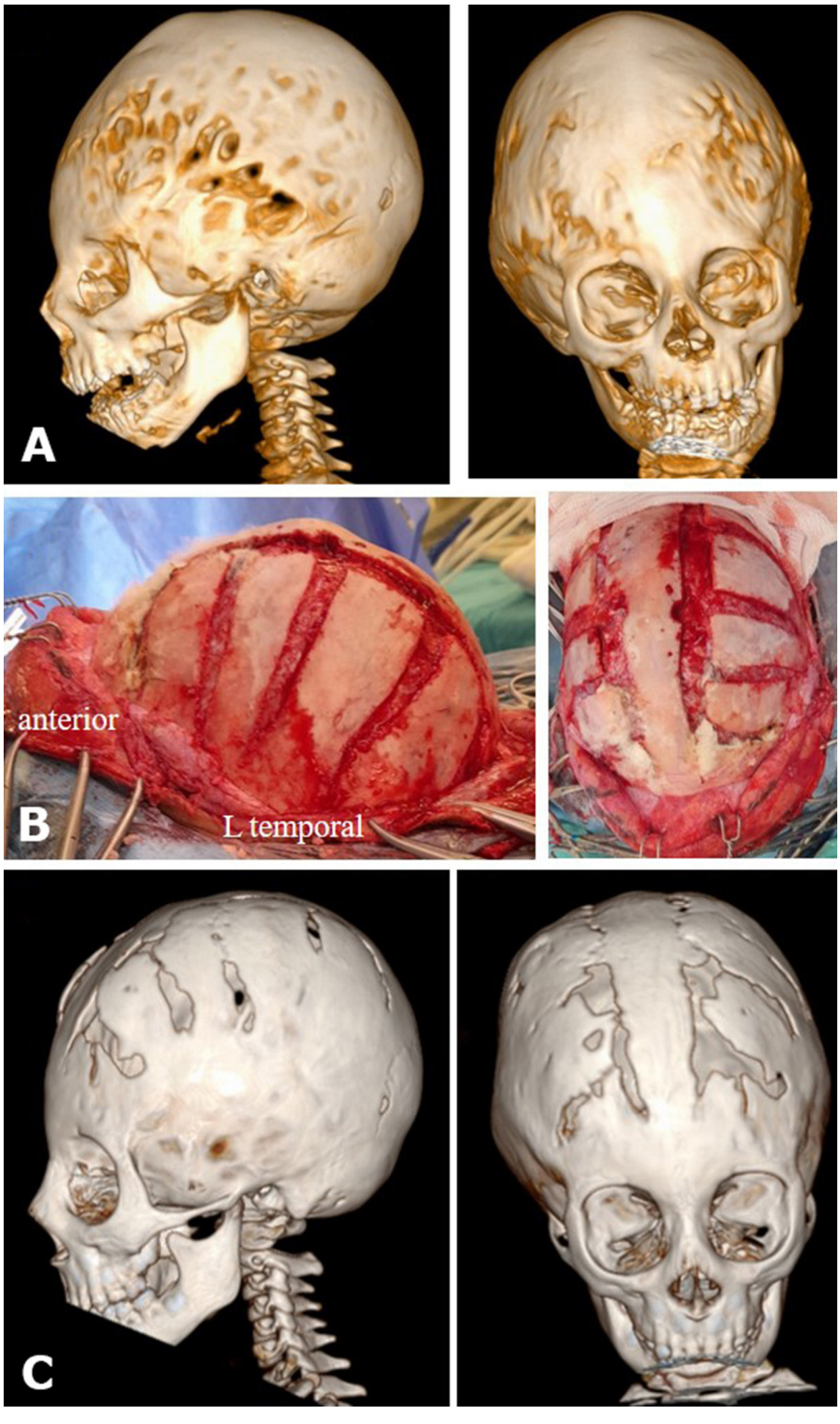

Fig. 1A. 3D head computed tomography, lateral and anterior views; fusion of the bilateral coronal, metopic, and sagittal sutures with signs of increased intracranial pressure with copper beaten appearance.

Fig. 1B. Peroperative image, lateral and superior view; osteotomy with symmetrical barrel staves in the parietal and frontal regions

Fig. 1C. 3D head computed tomography, lateral and anteior views; postoperative 15th month, showing improved flattening of the forehead, resolution of the copper beaten appearance with a widened biparietal diameter.

This article contains some figures that are displayed in color online but in black and white in the print edition.

Discussion:

In about 85% of cases, craniosynostosis is limited to a single suture. The anatomical classification is based on the involved suture [5]. The most common form, with a prevalence of 45% to 50% of all nonsyndromic craniosynostosis, is S synostosis. Recent epidemiologic studies have shown that about 25% of all patients have M synostosis, which is the second most common form [3]. C (unilateral or bilateral) synostosis accounts for 17%, while L synostosis is thought to account for 1-5% of all nonsyndromic craniosynostosis [6].

Approximately 15% of cases are syndromic synostoses, usually involving multiple sutures, including at least 2C sutures [3]. When the S+2C sutures are fused, the membranous bones of the calvarium expand between the sutures, giving the appearance of a cloverleaf as in Kleeblattschädel syndrome; or a high forward tilted head in the form of acrocephaly as observed in Apert syndrome. In craniosynostosis with 2C+L sutures, the forehead recedes, resulting in an upturned, posteriorly declined head and a pointed skull shape, which is associated with compensatory hypergrowth of the bregmatic fontanel in the form of oxycephaly as in Crouzon syndrome [7-9].

Aside from these syndromic craniosynostoses, there is a small subgroup of patients with a multisutural synostosis pattern in whom the underlying syndrome is not readily apparent. Czerwinski et al. retrospectively analyzed 858 patients who underwent craniosynostosis over an 18-year period and found only 37 (4%) cases of nonsyndromic multisutural craniosynostosis [4]. In this study, M+S suture synostosis (10 of 37), followed by 2L+S suture synostosis (7 of 37) were most commonly found [4]. In another study, S+L synostosis was found to be the most commonly observed form of nonsyndromic craniosynostosis (6 in 20 cases of nonsyndromic multisutural craniosynostosis) [6]. The simultaneous involvement of the S+M+2C sutures is exceedingly rare. Czerwinski et al. reported only three cases, while Boulet et al. identified only one case in their craniosynostosis series [4, 5].

This rare case of multiple suture synostosis is particular in terms of the characteristic head shape. This is basically the contrary of the shape that occurs in case of Mercedes-Benz pattern craniosynostosis in which the fusion of S+2L sutures led to a turricephaly in association with scaphocephaly. The main cranial characteristic feature of Mercedes-Benz pattern craniosynostosis is a frontal bossing associated with a posterior parietal flattening (S+2L: anterior oxycephaly with posterior flattening: "Mercedes-Benz pattern") [1, 10, 11]. It is important to note that the M suture is naturally a continuum of the S suture beyond the anterior fontanel [12] . Therefore in our presented case, as a contrary of Mercedes-Benz pattern, the flattening was frontal and a relative backward prominence of that head shape as the result of S and M synostosis with closed 2C sutures [4-5] (S+M+2C: posterior oxycephaly with anterior flattening: "Scapho-trigo-brachicephaly").

Conclusion:

We herein report a rare case of nonsyndromic, multisutural cranisynostosis involving the S+M+2C sutures, scapho-trigo-brachicephaly; and a characteristic flattening of the forehead, as a contrary of Mercedes-Benz pattern craniosynostosis.

Disclosure

Acknowledgements:

None.

Declaration of Interests:

The authors have no relevant financial or non-financial interests to disclose.

Funding:

The authors did not receive support from any organization for the submitted work.

Consent:

Written informed consent was obtained from the legally authorized representative of the patient for publication of this case report and any accompanying images.

Ethical statement:

The need for ethical approval was waived by Istinye University Ethics Committee.

Data Availability:

All data generated or analyzed during this study are included in this article. Further enquiries can be directed to the corresponding author.

Authors' Contribution:

Study conception and design: OB, TH. Data collection: OB, HŞÇ. Analysis and interpretation of results: OB, HŞÇ. Draft manuscript preparation: OB, HŞÇ, EU. Critical revision of the article: TH. Study supervision: TH. All authors (OB, HŞÇ, EU, TH) reviewed the results and approved the final version of the manuscript.

References:

1. Kajdic N, Spazzapan P, Velnar T. Craniosynostosis - Recognition, clinical characteristics, and treatment. Bosn J Basic Med Sci. 2018 May 20;18(2):110-116. doi: 10.17305/bjbms.2017.2083
2. Xue AS, Buchanan EP, Hollier LH Jr. Update in Management of Craniosynostosis. Plast Reconstr Surg. 2022 Jun 1;149(6):1209e-1223e. doi: 10.1097/PRS.0000000000009046
3. Yilmaz E, Mihci E, Nur B, Alper ÖM, Taçoy Ş. Recent Advances in Craniosynostosis. Pediatr Neurol. 2019 Oct;99:7-15. doi: 10.1016/j.pediatrneurol.2019.01.018
4. Czerwinski M, Kolar JC, Fearon JA. Complex craniosynostosis. Plast Reconstr Surg. 2011 Oct;128(4):955-961. doi: 10.1097/PRS.0b013e3182268ca6
5. Nagaraja S, Anslow P, Winter B. Craniosynostosis. Clin Radiol. 2013 Mar;68(3):284-92. doi: 10.1016/j.crad.2012.07.005
6. Boulet SL, Rasmussen SA, Honein MA. A population-based study of craniosynostosis in metropolitan Atlanta, 1989-2003. Am J Med Genet A. 2008 Apr 15;146A(8):984-91. doi: 10.1002/ajmg.a.32208
7. Vinchon M, Guerreschi P, Karnoub MA, Wolber A. Synostosis of the lambdoid suture: a spectrum. Childs Nerv Syst. 2021 Jun;37(6):1991-2000. doi: 10.1007/s00381-020-05003-9
8. Blaser SI. Abnormal skull shape. Pediatr Radiol. 2008 Jun;38 Suppl 3:S488-96. doi: 10.1007/s00247-008-0867-0
9. Bennis Y, Wolber A, Vinchon M, Belkhou A, Duquennoy-Martinot V, Guerreschi P. Les craniosténoses non syndromiques [Non syndromic craniosynostosis]. Ann Chir Plast Esthet. 2016 Oct;61(5):389-407. French. doi: 10.1016/j.anplas.2016.07.004
10. Balestrino A, Secci F, Piatelli G, Morana G, Pavanello M, Pacetti M, Cama A, Consales A. Pure Bilateral Lambdoid and Posterior Sagittal Synostosis (Mercedes-Benz Syndrome): Case Report and Literature Review. World Neurosurg. 2019

Aug;128:77-82. doi: 10.1016/j.wneu.2019.04.117
11. Dinis J, Junn A, Lu X, Lopez J, Persing J. Aberrant Morphologic Patterning of Combined Sagittal and Metopic Craniosynostosis. J Craniofac Surg. 2021 Sep 1;32(6):2184-2185. doi: 10.1097/SCS.0000000000007676
12. Pontell ME, Barrero CE, Wagner CS, Salinero LK, Swanson JW, Taylor JA, Bartlett SP. Oxycephaly-systematic review, case presentation, and diagnostic clarification. Childs Nerv Syst. 2023 Nov;39(11):3041-3049. doi: 10.1007/s00381-023-06048-2